JAPAN ADVANCED INSTITUTE OF SCIENCE AND TECHNOLOGY

DOCTORAL THESIS

---

# Scalable Eel-like Robot Using Series of Soft Actuators: Design Basis, Evaluation, and Applications

---

*Author:*
Dinh Quang NGUYEN

*Supervisor:*
Assoc. Prof. Van Anh HO

*A thesis submitted in fulfillment of the requirements*
*for the degree of Doctor of Philosophy*

*in the*

Soft Haptic Laboratory
Graduate School of Advanced Science and Technology

# Declaration of Authorship

I, Dinh Quang NGUYEN, declare that this thesis titled, "Scalable Eel-like Robot Using Series of Soft Actuators: Design Basis, Evaluation, and Applications" and the work presented in it are my own. I confirm that:

- This work was done wholly or mainly while in candidature for a research degree at this Institute.
- Where any part of this thesis has previously been submitted for a degree or any other qualification at this Institute or any other institution, this has been clearly stated.
- Where I have consulted the published work of others, this is always clearly attributed.
- Where I have quoted from the work of others, the source is always given. With the exception of such quotations, this thesis is entirely my own work.
- I have acknowledged all main sources of help.
- Where the thesis is based on work done by myself jointly with others, I have made clear exactly what was done by others and what I have contributed myself.

Signed:

_____

Date:

_____

JAPAN ADVANCED INSTITUTE OF SCIENCE AND TECHNOLOGY

# *Abstract*

School of Materials Science

Graduate School of Advanced Science and Technology

Doctor of Philosophy

**Scalable Eel-like Robot Using Series of Soft Actuators: Design Basis, Evaluation, and Applications**

by Dinh Quang NGUYEN

In this thesis, we developed an eel-inspired soft robot for both aquatic and terrestrial locomotion and showcased theoretically and experimentally how the structure and control parameters many benefit efficient swimming. In terms of theoretical approach, a hydrodynamic model that considers the effect of whole-body movement of the eel-like body's locomotion was constructed. The model was built based on the continuum approach, in which the reactive force at any point along the mid-line is determined. The model was then utilized to predict the propulsion of the eel robot at different working regimes. Also, the model brings in an approach for estimating the drag force coefficient of anguilliform movements, even when it is difficult to set up an experiment and conduct measurement due to the complex motion of the object. Regarding the practical aspect, a control regime was proposed for mimicking the anguilliform swimming of the eel soft robot built by a series of soft actuators. Here, pulse signals with the shifting phase are supplied into actuators. For the efficient generation of sine-waveform, four pairs of the actuators that were divided into three segments were chosen to construct the robot body, therein, the head segment was built from two pairs because it plays a role as a wave source, while the others work as propagation parts. Smooth propagation waves generation is considered the key to realizing swimming efficiency. Besides, three novel swimming strategies (C shape mode, passive body level 1 - one-fourth passive body, and passive body level

2 - a half passive body) that cannot be done by natural animals and traditional rigid robots were introduced. Surprisingly, differing from the natural eel and rigid elongated body robot, the soft eel robot with a passive tail and performing C shape can even swim with higher efficiency than the fully active one. This result is important for the development of the robot for long journey tasks for energy-saving purposes, also, enlarges the working conditions of the robot.

By scaling down the soft eel robot, we present the preliminary design and evaluation of a self-propelled soft colonoscopy robot employing a series of soft actuators, equipped with a control strategy for creating forwarding movement. The design permits the robot to move efficiently, thanks to creating transient bending segments between crest and trough segments, resulting in smooth propagating waves along the robot's body. Control parameters, including frequency, shifting phase (that characterizes the creation of propagation waves from head to tail,) and pressure of supplied air strongly affect the locomotion gait. The obtained results in this paper would be applied to the creation of an autonomous soft colonoscopy robot in the future.

**Keywords**: eel inspired robot, pneumatic actuator, anguilliform, body partially damage, colonoscopy robot

# *Acknowledgements*

Many people help me throughout my Ph.D. and made it possible for me to write this thesis. Firstly, I would like to express great gratitude to my advisor, Prof. Ho Anh Van, for giving me a chance to work in an exceptional environment, encouraging me to push our research forward, and providing me with excellent advice and valuable resources. Under Ho sensei motivating and supporting, I went through many interesting adventures and handled a vast variety of problems during the past three years. My knowledge and skills learned from Ho sensei are beyond this thesis. I also greatly like to thank my second supervisor Prof. Hiroshi Mizuta and my supervisor for minor research Prof. Mikio Koyano for all their advice and support through my Ph.D. The valuable conversations guided me to move faster on my research road. Additionally, I come up with many interesting ideas that helped me dig deeper into my research theme.

I also would like to thank all Ho Lab. members for supportive, collaborative, and friend environments. The discussions with lab members also provided many understandings from both academia and society. I am very happy to become a part of the lab and will always remember funny parties and outside activities. Many thanks also go out to all the JAIST staff, from whom I received kindly supports on both living and studying aspects. Without these things, this journey would have been much harder.

To my love Thu Van, no words can express your sacrifices. Thank you very much for your support and encouragement. Despite my absence over three years, you have taken good care of and raised our son. Thank you for all the inspiring conversations and all the loving words. I am looking forward to standing by you and creating everything together.

To my son Minh Thanh, you are a great source of motivation for me to overcome the difficulties of the past three years. Your smiles, your words dispelled my tiredness and stress. I am very happy to see you growing up day by day and strong interest in learning new things. Soon, we will do many things together.

Finally, my deepest gratitude goes to my dad and mom, who have always encouraged me to follow my dreams. Thank loving dad who has been quietly sacrificing and loving me. Thank loving mom who has been making endless sacrifices for me. I will remember video calls each weekend and since I was stressed through the past three years. Thank parents for always being healthy so that I can confidently pursue my dreams. I am looking forward to many more joyful years together.

# Contents

# List of Figures

# List of Tables

# List of Abbreviations

| | |
|---|---|
| **BCF** | **B**ody and/or **C**audal **F**in |
| **MPF** | **M**edian and/or **P**aired **F**in |
| **BL/s** | **B**ody **L**ength per second |
| **DoF** | **D**egree of **F**reedom |
| **PAM** | **P**neumatic **A**rtificial **M**uscle |
| **PneuNets** | **P**neumatic **N**etworks actuators |
| **DEA** | **D**ielectric **E**lastomers **A**ctuators |
| **EBT** | **E**longated **B**ody **T**heory |
| **PCC** | **P**iece-wise **C**onstant **C**urvature |
| **COT** | **C**ost of **T**ransport |
| **FEA** | **F**luidic **E**lastomer **A**ctuator |
| **PWM** | **P**ulse **W**idth **M**odulation |
| **PIV** | **P**article **I**mage **V**elocimetry |
| **MIS** | **M**inimally **I**nvasive **S**urgery |

# Physical Constants

| | |
|---|---|
| Gravitational acceleration | $g = 9.806\,65\,\mathrm{m\,s^{-2}}$ |
| Water density | $\rho = 997\,\mathrm{kg\,m^{-3}}$ |

# List of Symbols

| | | |
|---|---|---|
| $C_D$ | drag coefficient | |
| $\rho$ | fluid density | $\mathrm{kg\,m^{-3}}$ |
| $s$ | reference area | $\mathrm{m^2}$ |
| $v$ | velocity | $\mathrm{m\,s^{-1}}$ |
| $a$ | acceleration | $\mathrm{m\,s^{-2}}$ |
| $A$ | amplitude | m |
| $\beta$ | increment coefficient | |
| $\alpha$ | amplitude growth rate | |
| $\lambda$ | wavelength | m |
| $f$ | frequency | Hz |
| $T$ | cycle time | s |
| $s$ | shifting phase | % |
| $P_E$ | electrical energy | J |
| $P_A$ | air pressure energy | J |
| $g$ | gravitational acceleration | $\mathrm{m\,s^{-2}}$ |
| $\omega$ | increment coefficient | |

# Chapter 1

# Introduction

## 1.1 Soft robotic locomotors: chance and challenge

Animals have evolved their body shapes, interaction methods, and locomotion strategies to adapt to the living environments [1]. A few examples can be given to show the superiority of evolution in nature. Using joint structure is the most common method that animals use to move (by walking, running, flying, jumping, and swimming) from one place to another. Joints also permit animals to perform skill-full actions such as grasping, moving objects through space along complex lines. Body shape and skin are also changed to suit different goals. Taking speed as an example, sharks are the fastest predators which can reach a velocity of 16 m/s (10 times faster than the typical human swimmer). This speed is achieved because of the very low drag force that comes from hydrodynamic body shape resulting in reducing pressure drag and special structure cover scales resulting in reducing friction drag [2]. Therefore, learning from nature is a wise approach to creating effectively artificial moving robots. Traditionally, robots are made of rigid materials (steel, copper, rigid plastic, *etc*.) so that they can work fast, precisely, strongly, and repeatably. Such kinds of robots can only mimic the working principle of the natural creatures such as flapping [3], wave generating [4], and can create high speed, accuracy, and force application but have a low level of behavioral diversity, low level of bio-inspiration. One of the most important issues that accompany rigid robots is unsafe and low adaptability to operate in unexpected environments unless complex control measures are employed.

Most animals exploit soft body structures to perform maneuver locomotion in

complex terrain in natural and to create gentle contact with environments at unforeseen collisions. Higher animals even use stiff bone skeletons for bearing the body's weight but the rest which contributes a large portion is made up of soft tissues. Regarding ingenuity and flexibility, an elephant's trunk is a marvel of biology. Elephants use their trunks to explore surrounding environments by bending and/or extending. The trunk without any bone not only is able to lift a heavyweight such as a human or a long chunk of wood, but also move adaptively through narrow and complex structure [5]. Another example of this characteristic is the octopus that used tentacles to walk, swim, explore the environment, and search for food. Due to its soft and flexible body, the octopus can entrance very narrow space. Mimicking not only the locomotion/working principle but also the "soft" structure from nature will raise the level of bio-inspiration. The combination of traditional robotics and new material technology created soft robotics, in which robots are partially or fully constructed by soft and deformable materials (soft biological materials) such as silicone rubbers, urethanes, and hydrogels. In general, the new robotic field has been created bio-inspired robots with more flexibility and adaptability compared to those from traditional rigid robots [6], [7].

### 1.1.1 Key for bio-inspiration

Basically, the animal locomotion principle can be divided into three groups including flying, walking and crawling, and swimming. Although there are different movement methods, these activities are performed by muscle bundles. In soft robotics, soft biological materials have been utilized to fabricate actuators that play as muscles. Depending on locomotion characteristics and the working process of muscle bundles, materials are chosen and structures are designed.

#### Locomotion principles

Most flying animals flap their wings to create airflow that generates thrust and lift. Flying strategies by flapping wings are also very diverse, however, they can be categorized into two main groups including birds flying method and insect flying method. The former group use shoulder joints to perform complex movement of their wings including up and down, fore and aft, and supination and pronation for

flying. Additionally, the cross-section of the bird's wing has an airfoil shape that strongly supports flying such as permitting the bird to use natural airflow to hover without flapping movement. This geometrical characteristic is employed to design propellers and airplane wings [1]. To fly, the birds only need to flap their wing less than 10 times in one second (wingbeat frequency less than 10 Hz) [8]. Meanwhile, insects employ muscles to control the wing movement and elastic elements to store and release kinetic energy during flight. The insects' wings that are constructed from a membrane supported by a meshwork of veins only perform up and down strokes to create lift and thrust. An interesting characteristic of the insects' wings is the deformable ability (even fold) upon outside pressure (wind gut or collision) to reduce breakage. This characteristic was employed to create a novel safety drone propeller [9]. Differing from the bird, insects have to create a very high wingbeat frequency up to 1000 Hz (100 Hz in commonly) as flying.

Unlike aerial animals, terrestrial animals have a vast variety of locomotion strategies. Having four feet, however, quadrupedal mammals and quadrupedal reptiles have different locomotion gaits. Quadrupedal mammals move the left and right legs alternatively and the legs at front and rear are symmetrical [1], [10]. Due to the familiarity of quadrupedal animals with humans, many kinds of locomotion robots sharing the quadrupedal mammals' locomotion principles have been developed [11]. Meanwhile, lizards, besides moving their legs sequentially, undulate their body and tail to the support movement. Based on this principle, an amazing salamander robot was introduced. Investigation on robot locomotion gaits indicated that the combination of legs alternatively movement and undulatory movement of its body is very important to walking efficiency of the robot [12]. Terrestrial invertebrate animals such as worms use circular and longitudinal muscles to bend their body for locomotion. Besides bending the body, worms also have to use legs as an anchor in each movement step [13]. Another popular terrestrial animals locomotion type is jumping (rabbit, kangaroo, bush baby, frog, *etc*.). In this movement strategy, animals rapidly extend their leg with the extension acceleration time of 0.05 sec to 0.1 sec. The locomotion is performed by hind legs that play a role as spring as shortening to store energy then extending to jump [14].

Aquatic animals (except for some kinds of mammals such as seals, walruses) can

be classified into four groups including crustaceans (shrimp, crab, *etc*.), shellfishes (scallops, snails, *etc*.), fishes (salmon, eel, *etc*.), and animals with tentacles (octopus, squid, *etc*.). Most of the animals in the first and second groups travels by clawing apart from some kind of scallops that swim by jet propulsion [15]. Invertebrates with tentacles both use their tentacles for traveling and/or searching and getting food [16] and also use jet propulsion for locomotion [17], [18]. Fishes exhibit a large variety of swimming strategies that use different parts of their body to interact with ambient water. The classification of fish locomotion strategies is based on the combination of swimming propulsors (body and fins). Specifically, fishes are classified into two swimming types, based on how they use the body parts to create propulsion, including BCF (body and/or caudal fin) in which fishes bend their body or a part of the body to create propulsive waves or oscillatory motions for traveling, and MPF (median and/or paired fin) in which fins are utilized to create undulatory or oscillatory motions for locomotion. In BCF modes, another classification have been conducted based on how much the body is used and how are they operated, the mode can be divided into five swimming types sorted as anguilliform (eels, lampreys, most type of sharks, *etc*.), subcarangiform (trouts, salmons, cods, *etc*.), carangiform (bluefin trevallys, jacks, herrings, *etc*.), thunniform (tunas, billfishes, *etc*.), and ostraciiform (boxfish, torpedo rays, *etc*.) [19] [20].

In this section, the most important characteristics of an anguilliform swimmer are listed to make a foundation for the development of an eel-like soft robot. In anguilliform mode, a large portion of the fish body is undulated to generate propagation waves from head to tail for forwarding locomotion. The animal body in swimming mode forms sinusoidal waves with continuously increasing amplitude from head to tail [21], [22] resulting in a pronounced characteristic of the anguilliform swimmer is large lateral displacement of the tail segment at roughly 0.24 BL (Body length). Tail beat frequency varies from around 2.0 Hz to approximately 4.0 Hz depending on swimming conditions. Meanwhile, swimming velocity range from 0.2 BL/s (Body length per second) to 2.0 BL/s [23], [24].

A vast variety of investigations on locomotion principles of natural creatures that have been conducted clearly and meticulously provide a strong foundation for roboticists in developments on bio-inspired robots. Variability of life forms, which

might up to millions of types of species, provides a diverse source for scientists and engineers.

**Bio-inspiration rigid robots**

Bio-inspiration robots immensely diversify. They have been utilized not only for human, military services but also for investigating physical behaviors of living counterparts that might provide a deep understanding of the physical interaction between natural animals with the surroundings, which cannot be done or difficult conduct experiments on natural species. Such principle underlying, then, is transferred to the development of the robots. Traditional bio-inspired robots utilized rigid materials such as steel, copper and classical basic mechanisms such as gears, bearings, belts, chains, joints for robot body construction [25], [26], [27] or to build a novel mechanism for robot movements [28], [29]. Having a long development history combined with the precision of mechanical systems, control strategy, and sensor system, conventional rigid robots have many advantages including well-established, high precision, fast response, high force reaction, high-temperature resistance. They also have been used in a vast variety of applications such as industry, transport, medical service, military, and entertainment. Nonetheless, hard robots have demerit characteristics that are not suitable for many applications. One of the points worth noting is unsafe and limited adaptability to operate in unforeseen environments unless complex control and sensory systems are applied. Additionally, conventional robots that are commonly constructed from links connected by joints have an inherent property of discontinuity (finite DoF - Degree of freedom). To improve discontinuity property, an increase in the number of links is required, which results in an intricate control algorithm. Due to construction from rigid materials, traditional robots have high weight and low levels of bio-inspiration [30]. The appearance of soft-smart materials and novel structure made by them has opened up a new field in robotics called "soft robotics", in which investigation on robots made from soft and deformable materials. Such robots are expected to change their effective stiffness and morphology in order to provide a desired force or compliance when interacting with the surroundings. Besides, soft robots are able to create complex motion, absorb impact

force to reduce or even avoid injury, self-healing (relying on the material property). These characteristics seem to be suitable for biological robotics.

### Soft actuators and actuation methods

One of the most important components of robots is the actuator (motors, cylinders, *etc*.) that decide the working and controlling method. Actuator's type and size, normally, is chosen at the design phase based on the robot functions and characteristics such as working conditions, robot's size. This section will review some typical types of soft actuators that play an important role in designing suitable types of bio-inspired soft robots.

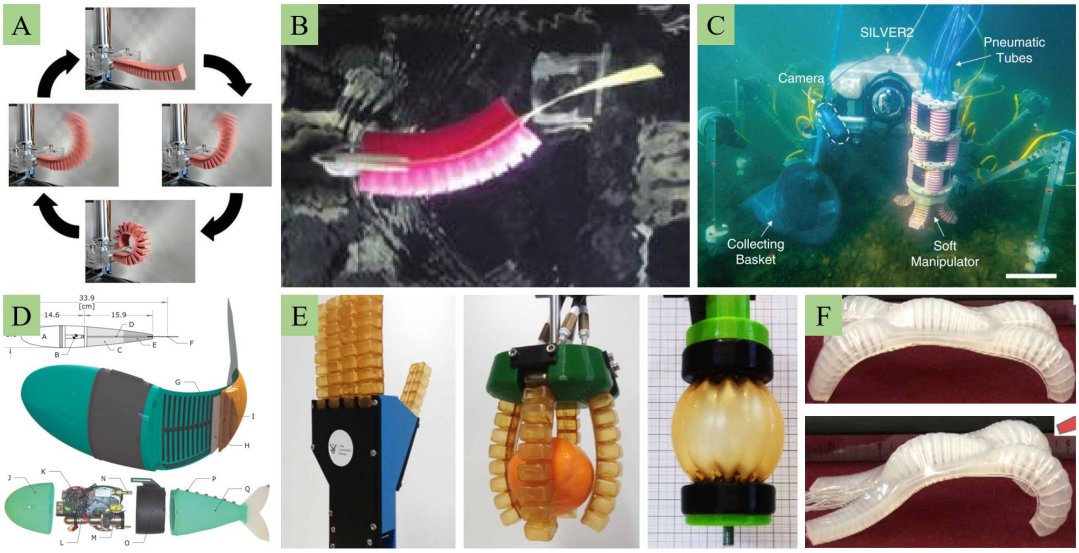


FIGURE 1.1: Pneumatic soft actuator (PneuNet - A [31]) and its variants. B - A pair of PneuNets were affixed symmetrically along a plastic plate to create flapping movement [32]. C - Soft actuators were used to construct a soft manipulator for collecting under sea objects [33]. D - Fluidic actuator (actuated by pressurized air) in customized shape for tail segment of a soft fish robot [34]. E - Special polymer was utilized to fabricate self-healing soft hand, gripper and muscle [35]. F - Multi gait locomotion soft robot shared the chamber structure with the PneuNets [36].

Pneumatic actuators use compressed air for actuation. There are two typical types including Pneumatic Artificial Muscle (PAM) (also known as McKibben Artificial Muscles) and Pneumatic Networks actuators (PneuNets). Fig. 1.1 shows working principle of a PneuNets and some variants for many kinds of applications. PneuNets that are made of soft materials and have chambered and segmented structures are popular actuators in soft robotics. In the original design, PneuNets can only be bent when inflated [31]. Up to now, many variations of the pneumatic actuator

have been introduced. The combination of chambered and segmented structure in PneuNets and idea of braid sleeve in PAM created reinforcement pneumatic actuator, in which actuator can enlarge working ability to bend, twist and also can work at higher pressure resulting in withstanding higher loads [37], [38]. Two or three pneumatic actuators are also combined to generate different kinds of movement such as omnidirectional steering [39], [40], two sides bending, or flapping [32], [41]. Fluid is also used instead of pressurized air for actuation [34]. By applying special functional polymer, soft actuators are able to heal microscopic and macroscopic damage [35]. The stiffness of actuators, and thus robots, can be varied by changing construction materials, actuators' wall thickness, and actuation pressure. Working frequency (taking flapping movement as an example) is quite low at lower than 2.0 Hz [32]-[42]. The segmented and chambered soft actuator is scalable and can change shape or morphology to adapt with robot size and natural animal types that are natural sources to inspire for soft robots [33], [36], [43], [44]. Soft pneumatic/hydraulic actuators, therefore, are suitable for bio-mimicking of low locomotion motions such as fishes, jellyfishes, turtles, worms, human hand movement.

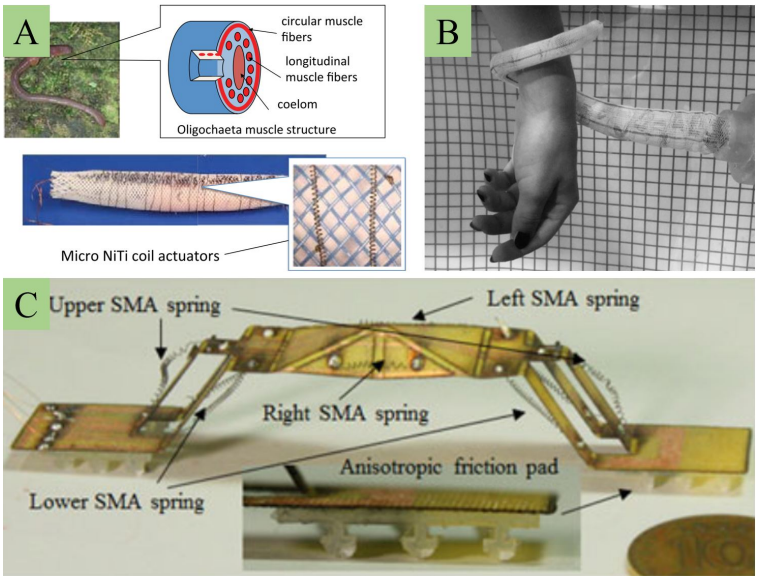


FIGURE 1.2: Some typical soft robots used SMA driven. A - SMA was used to generate peristaltic locomotion of a soft earthworm robot [45]. B - A soft octopus tentacle was driven by SMA springs for transverse deformation. The tentacle can perform some basic movements such as elongation, shortening, and bending in water [46]. C - Omegabot inspired by inchworm used customized SMA spring coil to work over a large pitch angle range [47].

Dielectric elastomers actuators (DEA) work with electroactive polymers which

deform when inducing an electric field. DEA has large actuation strains, rapid response rate, low cost and low noise, high energy density, and high efficiency. An interesting characteristic of this actuator type is that it can generate high-frequency movement when reaching the highest displacement at 700 Hz [48]. This property is very suitable for mimicking the flapping movement of a bird or insect's wing. However, requiring high voltage for actuation might consider as a demerit of the DEA. The high voltage consumption, which usually requires a large size power supply, prevent the development of untethered and/or compact bio-inspired robot [49], [50].

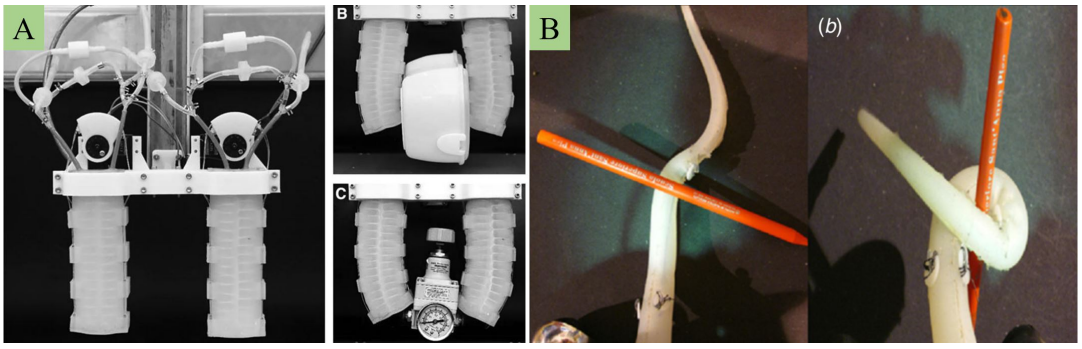


FIGURE 1.3: Examples on tendon-driven soft actuator. A - A soft self pumping actuator used tendon to generate gripping activity and used pressurized air to enlarge its stiffness [51]. B - Cable was embedded into a soft tentacle for actuation. The tentacle can pushing for locomotion or grasping objects [52].

Shape Memory Alloy (SMA) is also considered a typical type of soft actuator. SMAs are high force/weight ratio, low weight, and noiseless actuators that are suitable for soft and wearable robots, particularly for the construction of exoskeletons for soft locomotion robots. However, shape memory alloy has some disadvantages including low actuation frequency, complex controllability, and low energy efficiency [53]. For bio-inspiration soft robots, SMA was utilized to mimic peristaltic locomotion in an earth worm-like robot [45], omega-shaped in inchworm-inspired crawling robot [47]. SMA can also act as tendon-like actuators that create the movement of octopus tentacles [46].

Tendon-driven soft actuators are another approach to deal with actuation for soft actuators. This kind of actuator often drives robotic joint motion through a pulley system. As PneuNets, tendon-driven soft actuators can only work at low frequency. Nonetheless, it creates better precision motion, less vibration, and more stiffness

[51]. The principle was used to actuate the flapping motion of a soft fish robot [54] and embedded into a soft octopus arm to drive its movement [52].

### 1.1.2 Challenges

Although soft robots have been investigated for decades and also achieved some brilliant results that have been applied in the food industry [55] and have the potential to be applied in practice [56], there are still many issues to be tackled to get depth understanding in soft robotics from both theoretical (modelings, control algorithms, mechanical calculations, *etc*.) and practical (soft mechanism response, repeatability, efficiency, *etc*.) aspects.

The characteristic that brings advantages for the soft robots of adaptability, flexibility, and creating gentle contact ability is continuity. The soft robots can be considered to have infinite DoF. However, this property also is a difficult issue when working with soft robots especially creating mathematical/physical models. A precise mathematical/physical model is an effective tool for solving robot/machine-related problems. It has been used to predict the behavior of the robot/machine such as velocity, an interactive force with the surroundings, position in space at any working condition that scientists and engineers cannot conduct to examine due to lack of time or experimental facilities. These predictions permit researchers to save their time in optimization of the robot designs, and/or selection of the efficient working parameters. Another important merit of a precise model is to create suitable control laws that strongly affect the precision in motion of the robots. Due to the infinitive degrees of freedom, it is a challenge to build a precise model for soft robots. Today, the most common method is approximately discrete, in which a soft and continuum body is considered as many rigid links. This approach is quite effective in simple cases such as 2D (two-dimension) deformation [57], [58]. Another approach to model soft movement object is piece-wise constant curvature (PCC) that represent the soft structure with a certain number of arcs characterized by three factors including the radius, the angle of the arc, the bending plane [59]. Recently, the PCC method was also applied for dynamic modeling and experience in closed-loop control [60]. Nonetheless, this method still considers the soft continuum robot as a discrete object

when dividing the robot into $n$ curvature segment and do not include the properties of the material from which the robot was built. For taking into account large deformation and construction material properties (*i.e*. nonlinear behavior of hyperelastic materials - soft and resilient materials), Cosserat theory has been introduced [61]. Cosserat theory is usually used for hyper-redundant robots that are quite close to soft robots. The theory also has been applied to locomotion and manipulation of soft robots [62]. However, this method is considered difficult to use for control purposes or might be computationally expensive that is not suitable for the control algorithm of an untethered and compact soft robot. These disadvantages of the current modeling theories have motivated the researchers to come up with new ideas of a simpler approach for modeling soft robots that can capture both continuum and nonlinear characteristics.

Conventional robots have been mostly constructed from basic machine element parts such as motors, gears, chains, ball joints. Such foundations are not available for soft robots, therefore, to construct a new soft locomotion robot, scientists and engineers have to come up with the idea of the robot right from the design stage and have to go through the testing process that might take a long time for testing locomotion efficiency with limited support techniques. Researches on soft robots indicated that it is difficult to development of an efficient locomotion soft robot with basic characteristics such as being untethered, continuously working for a long time, waterproof, modularized so that damaged parts can be easily replaced. As a result, it can be seen that there is still a long process for the soft robot community to develop design standards from which soft robots can be easily and quickly designed and calculated (durability, kinetic and dynamic parameters, *etc*.) as done with conventional robots. This is the foundation for soft robot developments and applications of soft robots in the industrial field and social service area. Another disadvantage of the soft robots related to their structures is vulnerability. The soft robots (soft pneumatic actuator, soft balloon, *etc*.) easily break upon contact with sharp objects.

The nonlinear behavior of construction materials and the lack of modeling (as analysis aforementioned) lead to a big challenge in precisely controlling soft robots. Soft robots require power sources for actuation such as an air pump that applies pressurized air into the internal chamber of a pneumatic soft actuator constructing a

soft robot body, electrical source applies a voltage to a DEA making up a soft robot, or a motor pulls on cables embedded in a soft mechanism. Most soft robots developed in such ways have been used a low-level control approach. Taking a pneumatic soft actuator as an example, with this control method, the soft actuator is controlled its movement by pressure control using a pressure sensor or volume control using flow rate control or strain gauge. The soft robot movements are deployed based on this control strategy. In addition, soft robots have inherent compliance, therefore, they are easy to adapt their shape to unforeseen objects or environments. However, controlling a soft robot to reach exactly desired shape, position, and/or impact force on other objects especially at high frequency or high velocity challenge (unlike rigid robots that can be controlled precisely positions, velocity, and force by control motors' angles, displacement of a cylinder, *etc*). Because of the low durability of hyperelastic materials, which is changed their properties (hardness, toughness, resilient property, *etc*.) over time or when exposed to sunlight, heat, or reactive chemicals, the soft robots also require an adaptive controller and control algorithm toward these situations. Another challenge for control comes from the fabrication method mainly related to the 3D printing technique (pouring silicone molds, some kind of actuators) that results in big tolerances and variability attributing to the imprecise and inconsistency of the fabricated robots leading to errors in controlling.

## 1.2 Thesis objectives

In this thesis, we aim to develop a soft elongated body robot with a high softness level and high locomotion efficiency as shown in Fig. 1.4. The main objective is to create and evaluate an underwater soft robot inspired by the shape and movement of an eel, exploiting pneumatic actuators. The robot structure is scalable for a vast variety of applications. Details of the research purpose can be found below:

**A physical model of a soft eel robot**: Using a series of soft actuators to construct a soft eel robot that is capable of anguilliform locomotion with high swimming efficiency.

**Control strategy for aquatic soft elongated body robot locomotion**: Investigating on undulatory movement control to create anguilliform swimming performance

for the soft eel robot at several swimming mode (from active to passive ways).

**Hydrodynamic model for thrust force prediction**: A continuum model of soft and continuum bodies is being established. This model and its related establishment method can be utilized to predict the hydrodynamic behavior of the soft eel robot and exploited to develop control strategies.

**Miniature scale of the soft eel robot performing undulatory movement for colonoscopy applications**: Developing a mini soft eel robot using a series of soft actuators and undulatory movement control for a self-propelled colonoscopy soft robot.

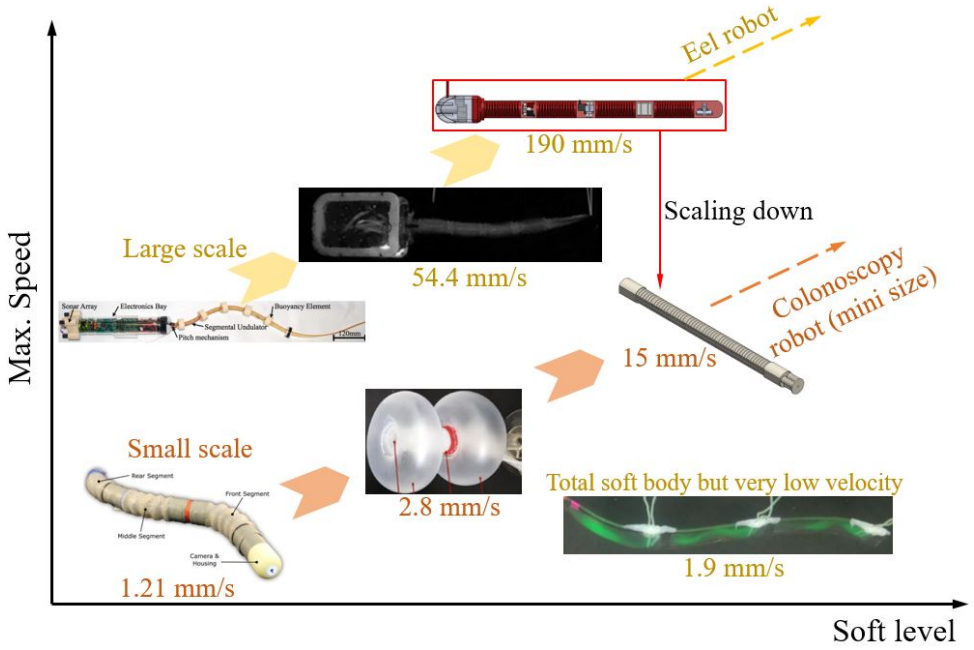


FIGURE 1.4: Development trend of bio-inspired soft robots and position of our research.

## 1.3 Approach methodology

Our development begins with the investigation of a soft pneumatic actuator to get a suitable shape and easily bend in the desired manner when inflated. Simulation is employed to support the design stage. Locomotion principles and related issues of anguilliform creature is deeply investigated for whole robot design and its working principles for mimicking natural one. Then undulatory movement control strategy is investigated to form anguilliform swimming locomotion. Along with them, a hydrodynamic model for underwater continuum locomotion is developed to predict

the thrust generation of an anguilliform swimmer. Additionally, the model is also used to calculate the drag force coefficient created by wave-like movements. Other efficient swimming strategies that can not be done by natural ones are introduced. Lastly, the miniature scale of the robot is investigated for colonoscopy soft robot.

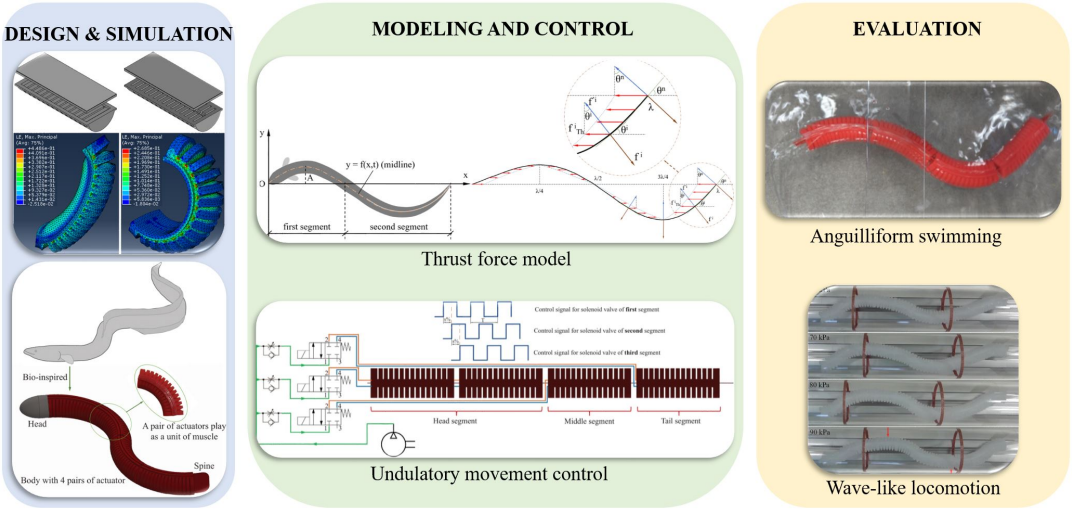


FIGURE 1.5: Approach overview for scalable eel-like robot using series of soft actuators: Design basis, Evaluation, and Applications.

In detail, a hydrodynamic model of an anguilliform swimmer based on continuum deformation opinion is founded. Using the model, thrust force generation at any swimming regime can be predicted. One of the most challenges in engineering is thrust and drag coefficient measurement. They require a complex experimental system. In this case, the difficulty is at a higher level due to the variation of geometrical morphology of the robot body when performing anguilliform gait. Therefore, the thrust model might supply an effective tool to determine the drag coefficient of an elongated body fish. Due to the nonlinear deformation of the robot body when inflated combined with the complex reaction in a fluid environment, experiments and Matlab fitting tools are employed to determine the variation of robot body parameters such as tail beat amplitude, wavelength versus controlling frequency, and pressure. This, in our point of view, is an appropriate tool for soft robots.

Chambered and segmented structure [31] is employed to design the soft pneumatic actuator. Due to the different shapes, sizes, and construction material, the design is simulated (using Abaqus) to get a suitable one, from which the actuator can bend and create flapping movement easily. The molding technique is used to

fabricate the actuator. Based on the actuator design, molds are designed and then fabricated by a 3D printing technique. A series of the pneumatic soft actuators are affixed symmetrically along a flexible polypropylene ribbon to construct the eel-like robot body that also is built based on natural anguilliform swimmer characteristics.

Because of the differences in fabrication and structure, the working bandwidth of the fabricated soft actuator must be identified. To determine a suitable working frequency range, in which the actuator work efficiently, experiment evaluation is conducted for a pair of the soft actuator. Pulse signals with shifting phase are employed to actuate the series of pneumatic actuator sequentially for creating sinusoidal waves from head to tail in order to forward locomotion. Besides tail beat frequency, other important control parameters including inflated pressure and shifting phase are examined.

In natural, eel that typical for the anguilliform locomotor swim by creating sinusoidal waves from head to tail. Additionally, some previous research indicated that natural eel can not perform well anguilliform swimming when its body is partly damaged. This conclusion is as same as with rigid elongated body robots. However, based on flexible and continuum characteristics, a soft robot might perform differently. We examined different swimming strategies based on air pipe order connection and varying control shifting phase to create un-anguilliform locomotion and deactivate partly body to create partly damaged body. Interestingly, the proposed soft eel robot performs new swimming strategies better than the traditional one.

One of the considerations of scientists is the scaling capability of their researches. Realizing the potential application of self-propelled soft robot in endoscopy. A miniature eel-like robot is deployed toward a colonoscopy soft robot. The difference in the working environment requires an investigation on modifying the robot structure. Series of pneumatic soft actuators with undulatory control are the foundation and are still utilized, however, the robot body is softened totally for safety purposes. Additionally, the air contribution principle is modified for efficient locomotion on land and constrained environments.

## 1.4 Thesis contributions

The thesis is not set a target of thoroughly addressing one or some of the aforementioned challenges, however, it intends to tackle some aspects in design, simulation, control, and evaluation methodology for underwater soft robots. The investigation contribute a brick for soft robotics castle that is believed to complete in the near future.

### 1.4.1 Design and fabrication for bio-inspiration soft robot

The thesis contributes to the design and fabrication method of robotic soft through the development of a soft pneumatic actuator that is suitable for anguilliform swimmer soft robots. Specifically, a semi-cylindrical soft actuator and suitable air connecting channel structure were proposed. The simulation method was utilized for time-saving. The fabrication process also detailed description. Additionally, the design of an eel soft robot that included a series of new design pneumatic soft actuators to provide undulatory movement via pulse control signals with a suitable shifting phase was introduced. The robot structure and soft actuator powering method permits the robot to perform large tail beat displacement mimicking the natural ones. The soft actuator is not only suitable for pneumatic powering but also hydraulic actuation.

### 1.4.2 Continuum model for hydrodynamic force prediction

We propose a new theoretical approach for determining the interaction between soft robot performing serpentine locomotion and surrounding fluid. A model of hydrodynamic force impacting the robot eel when swimming was constructed. The model includes the effect of whole-body movement on thrust generation and could be used to predict propulsion generated by anguilliform swimmers at any swimming regime (any control parameter). The model set a foundation for establishment a complete model which can be used for selecting design (robot size, materials, *etc*.) and developing closed loop control for anguilliform swimming performance of soft robots.

### 1.4.3 Undulatory movement control and novel swimming strategy

Undulatory movement control for elongated body soft robots was proposed, in which pulse signal controls were employed to actuate pneumatic soft actuator along the body sequentially. Characteristics of the control signals were detailed investigated and described. The combination of a series of soft actuator structures and the proposed control strategy create smooth propagation waves from head to tail for forwarding swimming. Besides natural swimming mimicking, other swimming strategies were introduced as follows:

- Creating a new "C" shape swimming strategy by changing the air pipe connection order and increasing control shifting phase value resulting in much higher swimming velocity.
- Proposing swimming strategy with a partly passive body (passive tail and a half passive body) copying the situation of the partly damaged body.

These swimming strategies enlarge not only the understanding of the locomotion method of the soft robot community but also the working conditions of the elongated body soft robot for different kinds of tasks.

### 1.4.4 Miniature scale for enlarging applications

A miniature scale of elongated body soft robot with undulatory movement was introduced for self-propelled colonoscopy robots. The main contributions of this part are as follows:

- Proposed the preliminary design of a soft robot (3.5 times smaller than the original one) using a series of soft actuators which can be fabricated by molding technique resulting in the miniaturized size of the robot that is suitable for colonoscopy task.
- Investigated on control strategy, in which pulse control signals with suitable shifting phase are found out, to provide undulatory movement (creating smooth propagation waves along the robot body) with high locomotion velocity.

## 1.5 Thesis outline

After introducing the changes and challenges for the development of biomimetic soft robots and the main contribution of our research, the thesis will review the previous investigation on the bio-inspiration underwater soft robots in Chapter 2. The hydrodynamic force model for anguilliform locomotor is presented in Chapter 3. This chapter is also mentioned previous opinions about the physical aspects of the anguilliform swimming movement. Chapter 4 shows the design and fabrication process of the soft eel robot from the pneumatic actuator to the whole robot body. In Chapter 5, the control strategy of the soft eel robot is described. The bandwidth (working frequency range) of the fabricated soft actuator is determined in this chapter. Control strategies for creating propagation waves from the anterior to the posterior part of the robot are investigated. Then, swimming ability including swimming velocity and COT (cost of transport) of the proposed robot and thrust force model is evaluated and validated, respectively. A novel swimming strategy type "C" shape is also deployed and evaluated in this chapter. The other swimming strategy with a partly damaged body is introduced in Chapter 6. Two levels of this swimming strategy including 25 % and 50 % are investigated in two separate sections. Chapter 7 is dedicated to describing miniature idea, design, fabrication, and evaluation of a wave-like locomotion soft robot toward endoscope applications. A new air contribution approach is introduced to achieve efficient serpentine locomotion inland and constrain conditions. Design and molding fabrication techniques that are appropriate for miniature size are described in Section 7.3. The last section is for the experiment and validation of the self-propelled soft colonoscopy robot. To conclude whole our work in roughly three years in Chapter 8, we offer a final discussion by providing a summary of this thesis, contributions list, limitation aspect. Finally, possible future developments and applications are revealed.

# Chapter 2

# Previous research on underwater soft robot

Aquatic creatures can mainly be sorted into vertebrate and invertebrate groups. In this chapter, we only mention underwater soft locomotion robots, but soft mechanisms manipulating in water environments such as tentacles or grippers. Vertebrate animals will be categorized as short body robots (fishes) and elongated body robots (eels, lampreys). Based on this categorization, this chapter will be divided into two sections: short body soft robot and elongated body soft robot. Invertebrate inspired soft robots are sorted as short body soft robots.

## 2.1 Short body soft robots

### 2.1.1 Soft invertebrate robot

Besides walking, there are two main methods for invertebrate species to locomotion, which are propulsion created by flapping or propagation waves and jet propulsion created by quickly expelling water out of the body. Hou *et al*. [63] proposed a squid-like soft robot that can both swim and fly out of the water by jet propulsion. The soft quid robot was composed of a rigid body shell that is made of photosensitive resin material. The body covers and protects the pneumatic system, water supplement unit, and electrical control system inside. Soft morphing fins and arms are employed to increase lift force during flying by spreading and decreasing drag force by folding during swimming. A pneumatic system is used to push suddenly water from an inside tank to outside for propulsion and is also utilized to control fin and

arm movement. A demerit of this prototype is that it cannot generate propulsion continuously. After each push cycle, the robot needs to take time for the complex collection water process for the next cycle. Propulsion by flapping movement can tackle

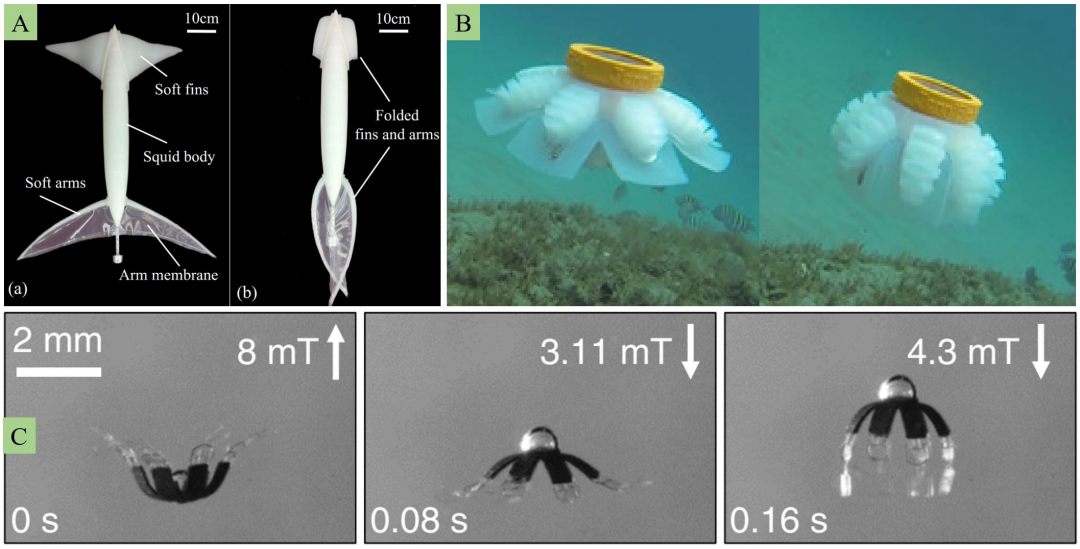


FIGURE 2.1: Typical examples of soft invertebrate robots. A - A soft morphing squid-like prototype used soft fin and arm driven by pneumatic source [63]. B - Soft robotic jellyfish with eight pneumatic network tentacle actuators [64]. C - An untethered miniature jellyfish-inspired robot constructed from magnetic composite elastomer actuated by external oscillating magnetic field [65].

this disadvantage. Jellyfish soft robots are typical for this swimming strategy [64], [66], [65]. Frame *et al*. developed a soft jellyfish constructed from eight segmented hydraulic actuators made by silicone rubber (Ecoflex). Two submersible impeller pumps were employed to actuate tentacles, each pump controlling the movement of four actuators. Another approach comes from Christianson *et al*., in which dielectric elastomer actuators (DEAs) are used to power a jellyfish-inspired soft robot. The untethered robot reaches an average velocity of 3.2 mm/s, and COT of 35 that is much better than a tethered robot (1.8 mm/s, and COT of 260) w.r.t. energy consumption. Requiring high voltage and low locomotion efficiency are the main disadvantages of the development. Recently, magnetic composite elastomer and external magnetic fields are utilized in soft robotics to develop untethered soft robots. Ren *et al*. proposed miniature soft body jellyfish-like swimming based on this technique. By oscillating external magnetic field (on, off, change magnetic field strength and direction), five swimming modes were discovered. Four robotics tasks that were suitable for the robot size and locomotion characteristics were realized by these modes.

### 2.1.2 Soft fish robot actuated by tendon/wire mechanism

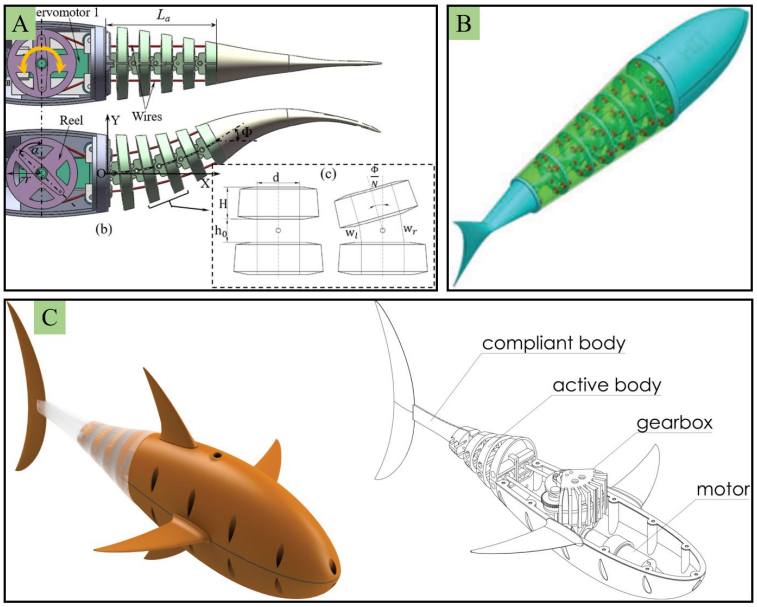


FIGURE 2.2: Soft fish robots actuated by tendon/wire mechanism. A - Robot fish with wire-driven active six links body and a soft compliant tail made of silicone [67]. B - Robotic fish body composed with a series of rigid segments linked with tensegrity [68]. C - High speed soft robotics fish used a simple DC motor to actuate an active body through tendons [69].

Tendon mechanisms are one of the most typical types of actuators that are utilized in soft robotics. They are considered as the lowest continuum level of soft actuator where most systems using the mechanism (using tendon to actuate rigid links) might be sorted as hyper-redundant. Zhong *et al*. [67] developed an untethered robot fish with tendon-driven activating six links active body and a long soft tail. The flapping movement of the fishtail was driven by one servo motor that was oscillated from 0.5 Hz to 3.5 Hz creating corresponding tail beat frequencies. The robot performed the highest speed of 2.15 BL/s (BL = 310 mm) at 3.0 Hz and can swim nearly 700 m in 40 min. A soft fish robot using tensegrity joints was introduced by Chen *et al*. [68]. Like other wire-driven actuators, a servo motor was used to actuate the flapping movement of the robot body. The difference comes from the elastic properties of tension elements. Although the platforms are rigid and discrete, this mechanism can achieve structural compliance. The robot was examined swimming ability from 1.0 Hz to 3.5 Hz. The results indicated that it reach the highest velocity at 0.7 BL/s (BL = 420 mm) at 1.72 Hz. A common characteristic of tendon-driven soft robot fish is that their tail beat amplitude can easily be controlled by controlling

motor rotation angle [54], [69], [70].

### 2.1.3 Soft fish robot actuated by pneumatic/hydraulic actuator

A typical and popular soft fish robot for this category is SoFi which is quite comprehensively developed to become the most stunning soft fish robot up to now. The first version was introduced in 2014 [34] when FEA (Fluidic Elastomer Actuator) actuated by pressurized air was employed to construct the main operating part of the robot. Two solenoid valves were used to control pressurization and depressurization of the actuator pair. The untethered robot can reach a velocity of 15 cm/s (0.44 BL/s) at 1.67 Hz. However, the robot only can perform 30 tail beats due to using an 8 g $CO_2$ pressure cartridge for actuation. To increase swimming time and reduce dependence

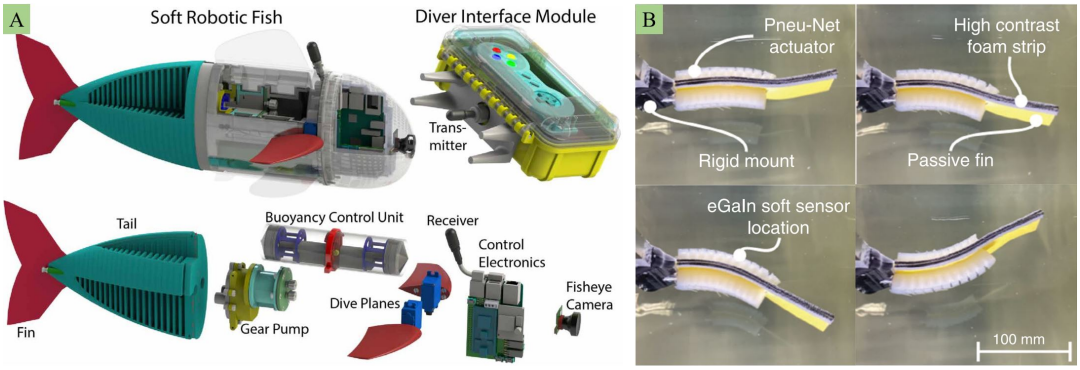


FIGURE 2.3: Soft robotic fishes use pneumatic/hydraulic actuators for body construction. A - Three dimensional swimming soft fish robot controlled by a miniaturized acoustic communication module for underwater life exploration [71]. B - Pneumatic soft fish robot body model integrated with a soft strain sensor for close loop control investigation [32].

on external air sources, a hydraulic pump was investigated to actuate the robot tail flapping movement [72]. An upgrade version was introduced with 3D swimming autonomously driven by hydraulic system [73]. The forwarding swimming speed of the robot was adjusted by controlling frequency and motor velocity. A soft robotic fish called SoFi with acoustically controlling was introduced in 2018 [71]. The robot can work underwater at a depth ranging from 0 to 18 m with an average velocity of 21.7 cm/s. The robot was intended to be used for oceanic exploration. Nonetheless, some existing limitations must be tackled including a short working period (40 min), requiring manual controlling, and short controlling range (0.9 m at ocean environment, and 2.8 m at swimming pool). Besides the research and development

of SoFi, some scientists have been investigated the working characteristic of a pair of soft pneumatic/hydraulic actuators for soft fish robot development. Jusufi *et al*. [32] investigated the undulatory movement of a pair of soft pneumatic actuators for a fish-inspired physical model. The model was tested at a flapping frequency ranging from 0.3 Hz to 1.2 Hz. The thrust force and midline kinematic measurement results indicated that the model is able to generate thrust force and could also enhance maneuverability by controlling the body shape changes such as inverting rapidly the body orientation. By adding soft strain sensing, Lin *et al*. [74] was introduced as a method to control the amplitude of flapping movement of a pair of the soft actuator. With the closed-loop control system, the tail tip can reach desired set point. The simple controller might allow the deployment of closed-loop control in an entirely soft robotic system.

### 2.1.4 Soft fish robot actuated by SMA or DEA

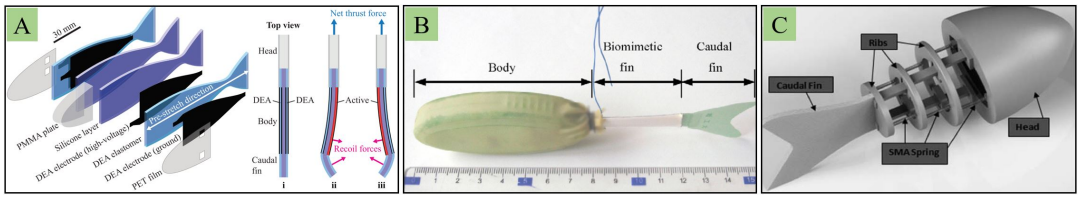


FIGURE 2.4: Soft fish robots use DEA/SMA for body construction. A - The robot consists of multi silicone layers wherein two DEAs are used in an antagonistic configuration, performing body caudal fin swimming strategy [75]. B - Micro-robot fish prototype with biomimetic fin made of SMA performing carangiform and subcarangiform swimming types [76]. C - Bionic robotic fish using SMA spring to actuate three links body [77].

Creating a sandwich structure of DEAs, Shitake *et al*. [75] developed a soft biomimetic fish robot. By applying a high voltage (5kV) and varying driving frequencies (from 0.25 Hz to 2.75 Hz), the robot performed three different flapping modes.The soft fish robot velocity reach a peak of 37.2 mm/s (0.25 BL/s) at 0.75 Hz. Meanwhile, thrust force has peaked at 1.25 Hz and 2.75 Hz. Shape memory alloy actuators also were utilized to develop soft bionic robotic fish [76], [77]. Wang *et al*. used SMA wire to construct the peduncle of an untethered micro-robot fish connecting the fish body and its caudal fin. Tail beat frequency was varied from 1 Hz to 11 Hz. The maximum velocity of forwarding swimming was 112 mm/s at 2.5 Hz. There was a special phenomenon with the robot when the swimming velocity decrease corresponding to

the increase of frequency from 2.5 Hz. Meanwhile, Muralidharan *et al*. [77] employ SMA spring to actuate three links of a posterior body of a tethered fish robot. A big soft caudal fin was used to increase thrust generation efficiency. Only two frequencies (0.5 Hz and 1.0 Hz) were examined. The robot has maximum velocity and thrust force of 25.5 mm/s (0.102 BL/s) and 0.39 N, respectively.

## 2.2 Elongated body soft robot

Most recent studies of soft aquatic robots have focused on systems inspired by short species such as fish, jellyfish, or squid as aforementioned in the previous section. Because of their complexity, few studies have focused on systems inspired by long species, which may account for the relatively slow development of elongated body fish-inspired soft robots. In the comparison with short species swimming in carangiform or thunniform, elongated body fish that performs anguilliform movement reveal a high propulsive efficiency due to their swimming strategy which could create zero wake-induced drag [78]. In addition, an anguilliform swimmer can swim forward and backward, which is useful for working in narrow and constrained environments, in which the other aquatic animals cannot turn around to change the swimming direction[19]. Consequently, despite the complex structure of elongated body robots, they are of interest in the development of promising search and surveillance devices with low-cost energy for narrow spaces such as shipwrecks and coral reefs.

In some works, shape memory alloy (SMA) was used to construct the robot body and create undulatory movement. Low *et al*. [79] was introduced a simple untethered robot that consists of three segments made of flexible polyurethane connecting two pieces of rigid acrylic ribs, which is actuated and controlled using shape memory alloy wires. The undulatory movement of the robot was created by sequential pulses. The swimming ability of the robot was examined at very low tail beat frequencies from 0.14 Hz to 0.34 Hz. The maximum forward swimming velocity of just over 8 mm/s was observed at 1/5.4 Hz and actuation current of 1200 mA. Basing on this research, Westphal *et at*. [80], [81] was proposed an untethered biomimetic robot based on the sea lamprey. Shape memory alloy actuators that were arranged in

five segments of a polyurethane strip were utilized to generate propagating flexion waves. The movement of the robot was controlled by an electronic nervous system (ENS) composed of networks of discrete-time map-based neurons and synapses that execute on a digital signal processing chip. The robot can perform both forward and backward swimming capability, and turning swimming as well. This research was quite interesting, however, the authors only focused on the development of the control system, thus, swimming strategies were not deeply investigated.

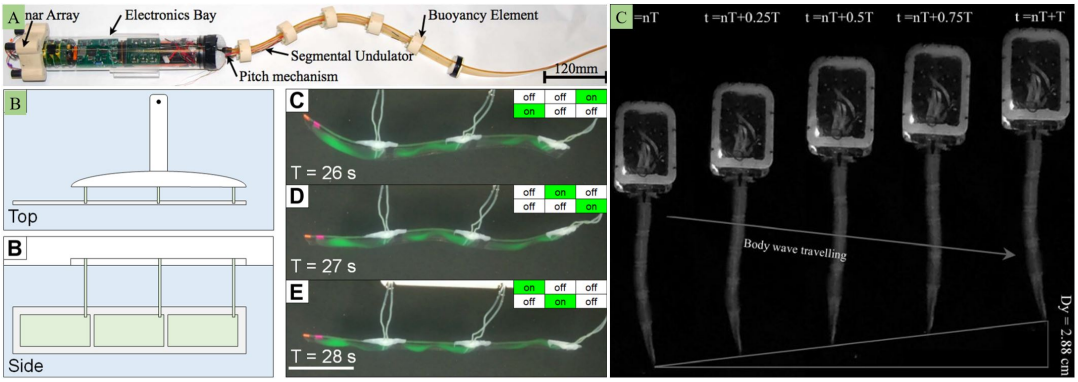


FIGURE 2.5: Elongated body soft robots. A - Lamprey robot constructed from five segment and actuated by nitinol actuator (a type of shape memory alloy) [80]. B - Untethered soft eel robot consist of three segments made of DEAs [50]. C - Eel-inspired robot with a four segments body constructed from fiber-reinforced soft fluidic elastomer actuators [82].

Dielectric elastomer actuators are also used for soft elongated body robot construction due to their large actuation strains, rapid response rate, low noise. To create flapping movement from DEAs, Christianson *et al*. [50] developed a fluid electrode DEA biomorph that consists of two separate fluid chambers enclosed by three layers of dielectric elastomer. This structure permits the actuator bending when supplying high voltage due to the compression of the actuated dielectric layer. Alternative actuation (on/off orderly) generates flapping movement of the soft actuator. Three designed actuators were used to construct the robot body with 22 mm in length. To produce propagation waves along the body, six fluid electrode chambers were actuated in sequence. At a driving frequency of 0.33 Hz, the robot can swim forward at a velocity of 1.9 mm/s. When increasing actuation frequency to 0.5 Hz, the robot speed gone up 12 %. There was no swimming evaluation at any different tail beat frequency. The main advantage of the translucent soft robot is that it consumed quite low energy at 1 W and it is noiseless. However, very high voltage is required

to operate (7.5 Kv) and a low bending angle of the actuator prohibits thrust force generation. This might prevent the development of an untethered soft robot.

Feng *et al*. [82] proposed a prototype of an eel-inspired robot using an array of fiber-reinforced soft fluidic elastomer actuators to construct the robot body. An array of four segments of FEAs were employed to construct the robot body. Each segment that was composed of two opposite bending units creating bidirectional bending FEA was driven by a gear fluidic pump controlled by Pulse Width Modulation (PWM) signal. To create wave generation, four pumps were actuated with a phase lag of T/4. The authors succeeded in the creation of propagating waves from the anterior to the posterior part of the robot body, and the robot was able to swim with the highest forwarding speed of 5.45 cm/s at a tail beat frequency of 0.67 Hz. The characteristic of an anguilliform swimmer is a large tail beat displacement that creates appreciable thrust that will be detailed described in the next chapter. However, such FEAs' structure seems to be quite "stiff" that require high actuation pressure to bend resulting in the low tail beat amplitude of the robot or requiring a high power pump. This claim is proved at the swimming performance of an untethered robot. Even using four pumps for four FEA segments, the robot was showed small tail beat amplitude with the supporting of a passive tail. Regarding the untethered design of the robot, four pumps, batteries, and control circuits were placed at the bulky head resulting in the disproportion between the head and the remains. This may negatively affect the swimming performance of the robot due to the increment of drag force. It is also a challenge toward a totally untethered design of soft, elongated-body fish robots.

The brief review on soft bio-inspired robots indicated that scientists put much effort into the development of soft aquatic robots from both quality and quantity. Various types of soft actuators with various designs have been used and introduced for the creation of many kinds of soft biomimetic robots. The researches have been put foundations for the soft robotics community, also, revealed demerits and given the change to develop complete and more efficient swimming soft robots. The development might come from all soft robot aspects: soft actuator design and working principle, modeling, control, and mechanical structure design.

**Chapter 2 conclusions**

The chapter provided an overview of how aquatic soft robots, whichwere categorized into short and long (elongated) body fish-inspired, were constructed from various types of soft actuators including SMA, wire driven, DEAs, and pneumatic/hydraulic actuators. Also, the control strategies and locomotion efficiencies of those robots were revealed. We pay special attention to soft elongated body robots which have only been studied at very early stages and have achieved very limited results on both structure and control strategies. They supplied a foundation for us to come up with the idea of a soft eel-inspired robot that can improve swimming ability, can perform novel swimming modes with high efficiency and is also scalable for other applications.

# Chapter 3

# Thrust force modeling

Modeling is one of the most important issues in robots development. The mathematical model represents the dynamic behavior of an object in relation to the surrounding environment (*i.e.* interact with ambient materials or nearby object). In robotics, the model is used to predict the physical behaviors of a machine depending on physical areas (force, heat, light, electric, magnetic, sound) that it describes, also, the model might put a foundation to establish control laws.

Aquatic animals swim by moving their body/ body parts to interact with ambient fluid to create balance force and thrust force. One of the physical behavior that is usually examined to evaluate the swimming performance of aquatic species is wake structure. Wake is a staggering array of vortices rings that are generated as the tail moves back and forth. Together with Reynolds number and (Re) and Strauhal number (St) form a set of parameters is used to evaluate the swimming efficiency of natural swimming animals. Nonetheless, they are only employed for aquatic bio-inspired robots at the final stage when the robots are finished for both structure and surface morphology (*i.e.* skin to reduce drag). At the dawn of such researches, body movement (*i.e.* flapping, wave generating), swimming velocity, cost of transport (COT), thrust generation are of interest for evaluation instead of the set of three parameters.

## 3.1 Review on thrust force model of fish robot

### 3.1.1 Large-amplitude elongated body theory of fish locomotion

In 1971, Sir Jame Lighthill proposed Elongated Body Theory (EBT) [83] which assumes that propulsion creating from reactive forces between the body surface and the surrounding fluid. Also, EBT assumes that the body is slender, in which cross section is thin and very small compare to the body length. A Lagragian coordinate $a$, which take value from 0 to $l$ (the length of the fish), was used. The body was considered as an inextensible line consisting of points $P(x(a,t), y(a,t))$. Reactive force on the body can be calculated as:

$$F_{thrust} = \left[ mv\frac{\partial y(a,t)}{\partial t} + \frac{1}{2}mv^2\frac{\partial x(a,t)}{\partial a} \right] - \frac{d}{dt}\int_0^L mv\frac{\partial y(a,t)}{\partial a}da$$

where $v$ is perpendicular velocity component of point $P$, and is calculated as:

$$v = \frac{\partial x(a,t)}{\partial t}\frac{\partial y(a,t)}{\partial a} - \frac{\partial y(a,t)}{\partial t}.\frac{\partial x(a,t)}{\partial a} + U\frac{\partial y(a,t)}{\partial a}$$

U stands for forward velocity of the body. EBT is used in some researches to predict thrust generation for both short and elongated body robots. Li *et al*. [84] developed a sub-carangiform robotic fish with three links posterior body driven by three motors and a passive caudal fin. Thrust force was evaluated based on Lighthill's theory and the variation angle of three joints. A dynamic model was established and used for control law. Swimming of robotic fish verifies that the bottom-level motion control and the controller are accurate and robust. In this research, there was no thrust measurement for validation of the proposed thrust formula. Wen *et al*. [85] used EBT to provide a dynamic model for the robot body with a number of planar or 3-D motions under inviscid conditions. Combining with kinematic modeling of body and caudal fin, caudal fin thrust force model, and drag force model, the authors built a force balance equation, from which the velocity of the robot fish can be solved. Comparison between simulation (using the established model) and experiment proved the adequacy of the model that then was used to come up with the idea of a fuzzy control method. Meanwhile, Webb *et al*. [86] used EBT model to predict thrust force generation and compared these data with experimental data. The results indicated

that there were a large different between two data set and further improvements to the EBT model are required to model the hydrodynamic forces in underwater undulatory swimming.

### 3.1.2 Euler-Lagrange dynamic formulation and others analytical approaches

A nonlinear, dynamic, carangiform locomotion model that was derived by using a planar four-link model was introduced by Pichet Suebsaiprom and Chun-Liang Lin [87]. The Euler-Lagrange dynamic formulation was employed to describe total force (hydrodynamic force included) on link $i$. The dynamic fish robot model was achieved by using:

$$M(\boldsymbol{\theta_i})\ddot{\boldsymbol{\theta}}_{\boldsymbol{i}} + C(\boldsymbol{\theta_i}, \dot{\boldsymbol{\theta}}_{\boldsymbol{i}})\dot{\boldsymbol{\theta}}_{\boldsymbol{i}}^{\,2} + B\dot{\boldsymbol{\theta}}_{\boldsymbol{i}} + K\boldsymbol{\theta_i} = \boldsymbol{F_i}$$

where $M(\boldsymbol{\theta_i})$ is a matrix of moment of initial, $C(\boldsymbol{\theta_i}\dot{\boldsymbol{\theta}}_{\boldsymbol{i}})$ is a Coriolis matrix, B is matrix of damping coefficient, K is matrix of spring constant. $\boldsymbol{F_i}$ is total exerted force on the link $i$ including hydrodynamic force. Theoretical control method for carangiform swimming fish was built based on this approach.

Four links posterior body fish robot, which mimics carangiform motion, was proposed by Korkmaz *et al*. [88]. A simple propulsive model was introduced, in which body movement was modeled as sinusoidal waves with continuously increasing amplitude from head to tail. Experimental measurements, from which the robot performed tail beat flapping frequency up to 2.5 Hz, verified partially the capability of the model in the prototype of the four-link fish robot. Nonetheless, only the movement kinematics of the robot was examined so that a simple propulsive model is achieved in experimental investigation. For soft robotic fish, Lin *et al*. [74] treated the soft robot fish body as a chain of rigid elements connected by hinges with nonlinear stiffness functions. Slender body theory is used to apply point load on individual elements for describing hydrodynamic forces. The model, then, was implemented in Matlab/Simulink and was used as one of the input parameters for actuator motion prediction. The comparison between model prediction and experimental data showed a similar movement direction (flapping to the left or right) but a difference

in the flapping posture especially in water. This might come from the hydrodynamic force model.

### 3.1.3 Navier-Stockes equation

The Naviver-Stockes equation govern the motion of fluids and can be seen as Newton's second law of motion for fluids. In the case of a compressible Newtonian fluid, it can be expressed as

$$\rho\left[\frac{\partial u}{\partial t}+u\nabla u\right]=-\nabla p+\mu\nabla^2 u+F$$

where $u$ is fluid velocity, $p$ is fluid pressure, $\mu$ is fluid dynamic viscosity, and $F$ is external force. The equation usually use for simulation. Kern *et al*. [89] employed the Navier-Stokes equation solving by commercial sofware STAR-CV to get the information of 3-D fluid-body interaction for optimization of anguilliform swimming. Meanwhile, Feng *et al*. [90] utilized a open source tool box OpenFOAM for solving the N-S equation to simulate self-propelled anguilliform swimming. The solver is modeled 2-D information of an anguilliform swimmer and also can compute force on each individual immersed boundary interface processing

In general, researchers currently employ two approaches for fish hydrodynamic modeling including numerical and analytical tools. Numerical methods are systematic in approach but arduous as it necessitates solving complex Navier-Stokes equations, whereas analytical methods are direct and realistic [91]. Regarding analytical methods, resistive theory, waving plate theory, Lighthill's theory, and airfoil theory have been usually employed. The resistive theory assumes that fluid force is composed of longitudinal skin friction force and lateral drag forces. The main drawback of this theory comes from the neglecting of inertial forces. Waving plate theory considers fish as undulating of a 2-D plate with a specific height. Meanwhile, Lighthill's elongated body theory (EBT) describes the dynamic forces experienced by a fish in a horizontal plane and is widely used for dynamic modeling. However, EBT is a simple model and neglects many effects [23], [92] and some of them could enable thrust generation along the length of a body of an elongated body fish. The impositions of the aforementioned measures for hydrodynamic force models for conventional

robot fishes and soft robot fish yield quite different results, in which rigid aquatic robots revealed compatible results between theoretical and practical data but a soft aquatic robot. The conclusion raises a requirement for further investigation on hydrodynamic models that are more compatible with a soft robot.

## 3.2 Thrust force model for anguilliform movement

Previous researches on aquatic animals have played an important role in the development of bioinspired robots as detailed analysis in Chapter 1. Analysis of movement strategies of underwater species has given researchers ideas to develop robot structures and their control that mimic those of natural ones. The functions and movement methods of fish body parts such as the tail and fins have been investigated [19]. Additionally, the reaction forces of ambient fluid on swimming fishes including pitch, yaw, and roll have been also defined [93]. There have been studies of elongated body fishes such as eel and lamprey that use entire muscles along their body to create a transport wave from head to tail with continuously increasing amplitude [22], [23]. Webb [94] hypothesized that in undulatory locomotors thrust is generated by two propulsive elements locating near their head and tail. When the body wave passes from head to tail, the elements move laterally and exert force on the nearby water. Due to the inclined posture of the elements, the reactive force of the nearby water pushes the anguilliform swimmers moving forward. Meanwhile, Gemmell *et al*. [22] indicated that instead of pushing against the ambient water, anguilliform swimmers pull themselves through water via suction which is created by the dominance of negative pressure over positive pressure resulting from wave propagation from anterior to posterior body part.

The movement of an aquatic animal's body has the purpose of interacting with ambient fluid to generate propulsion for balance and swimming. In this section, reaction forces between a swimming eel and surrounding water are examined to build a hydrodynamic forces model. The model can be used to predict the propulsion of an elongated fish robot based on design and control features. This may be useful for selecting design (robot size, materials, *etc*,.) and control strategies to make a suitable robot model.

### 3.2.1 Hydrodynamic forces acting on a moving object in fluid

Any object in a fluid is always subjected to gravity force and buoyant force. If the object moves at a constant velocity, it will also be subjected to drag force as shown in Fig. 3.1. Drag force can be calculated as:

$$f_{drag} = \frac{1}{2} C_D \rho s v^2, \tag{3.1}$$

where: $C_D$ is the drag coefficient associated with a particular surface area, $\rho$ is fluid density, $s$ is reference surface area and $v$ is object velocity [95].

For movement at variable velocities $v(t)$, added mass should be taken into account for the total reaction force on the body [96]. In this case, total reaction force at the moving direction can be expressed as:

$$f = f_{drag} - m\dot{v}. \tag{3.2}$$

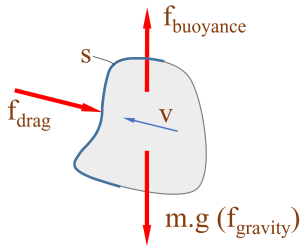


FIGURE 3.1: Forces exerted on a moving body in fluid.

### 3.2.2 Hydrodynamic forces acting on a swimming eel

An eel swims by repetitively bending sections of its whole body in a sinusoidal wave from head to tail [94]. Fig. 3.2 (A) shows the dorsal view of a swimming eel at the *maximum bending stage* of her body. A cartesian coordinate system is assigned with the origin point $O$ set at the location of the eel head for the construction of the eel's movement model. The midline, along the path of the eel's spine, describes a sine curve with increment in amplitude [22], [23]. Expression $Ae^{\beta x}$ with $\beta > 0$ is used to describe increase in amplitude along the $x$ axis, and $\sin\left(\frac{2\pi}{\lambda}x - 2\pi f t\right)$ is characterized as periodic variation of amplitude $A$ with time $t$ and the movement of

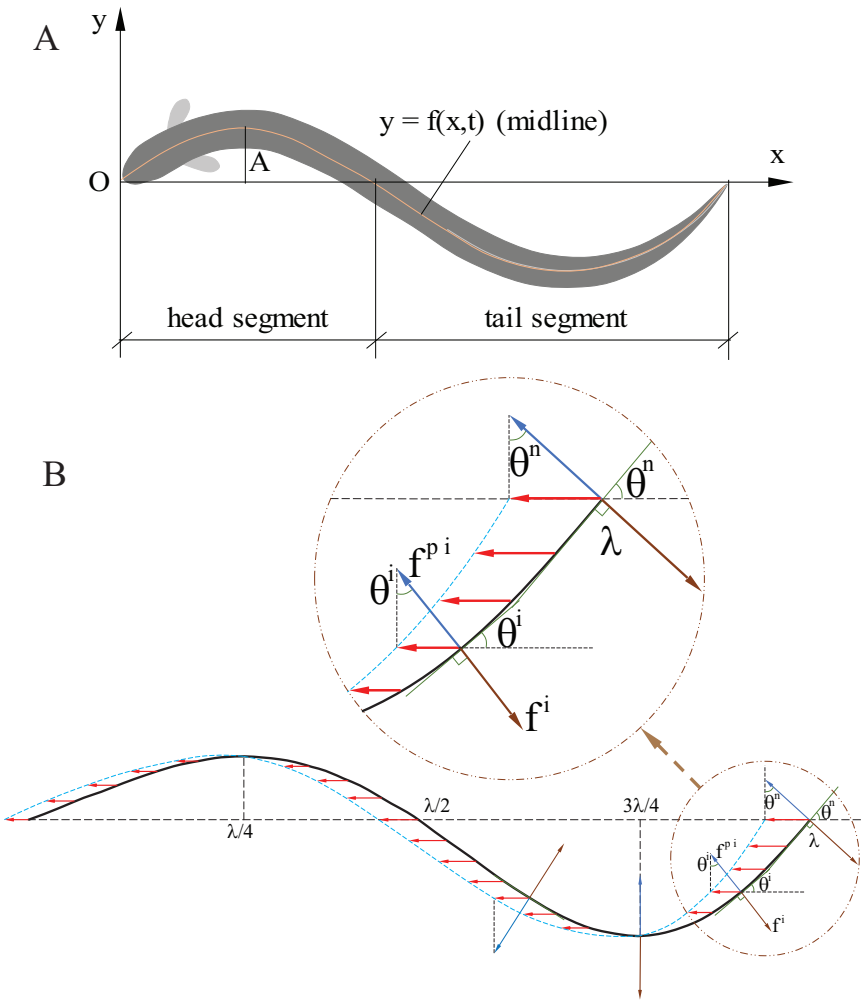


FIGURE 3.2: Reaction forces exerted on an eel body. (A) Model of a swimming eel at her maximum bending posture, which is in the shape of a sinusoidal wave with increasing amplitude from head to tail that conforms to Eq.(3). (B) Schematic distribution of reaction forces along the eel's spine on ambient fluid with maximum bending of her body.

each point $P(x, y)$ on the corresponding sine wave. Thus, movement of the midline is a function of position $x$ and time $t$, and is described as followed:

$$y = f(x,t) = Ae^{\beta x} \sin\left(\frac{2\pi}{\lambda}x - 2\pi f t\right), \tag{3.3}$$

where: $A$ is the initial amplitude of the curve. $\beta$ is the increment coefficient which characterizes rise of amplitude from head to tail. $\lambda$ is the wavelength and $f$ is the tail beat frequency.

Velocity and acceleration can be calculated as Eq. (3.4) and Eq. (3.5), respectively.

$$v(x,t) = \frac{\partial y(x,t)}{\partial t} = -2A\pi f e^{\beta x} \cos\left(\frac{2\pi}{\lambda}x - 2\pi f t\right), \tag{3.4}$$

$$a(x,t) = \frac{\partial^2 y(x,t)}{\partial t^2} = 4A\pi^2 f^2 e^{\beta x} \sin\left(\frac{2\pi}{\lambda}x - 2\pi f t\right). \tag{3.5}$$

The eel body interacts with ambient fluid to generate propulsion in order to move forward. To examine the total thrust force created by the whole body, the hydrodynamic force at points on the midline is considered. Fig. 3.2 (B) shows the hydrodynamic forces $\boldsymbol{f}^i$ acting at each point along the midline. These forces are divided into two components. The vertical component is mainly used to form vortex according to [23], which is not considered in this research. Instead, horizontal component $\boldsymbol{f}^i_{\boldsymbol{Th}}$, or thrust force, which involves forward swimming of the eel is examined. The direction of $\boldsymbol{f}^i_{\boldsymbol{Th}}$ at each point depends on its movement direction. Based on Eq. (3.4), the velocities of body sections from $x = 0$ to $\lambda/4$ and from $x = 3\lambda/4$ to $\lambda$ are negative, while the velocities of the others are positive. This means that the body sections from $x = 0$ to $\lambda/4$ and from $x = 3\lambda/4$ to $\lambda$ are traveling downward, while the others are traveling upward. Considering a point $i$ at the tail segment, since the tail segment is traveling downward, action force $\boldsymbol{f}^i$ (brown colored vector) of the body at the point $i$ on fluid has the direction as shown in Fig. 3.2 (B). Reaction force $\boldsymbol{f}^{pi}$ (blue colored vector) has the opposite direction. Similarly, the reaction force spectrum is constructed as followed:

$$f^i_{Th} = f^{pi} sin\theta^i, \tag{3.6}$$

where: $f^{pi}$ is the reactive force at any point along the midline, $\theta^i$ is the angle between $\boldsymbol{f}^{\boldsymbol{pi}}$ and horizontal direction at the point $i$. Based on the geometrical relationship as shown in the inset illustration of Fig. 3.2 (B), angle $\theta^i$ is equal to that of tangential direction and movement direction at the considered point. Therefore, angle $\theta^i$ can be calculated based on followed equation:

$$\tan\theta = \frac{\partial y(x,t)}{\partial x} = A\beta e^{\beta x}\sin\left(\frac{2\pi}{\lambda}x - 2\pi f t\right) + A\frac{2\pi}{\lambda}e^{\beta x}\cos\left(\frac{2\pi}{\lambda}x - 2\pi f t\right). \tag{3.7}$$

From Eq. (3.1) and Eq. (3.4), drag force at time $t$ can be calculated as:

$$\begin{aligned} F_{drag}(t) &= 2\rho C_D S A^2\pi^2 f^2 \int_0^{\lambda} e^{2\beta x}\cos^2\left(\frac{2\pi}{\lambda}x - 2\pi f t\right) dx \\ &= \rho C_D S A^2\pi^2 f^2 \frac{(e^{2\beta\lambda}-1)[4\pi^2 + \beta^2\lambda^2 + \beta^2\lambda^2\cos(4\pi f t) - 2\beta\lambda\sin(4\pi f t)]}{4\beta(\beta^2\lambda^2 + 4\pi^2)} \end{aligned} \tag{3.8}$$

Eq. (3.8) indicated that drag force reaches its peak as $[\beta^2\lambda^2\cos(4\pi ft) - 2\beta\lambda\sin(4\pi ft)]$ is maximum. This equivalent to:

$$\begin{cases} \cos(4\pi ft) = 1 \\ \sin(4\pi ft) = 0 \end{cases} \Leftrightarrow 4\pi ft = 2n\pi \Leftrightarrow t = \frac{n}{2f}(n \in N) \qquad (*)$$

or

$$\begin{cases} \cos(4\pi ft) = 0 \\ \sin(4\pi ft) = -1 \end{cases} \Leftrightarrow 4\pi ft = \frac{2n+1}{2}\pi \Leftrightarrow t = \frac{2n+1}{8f}(n \in N) \qquad (**)$$

To create comparable data sets between theoretical data and experimental data, hypothetical conditions used to build a thrust model must be as similar as possible to the experimental setup used to measure thrust force. Regarding measuring thrust force, the eel robot body will be fixed at the very first point of its head, which is detailed later in Section 4.3. Replacing alternatively $t$ from (*) and (**) to Eq. (3.3), it is sufficient to conclude that condition (**) does not meet the requirement of the robot that is fixed at the very first point ( *i.e.*, $x = 0$ then $y = 0$) since in this case if $x = 0$ then $y = 1$. Therefore, the condition (*) was chosen. Choose $n = 0$ then $t = 0$. Replacing $t = 0$ to Eq. (3.3), we are able to obtain an equation corresponding to the maximum bending stage of the eel body. At this stage, the resulting velocity and acceleration can be calculated as:

$$v(x,0) = -2A\pi f e^{\beta x}\cos\left(\frac{2\pi}{\lambda}x\right), \qquad (3.9)$$

$$a(x,0) = 4A\pi^2 f^2 e^{\beta x}\sin\left(\frac{2\pi}{\lambda}x\right). \qquad (3.10)$$

From Eq. (3.1) and Eq. (3.9), the equation for calculating drag force can be written as:

$$f_{drag} = \frac{1}{2}C_D\rho B4A^2\pi^2 f^2 e^{2\beta x}\cos^2\left(\frac{2\pi}{\lambda}x\right)dl, \qquad (3.11)$$

where: $B$ is the diameter of eel body cross section and $dl$ which is a derivation of the body length can be calculated as:

$$dl = \sqrt{dx^2 + dy^2} = \sqrt{1 + \left(\frac{dy}{dx}\right)^2} dx = \sqrt{1 + \dot{y}_x^2} dx$$
$$= \sqrt{1 + \left(A\beta e^{\beta x} \sin\left(\frac{2\pi}{\lambda}x\right) + A\frac{2\pi}{\lambda} e^{\beta x} \cos\left(\frac{2\pi}{\lambda}x\right)\right)^2} dx. \quad (3.12)$$

Deviation of the added mass component caused by bending with variation of velocity can be expressed as:

$$f_a = \frac{1}{4}\pi\rho B^2 4A\pi^2 f^2 e^{\beta x} \sin\left(\frac{2\pi}{\lambda}x\right) dx, \quad (3.13)$$

where $\frac{1}{4}\pi\rho B^2$ is the virtual mass. From Eq. (3.6), Eq. (3.11) and Eq. (3.13), the hydrodynamic forces on point $i$ can be calculated as:

$$f_{Th}^i = 2C_D\rho B A^2\pi^2 f^2 e^{2\beta x} \cos^2\left(\frac{2\pi}{\lambda}x\right) dl \sin\theta + AB^2\pi^3\rho f^2 e^{\beta x} \sin\left(\frac{2\pi}{\lambda}x\right) \sin\theta dx. \quad (3.14)$$

Thrust force which is created by movement of the whole robot body can be calculated as :

$$F_{thrust} = 2C_D\rho B A^2\pi^2 f^2 \int_0^\lambda \left\{ (e^{2\beta x} \cos^2\left(\frac{2\pi}{\lambda}x\right) \sin\theta \right.$$
$$\left. \sqrt{1 + \left(A\beta e^{\beta x} \sin\left(\frac{2\pi}{\lambda}x\right) + A\frac{2\pi}{\lambda} e^{\beta x} \cos\left(\frac{2\pi}{\lambda}x\right)\right)^2} \right\} dx$$
$$+ AB^2\pi^3\rho f^2 \int_0^\lambda e^{\beta x} \sin\left(\frac{2\pi}{\lambda}x\right) \sin\theta dx \quad (3.15)$$

Eq. (3.15) can be used to calculate generated thrust force by eel performing movement for swimming but cannot move forward (fixed at the very first point of their head). This condition is similar to the experimental setup for thrust force measurement in Section 5.2. This will create comparable data between theoretical calculation and practical measurement. In Eq. (3.15), $C_D$ can be determined approximately by object shape, in the present case, the eel robot body may be regarded as a cylinder moving in a turbulent flow. Parameters $A$, $B$, $\beta$, and $\lambda$ depend on properties of the

eel body including size and stiffness, meaning eels with different body characteristics have different swimming abilities (generated thrust force, swimming velocity). Therefore, similar individuals were selected to analyze swimming ability and build a dataset for a particular eel [22]. With regard to our eel-inspired robot, parameters had to be determined to calculate thrust forces. This required experiments at specific frequencies chosen from a range of operating frequencies.

Variation of swimming parameters ($A$, $B$, $\beta$, $f$ and $\lambda$) affects the value of thrust force. With respect to $B$ and $f$, Eq. (3.15) can be written as:

$$F_{thust} = Bf^2P(A,\beta,\lambda) + B^2f^2Q(A,\beta,\lambda),$$

where $P$ and $Q$ represent expressions depending on $A$, $\beta$, and $\lambda$. Fig. 3.2 (B) indicated that the vector thrust force at any point on the eel body orient a positive direction implying that the first component in Eq. (3.15) relating to the drag force is positive. Meanwhile, any point in the eel body in this case tends to travel from the farthest points to the equilibrium position as described when determining the moving direction of the eel body. The acceleration, therefore, is increasing resulting in the positive value of the second component in Eq. (3.15). As a result, $P$ and $Q$ are positive. Therefore, an increase in the two parameters ($B$ and $f$) results in increased propulsion. Other parameters relating to the effects of swimming posture of the eel on thrust force require a more detailed analysis based on body shape formation because $A$, $\beta$, and $\lambda$ are interdependent. For example, the increase in $A$ and $\beta$ leads to the decrease in $\lambda$ and vice versa. In other words, these parameters must be measured in certain working regimes, then by using Eq. (3.15), the influence of each parameter on the thrust force can be estimated.

**Chapter 3 conclusions**

We proposed a model to predict the thrust force generation of an anguilliform swimmer. The model was built based on the continuum approach, in which the reactive force at any point along the mid-line was determined. In addition, the model might bring in an approach for estimating the drag force coefficient of anguilliform locomotion, even when it is difficult to set up an experiment and conduct measurement due

to the complex motion of the object. The limitation of the model is that it is not taken into account the body morphology which strongly affects swimming efficiency.

# Chapter 4

# Anguilliform swimmer soft robot design and fabrication

Based on the reviews on soft actuators in Chapter 1, we realize that a segmented and chambered actuator is suitable for the construction of bio-inspired anguilliform swimmers, which perform a large tail beat amplitude, due to easily bending with a large curvature at low supplying air pressure. Research on designing soft actuators is one of the most interesting topics in the soft robotic community. Soft robots have been designed for different purposes and tasks that require various body shapes and sizes and have either incorporated previously design actuators or newly designed actuators to enable the performance of novel tasks. This chapter aims to tackle the following issues:

- Designing a soft pneumatic actuator that is suitable for the construction of the soft eel robot body.
- Designing molds for fabricating the designed soft actuator.
- Proposed the design of the robot body that can perform the anguilliform movement.
- Proposed fabrication process of the soft actuators.
- Fabricated the soft eel robot body using a series of the fabricated soft actuator.

## 4.1 Soft actuator design

### 4.1.1 Design selection by simulation

As mentioned above, elongated body fish swim by successively undulating their body in the shape of a sinusoidal wave from head to tail. To mimic this swimming style, a robot would require a combination of actuators to bend its body left then right when pressurized sequentially. Imitating an eel body cross-section (circular) for better hydrodynamic performance, semi-cylinder actuators were developed. The proposed actuators share the segmented, chambered structure with PneuNets [31]. In this research, two inside structures relating to the air connection method between chambers were examined. These detailed designs that were finished on SolidWorks (Dassault Systems) are shown in Fig. 4.1. The difference between the two designs comes from the dimensions of air connecting channels, in which the first design (Fig. 4.1 (A)) use a wide channel of 21 mm in width that might contribute to transporting pressurized air to all chambers quickly and easily, meanwhile, the second one (Fig. 4.1 (B)) use a narrow channel of 5 mm in width that might contribute to largely deforming of the actuator due to the constrain between chamber bottoms and a base plate.

Abaqus/CAE (Dassault Systémes Simulia Corp., 2018) was employed to determine the better design. The usage of the simulation tool saved time for choosing a suitable actuator. A pressure of 0.03 MPa was supplied to two designs. Based on their behaviors, the better one was chosen. Silicone rubber brand Dragon skin 20 (Smooth-on, USA) was intended to use for actuator fabrication. Dragon skin 20 is a non-linear, hyper-elastic material, thus, it can be represented using the Yeoh model. The parameters for Yeoh's model are shown in Table. 4.1 below:

TABLE 4.1: Coefficients for Yeoh model Dragon skin 20

| Parameters/ Coefficients | Mass density (tonne.$mm^{-3}$) | Constant C10 (MPa) | Constant C20 (MPa) | Constant C30 (MPa) |
|---|---|---|---|---|
| Value | $1028.10^{-12}$ | 0.04378 | 0.005472 | $-2.10^{-7}$ |

Simulation results are shown in Fig. 4.2 (A) and (B) for the wide and narrow connecting channels, respectively. In the former one, the soft actuator did not bend

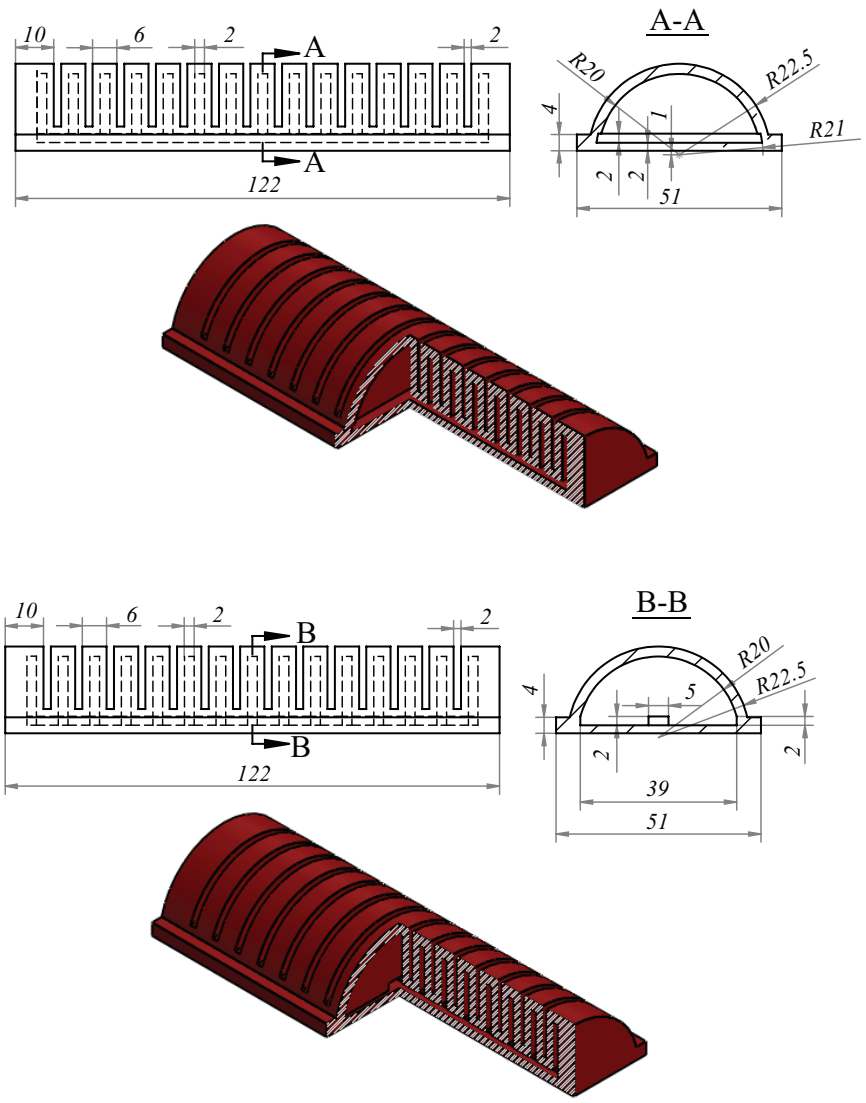


FIGURE 4.1: Two proposed design of semi cylindrical soft actuator. A - The design with a wide air connecting channel. B - The design with a narrow connecting channel.

in the same curvature radius at any actuator's section. The wide connecting channel created a large deformation area at the base plate which concentrated stress at this side. This inhibited deformation at segmented sections which play the main role in bending. However, change in the narrowing connecting channel achieved good results as shown in Fig. 4.2 (B). In this design, pressurized, stress accumulated at segmented, chambered section resulting in the actuator bending in a perfect curve shape. Therefore, the latter design was chosen to mimic muscle in the eel robot. The bending ability of a pair of soft actuators that plays as a muscle unit was also examined. Fig. 4.3 shows a simulation of two actuators in two contrasting situations

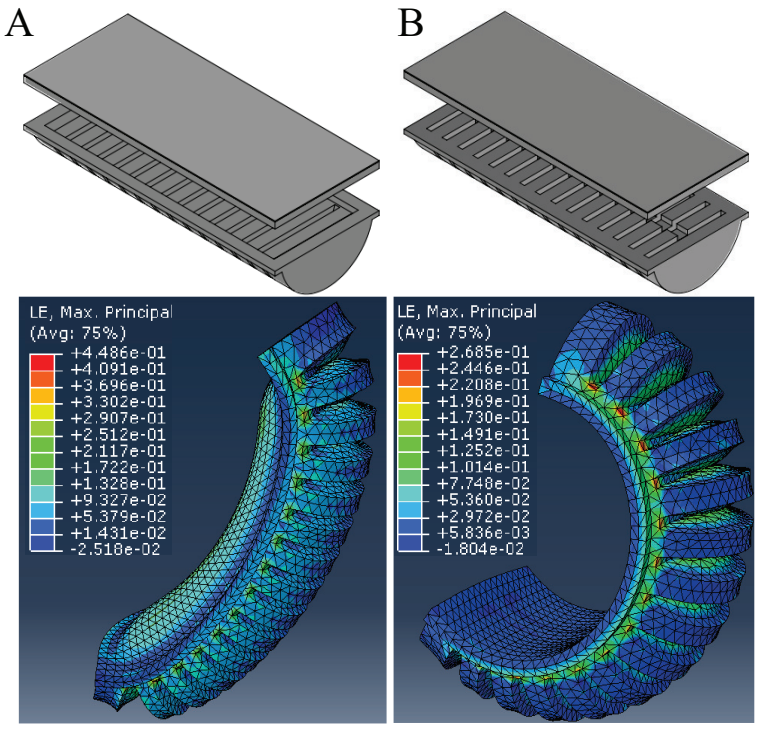


FIGURE 4.2: Design and simulation of soft actuators' pressurized situation. A - The soft actuator with a wide air connecting channel. B - The soft actuator with a narrow connecting channel. The inset legend shows results in stress components

- pressurized and unpressurized. The simulation result indicated that the combination of the two soft actuators with a suitable sequence of pressure alternation would induce undulatory movement. This is the groundwork to design the soft robotic eel's body.

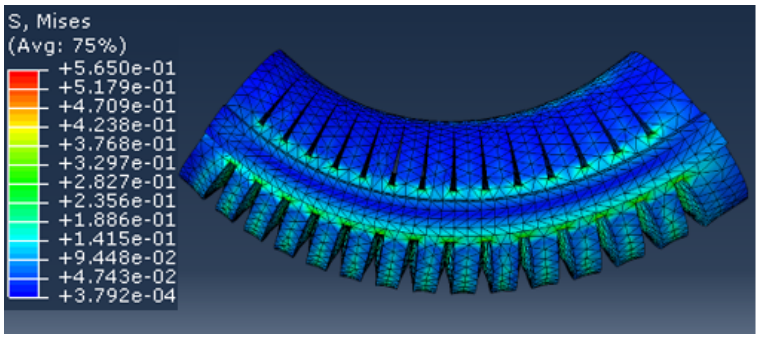


FIGURE 4.3: Simulation of a pair of actuators (downer actuator in pressurized stage of 0.06 MPa). The inset legend shows results in stress components

### 4.1.2 Mold design

Silicone pouring molds were designed based on the actuator's design. Due to the complex structure, to make it easy for molding, the actuator was divided into two

parts: base plate and segmented part as shown in Fig. 4.2 (B). SolidWorks (Dassault Systems) was utilized again to create mold design for the soft pneumatic actuator parts that were used as cores for mold parts generation. Fig. 4.4 (A) and (B) show the detailed designs of two main parts of the mold for the segmented part of the actuator. For creating a hole on the part for air pipe connecting, a pin was employed as shown in Fig. 4.4 (D). Detail design of the base plate mold is shown in Fig. 4.4 (C).

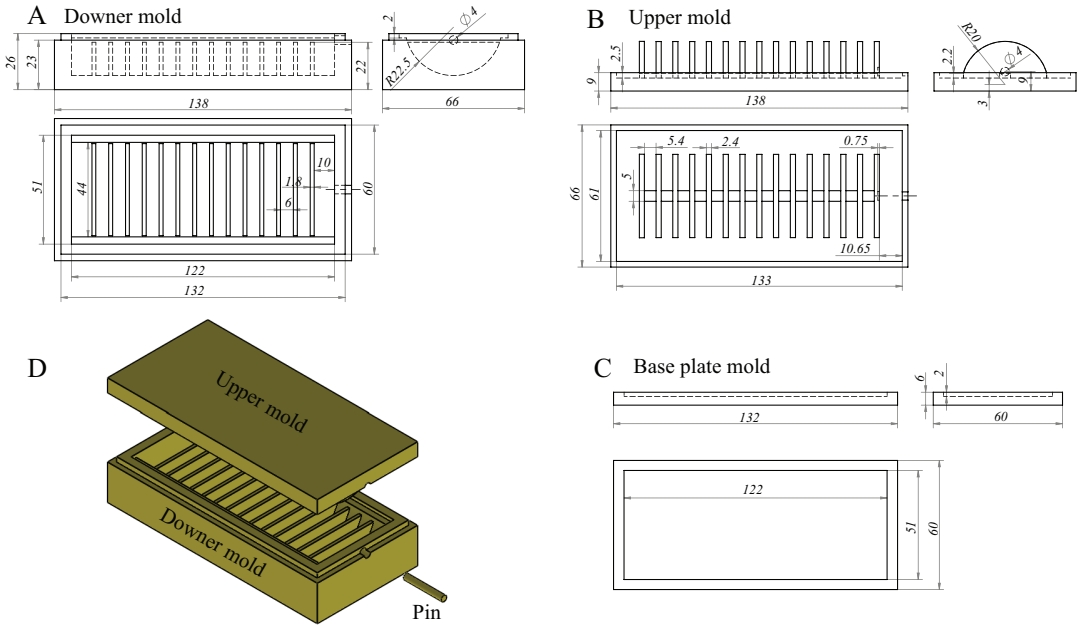


FIGURE 4.4: Silicone pouring molds for the soft actuator. A - Downer mold for segmented part. B - Upper mold for segmented part. C - Mold for base plate. D - Exploded view of the mold set for segmented part. Pin is used to make hole for air pipe connection.

## 4.2 Eel soft robot design

To create propagation waves from the anterior to the posterior body, a series of soft pneumatic actuators are employed for the robot body construction. Fig. 4.5 shows the preliminary design of a soft robot eel comprising three main parts: the head contains the control system; the body is constructed from soft actuators that are controlled to generate eel-like movement, and the spine is made of a non-stretch flexible polymer material. In the swimming performance evaluation stage, the constructed robot body is similar to one illustrated in Fig. 4.5, except it is tethered. The design of the soft eel robot body is shown in Fig. 4.6

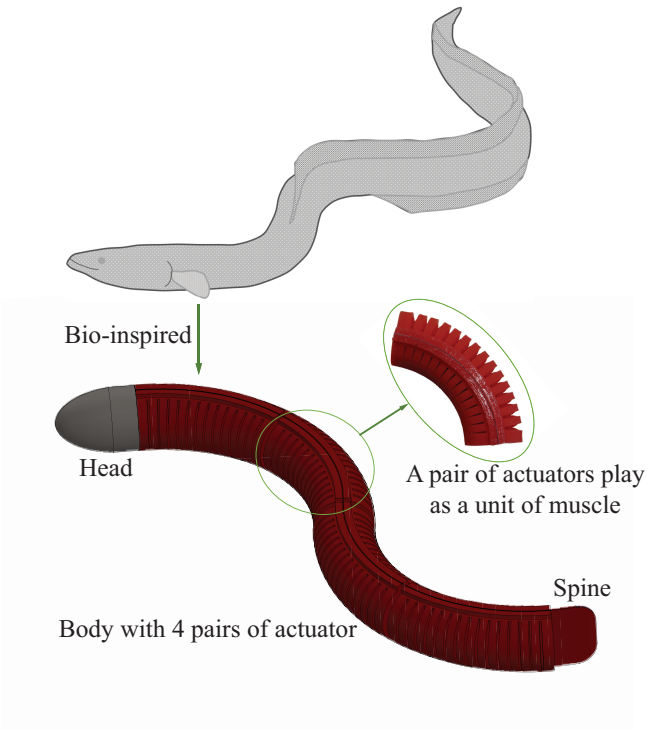


FIGURE 4.5: An ultimate design of an eel inspired robot that employs a series of soft actuators for accomplishment of anguilliform swimming performance.

Previous reports on soft robots with undulatory movement ([50], [82], [97]) indicated three or four segments were required for efficient generation of sine-waveform of the body. Nonetheless, the increase in the number of segments leads to more independent controls, resulting in difficulties in the design of an untethered system [82], on which power source, control parts, pipe, connectors need to be loaded. Thus, we decided to limit the current design of this eel robot with three independently controlled segments. Besides, for anguilliform swimmers, the head segment plays a role as a source of the sine wave, while others work as wave propagation parts [93], [98], [99]. Therefore, in this design, the first segment of the eel robot body was constructed from two pairs of soft actuators, which allows the robot to easily bend and then release more energy compared to a structure with only one pair. Another reason for this design is to test the critical case of the robot when the tail segments are broken, and the robot needs to perform anguilliform swimming with a *passive tail* (This swimming strategy was investigated and will be detailed described in Chapter 6.).

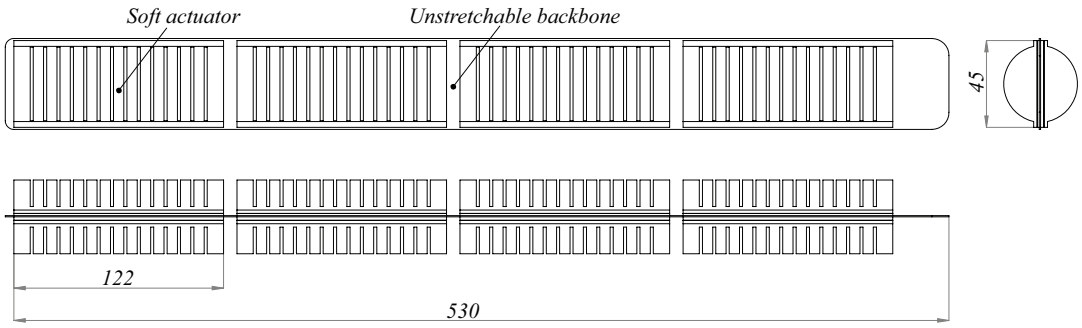


FIGURE 4.6: Design of the soft eel robot body with four pairs of soft actuator affixing in symmetrical way from both sides of backbone plate.

## 4.3 Fabrication process

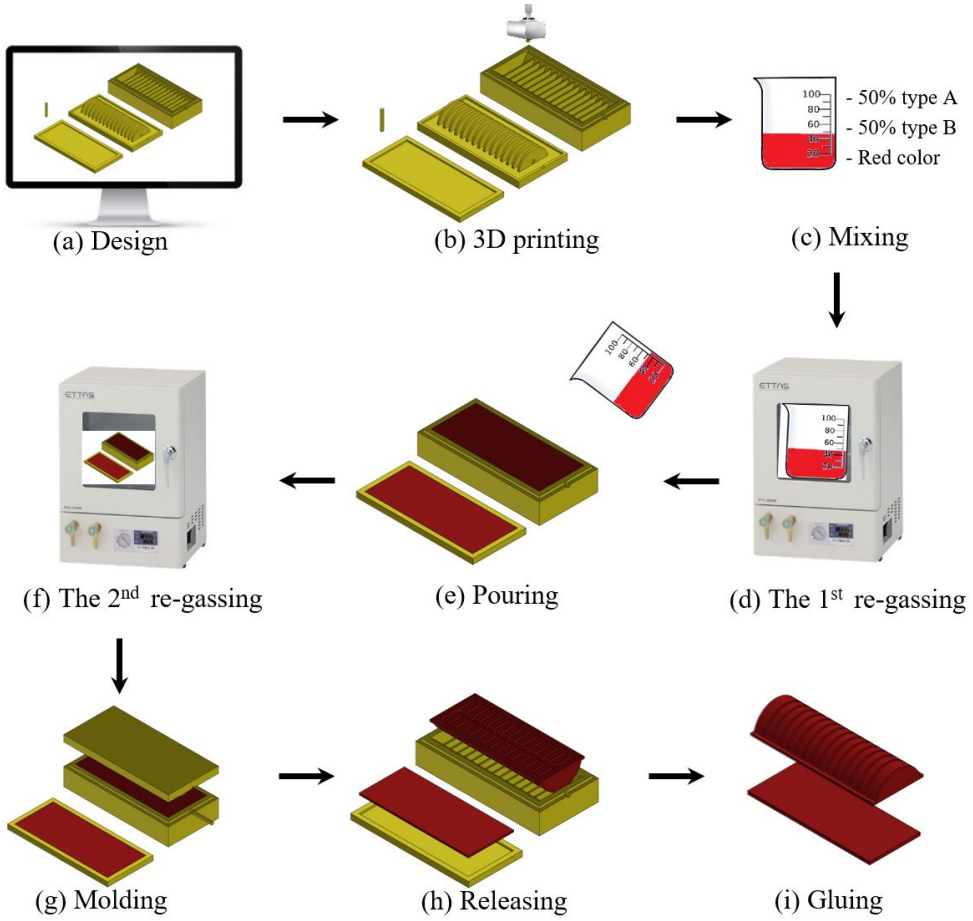


FIGURE 4.7: The pneumatic soft actuator fabrication process.

The soft actuator material was silicone rubber Dragon skin 20 (Smooth-On, Inc., USA). The actuator was fabricated by the molding method. All mold parts were designed using SolidWorks (Dassault Systems) and formed by a 3D printing technique (printer M200, Zortrax). Liquid silicone was poured into a mold to form the

segmented, chambered structure after mixing type A and B in a mass ratio of 1:1 and degassing in a vacuum chamber. The liquid silicon *in situ* on the mold was cured at 22 Celsius degrees for 4 hours. After finishing, two parts (segmented part and base plate part) were glued together using liquid silicon (Dragon skin 20). The nine steps fabrication process of the soft actuator is shown in Fig. 4.7. Air pipe, then, was attached to the actuator using a silicone epoxy (Sil-poxy, SmoothOn, Inc., USA).

After fabrication, soft actuators were attached in symmetry to either side of the spine (backbone) consisting of polypropylene $530 \times 55 \times 0.75$ mm long, wide, and thick, respectively. Silicon epoxy (Sil-poxy, Smooth-On, Inc., USA) was used to affix the actuators to the spine. Fig. 4.8 shows the fabricated soft robot eel body with 4 pairs of actuators grouped in three independently controlled segments.

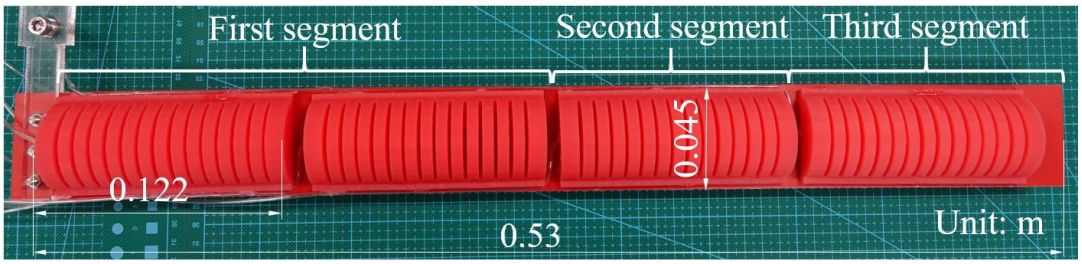


FIGURE 4.8: Fabricated soft robot eel body with four pairs of actuators and divided into three segments.

**Chapter 4 conclusions**

The soft eel-inspired robot body with four pairs of soft actuators was presented. We also introduced a process for choosing a suitable soft actuator shape and size by simulation. A process for fabrication of the soft actuator and whole robot body was revealed.

# Chapter 5

# Control strategy and validation

As mentioned in Chapter 3, eels bend the whole body to generate propagation waves along their body for swimming. This movement might achieve by activating a series of soft actuators orderly. Previous researches also indicated that the working frequency range of soft chambered, segmented depend on their shapes, sizes, and constructed materials. Thus, determining this parameter is obviously required for the first step of investigating soft eel robot locomotion. After that, the control-related issues and swimming performance evaluation are implemented. Specifically, this chapter aims to tackle the following subjects:

- Determining efficiency working frequency of the fabricated soft actuator.
- Investigating on the control strategy for generating propagation waves along the soft eel robot body.
- Validating the thrust force model by experiment.
- Evaluating anguilliform swimming efficiency at different working conditions and a novel swimming strategy based on changing the swimming gait.

## 5.1 Soft actuator bandwidth determination

To swim forward, an eel performs two activities with body muscles including actuating the muscles along one side of the spine orderly from head to tail, and activating the muscles on the other side in a similar way but in opposite phase. Thus, we divide the robot body movement into two activities involving flapping and wave

propagating. In this section, a range of flapping frequency, which a pair of the fabricated actuators can perform efficiently, is investigated. This range is preliminarily chosen based on natural anguilliform swimmers tail beat frequency (bellow 4.0 Hz) and soft segmented, chambered flapping frequency ability (lower than 2.0 Hz). This information is detailed mentioned in Chapter 1. To determine the suitable operating frequency range, a pair of soft actuators were fabricated and tested at frequencies of 0.83, 1.0, 1.25, 1.67, 2.0, and 2.5 Hz. A performance program used to control the open/shut status of solenoid valves (VQD 1121-5L, SMC, Japan) with a power circuit (MOSFET 4, UO 4) was written on Arduino (Arduino, Uno R3, Italy). Pressurized air was generated by a JUN – AIR generator (JUN-AIR, USA), and fed through an adjustable flow control valve (AS2052F, SMC, USA) to control the airflow rate to the solenoid valve which directed compressed air to the soft actuators. The 2 mm diameter pipe (TU0212C-20, SMC polyurethane tube) was used to supply pressurized air to the actuator. The test system diagram is shown in Fig. 5.1. High precision digital pressure sensor (ZSE30AF, SMC, Japan) was used to measure the variation of pressure in a chamber of the actuator.

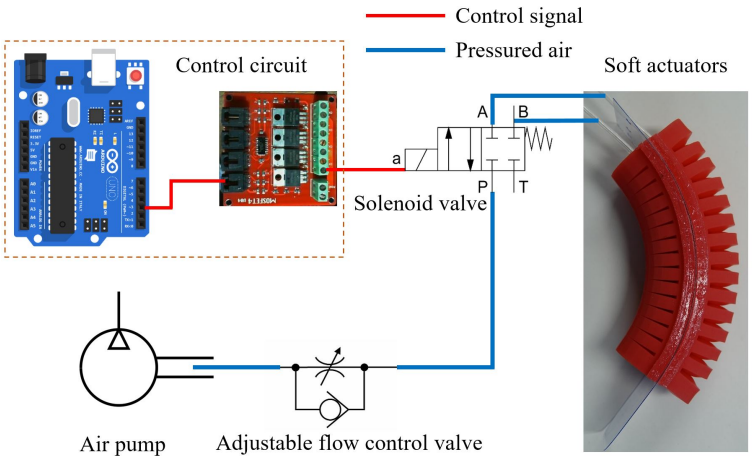


FIGURE 5.1: Diagram of experiment for determining working frequency range of a pair of the soft actuators.

Fig. 5.2 (A) shows maximum bending of the soft actuator for 6 different frequencies when compressed air was input to the upper and lower chambers in opposite phases to generate flapping motion. Bending angle, which is determined by a line connecting the first and last point on the middle spine of a pair of actuators and tangent of the middle spine at the bending stage, was considered as bending efficiency.

Based on visual recognition, from 0.83 Hz to 1.25 Hz, sufficient bending under pressurization was achieved, while the bending efficiency was noticeably downgraded at and above 2.0 Hz. At low frequencies, compressed air seems to be completely exhausted at the resting chamber (for example, upper one) while the working chamber (for example, the lower one) was at maximum pressure value, resulting in the maximum bending shape of the actuator. Meanwhile, at higher values of frequency, pressurized air remained in the resting actuator during the rapid change in status of the solenoid valve, *i.e.*, thus maximum bending could not be recognized. Fig.

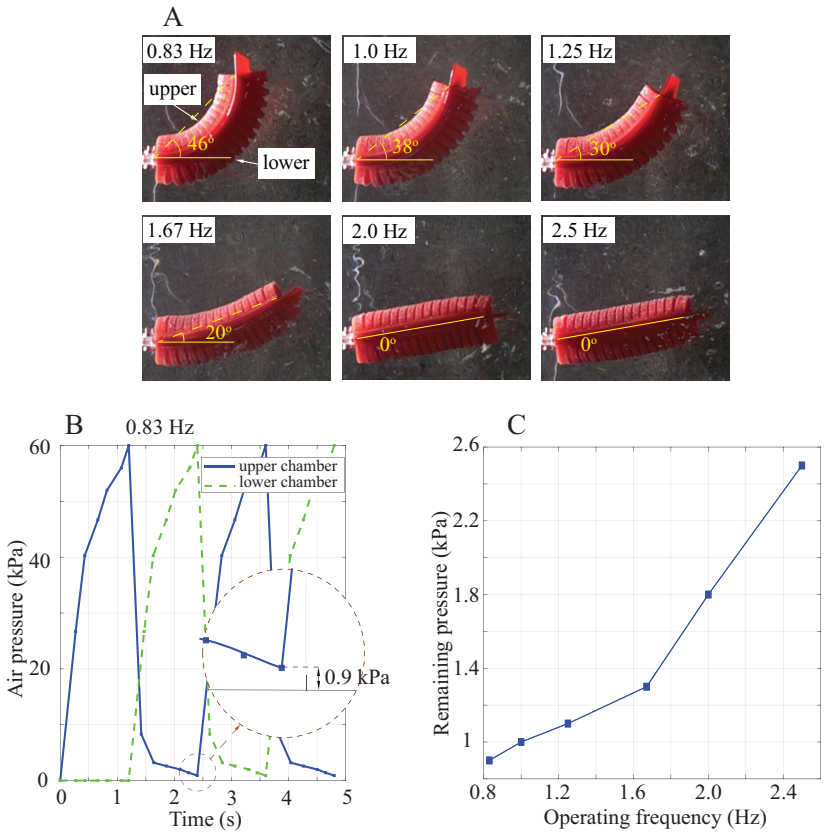


FIGURE 5.2: Experimental setup for evaluation of the flapping ability of a pair of soft actuators, including upper and lower chambers, at different frequencies. (A) The maximum bending posture of the soft actuator at 6 different frequencies. (B) The variation of measured pressure in two chambers of the actuator at 0.83 Hz. The inset picture shows the remaining pressure value (0.9 kPa) in the resting phase of one chamber. (C) The variation of remaining pressure in an actuator at different frequencies. When the remaining pressure increases, the actuator cannot perform the expected maximum bending posture.

5.2 (B) shows the variation of air pressure signal at 2 actuators in a pair flapping at 0.83 Hz. The air pressure signals, which were used to construct graphs, were measured using the pressure sensor. At other frequencies, the signals went with a

similar tendency but different remaining air pressures. The variations of remaining air pressure inside the actuator's chambers at different frequencies are shown in Fig. 5.2 (C). At frequencies from 0.83 Hz to 1.25 Hz, the remaining air pressure at the resting stage of the actuator is around 1.0 kPa. These values go up significantly to 1.8 kPa and 2.5 kPa at 2.0 Hz and 2.5 Hz, respectively. The higher the remained pressure of the resting chamber is, the less the actuator bends. This supports the above explanation on the maximum bending state of the actuator. As a result, the design of soft actuator pairs cannot perform at frequencies of and above 2.0 Hz. At 1.67 Hz, pressure remained at 1.3 kPa in the resting chamber when its counterpart chamber was energized, however, the actuator could perform a sufficient degree of flapping movement. Therefore, the frequency range from 0.83 Hz to 1.67 Hz was chosen for investigating the swimming movement of the robot eel.

## 5.2 Creating propagation waves by series of soft actuators

### 5.2.1 Control strategy

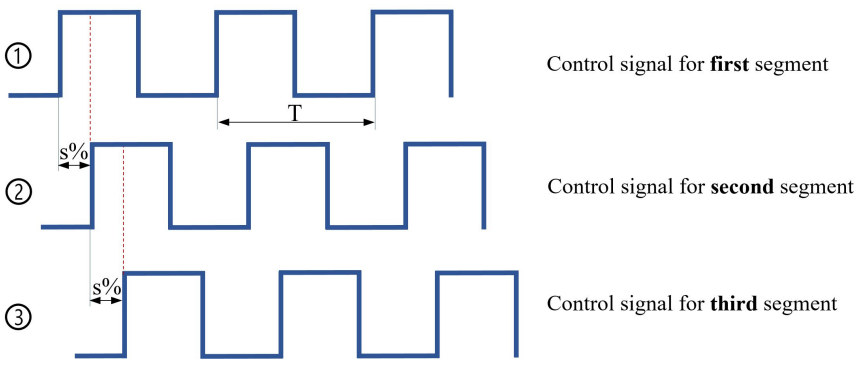


FIGURE 5.3: Diagram of control signals for 3 segments of the eel robot, where $T$ is cycle time, and $s$ is shifting percentage ($s = 100\%$ corresponds to half of the cycle $T$).

Pulse signals with shifting phase were used to control the operation of solenoid valves directing pressurized air to and from the soft actuators, in turn, to generate a sinusoidal wave from head to tail. The robot eel body with four pairs of soft actuators are divided into three segments as shown in Fig. 4.8. First, two pairs of actuators are grouped into the first segment (head segment) that share the same control signal, while other segments (middle and tail segments) have separated control inputs. The diagram of control signals is shown in Fig. 5.3. Signal phases were shifted $s$ percent

of $T$ (cycle time) compared to its previous. It can be seen that wave propagation capability strongly depends on shifting phase value. Thus, the influence of $s$ value on swimming velocity will be investigated.

The system used to control the solenoid valves (VQD 1121-5L, SMC, Japan) included a 4-channel switch (MOSFET 4, UO 4) connected to a micro-control board (Arduino, Uno R3, Italy). Arduino code using multitask algorithm for controlling solenoid valves' stages is shown in Appendix B - Program for multitask. One solenoid valve was employed for each of the four pairs of actuators in the three segments. The solenoid valve is 4/3 way including 4 ports named 1 to 4 in which port 1 is the inlet port, port 3 is the exhaust port, and ports 2 and 4 are outlet ports. Air pressurized by a compressor (JUN-AIR, USA), was fed through throttle valves (AS2052F, SMC, USA) to the solenoid valves that connect the actuators. The smallest possible pipe size of 2 mm diameter (TU0212C-20, SMC polyurethane tube) was used to supply pressurized air to the actuator. The pipe is flexible so that it can reduce the influence of the wiring problem of the tether system on swimming speed measurement as shown in Section 5.3. The polyurethane pipes can work with a maximum pressure of 8 bar ($\sim$ 800 kPa). The control board is shown in Fig. 5.4. Before reaching the solenoid valve, pressurized air was gone through a throttle valve that was utilized to adjust the flow rate of the supplied air independently for each segment.

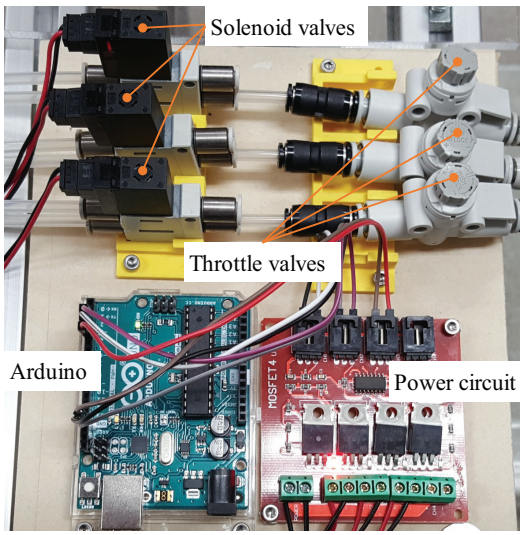


FIGURE 5.4: Control board for distribution pressurized air to the eel soft robot body.

### 5.2.2 Pipe connection

For creating propagation waves along the robot body, the actuators at one side of the backbone (the upper side as shown in Fig. 5.5) are connected to ports number 2 of the solenoid valve, meanwhile, the others are connected to ports number 4. Regarding connection order, at the upper side, two actuators of the head segment, the actuator of the middle segment, and the actuator of the tail segment are coupled to port 2 of solenoid valve numbers 1, 2, and 3 that are actuated by control signal ①, ②, and ③, respectively. The actuators at the downer side are connected in a similar order to ports number 4 of three solenoid valves.

For the C mode swimming strategy, the two pairs of actuators in the first segment were operated in unison with one side connected to port 2 of the solenoid valve 1 and the other to port 4. The connection order to solenoid valve 2 was inverted for the pair of actuators in the middle segment. Meanwhile, the connection order to solenoid valve 3 for the pair of actuators in the tail segment was similar to that for the first segment.

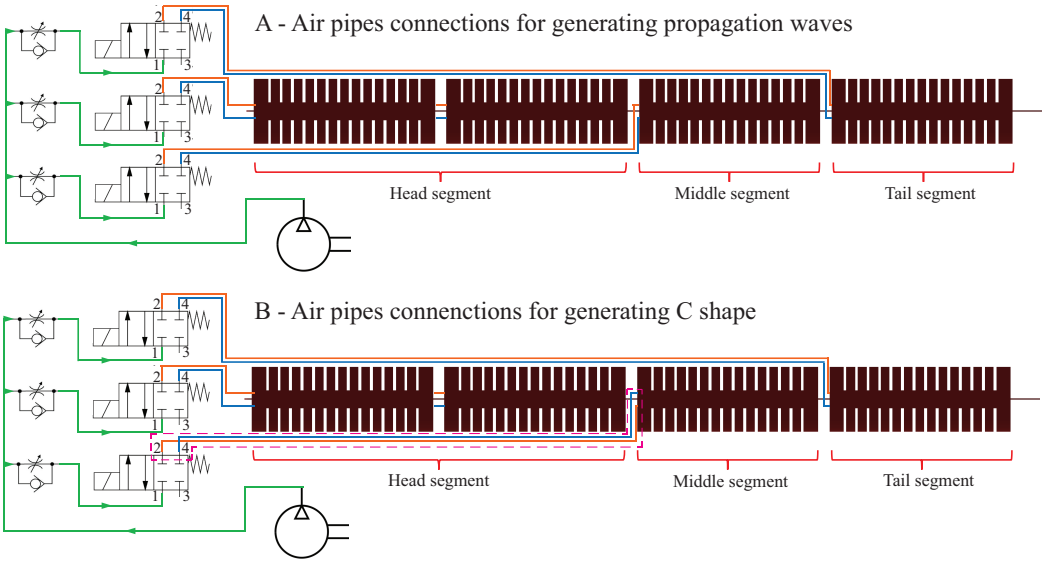


FIGURE 5.5: Diagram of pressurized air connection to three segments of the eel soft robot body. A- Conventional connection for propagating wave from end to end as ports 2 of all three solenoid valves are connected to actuators at one side of the robot and ports 4 for the others. B - Connection for generating C shape swimming gait as reserving ports 2 and 4 at the middle segment (The change is the highlight in the red dash line area.)

Detail investigations on swimming gaits, swimming efficiency of two swimming modes that also strongly depend on control parameters such as tail beat frequency, shifting phase will be described in Section 5.4 and 5.5.

## 5.3 Thrust force validation

### 5.3.1 Experimental setup

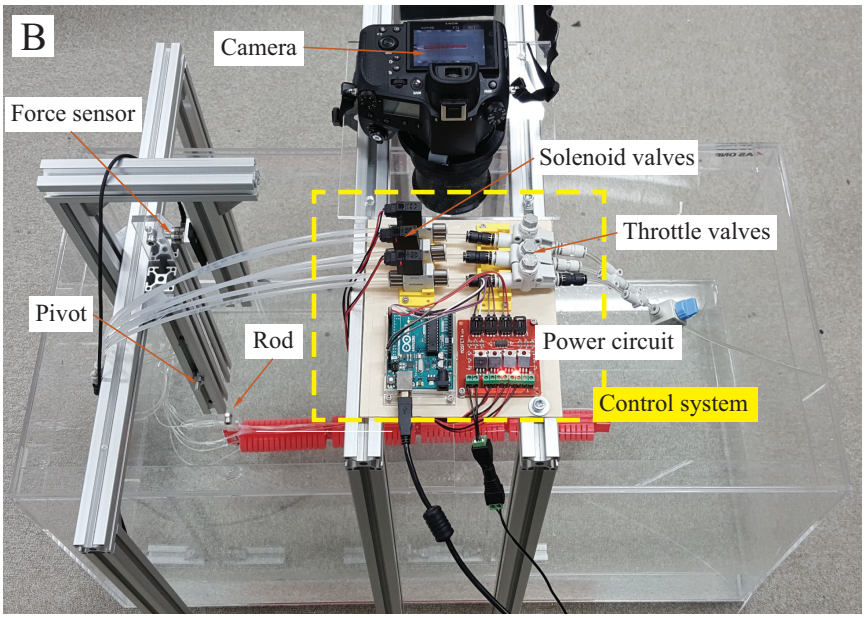


FIGURE 5.6: Experimental setup for measuring thrust forces and recording robot's swimming parameters.

In this experiment, the robot body was attached to a supporting rod from the interior of the spine and performed in still water in a tank ($450 \times 450 \times 900$ mm in length, width, and depth, respectively). A high-speed camera (DSC-RX10M4, Sony, Japan) was used to record sequent images of the robot's swimming postures. The camera's speed was set at 240 fps (frames per second). The supporting rod was hung on a pivot such that when the body created a sinusoidal wave, the body and supporting rod could rotate around the pivot and impact force to a force sensor (see Fig. 5.6). A force-torque sensor (Nano17, ATI Industry Automation, USA) was used to measure propulsion generated by the soft robot eel body. Matlab code for collecting and converting data (Analog-to-Digital Converter) is shown in Appendix C - Matlab code for collecting thrust force data. The pivot was set midway between the force sensor and the robot. Impact forces on the force sensor, therefore, were equal to the thrust forces that the eel robot generated when swimming.

### 5.3.2 Determining swimming parameters of the robot body

As mentioned in Chapter 3, swimming parameters ($A$, $B$, $\beta$, $\lambda$, and $\theta$) are affected by several variables and properties of the eel robot's body, including body length, body diameter, material stiffness, the bending ability of actuators, and so on. In this thesis, the robot was operated at chosen frequency range for determining such swimming parameters. The control shifting phase was set at 50 % for propagation wave mode or 40 % for C shape mode (two swimming mode will be detailed explanation in the next Section), in which the robot perform smooth propagation waves from head to tail. Meanwhile, air pressure at three segments from head to tail was set at 65 kPa, 50 kPa, and 30 kPa, respectively. All image data at four different operation frequencies (0.83, 1.0, 1.25, 1.67 Hz) was extracted using Matlab R2018b (MathWorks). Matlab code for extracting images from a video is put in Appendix D - Matlab code for extracting images. The information on the robot's amplitude $A$ and body wavelength $\lambda$ was extracted by measuring manually on images data using a reference rule with a resolution of 1 mm added to each image. Amplitude growth rate $\alpha$, then, was calculated by dividing the amplitude of the tail segment by amplitude of the head segment. Eq. (3.3) was used to calculate $\beta$. These data were processed to extract information on the robot's amplitude $A$, body wavelength $\lambda$ and amplitude growth rate $\alpha$, and then $\beta$. Angle $\theta$ was calculated using Eq. (3.7) and the parameter $B$ is the diameter of the body's cross-section area. The maximum bending postures of the robot, which were used to determine swimming parameters, depended on the frequency and are shown in Fig. 5.7.

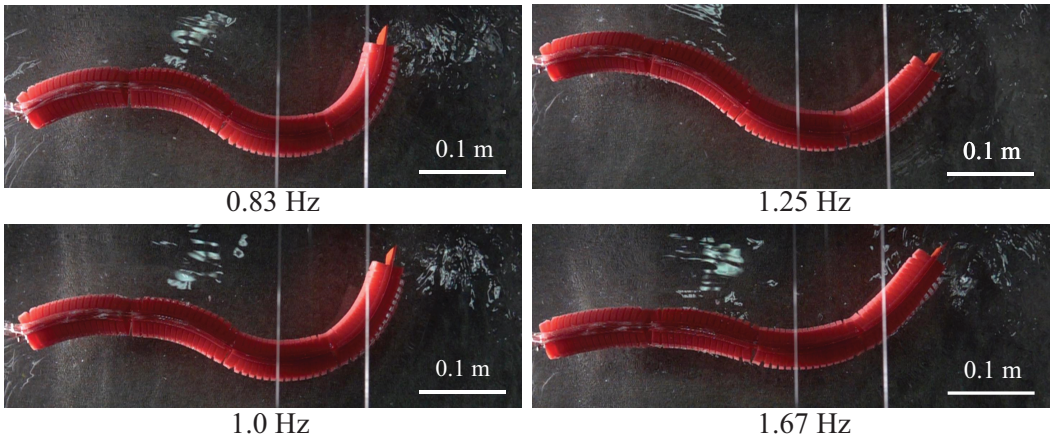


FIGURE 5.7: Maximum bending of robot eel body at four frequencies.

Table 5.1 shows the robot eel body swimming geometrical parameters for four frequencies. This information will be utilized for calculation of thrust force in the followed section.

TABLE 5.1: Eel robot body swimming parameters

| Swimming frequency, f (Hz) | 0.83 | 1.0 | 1.25 | 1.67 |
|---|---|---|---|---|
| Amplitude, A (m) | 0.026 | 0.024 | 0.022 | 0.018 |
| Amplitude growth rate, $\alpha$ | 2.8 | 2.8 | 2.9 | 2.8 |
| Body wavelength, $\lambda$ (m) | 0.416 | 0.424 | 0.444 | 0.448 |
| Increase coefficient, $\beta$ | 4.95 | 4.86 | 4.8 | 4.6 |

### 5.3.3 Thrust force calculation

Generated thrust forces are calculated using Eq. (3.15). Propulsion, however, is a function of multiple swimming parameters. As a result, thrust force values can only be calculated at certain frequencies based on parameters measured directly from the kinematics of the robot body. Thus, to predict the variation of thrust force, functions of the other swimming parameters w.r.t variable frequency is required. In other words, Eq. (3.15) will become a function of only variable frequency $f$. Curve fitting tool (Matlab R2018b) was used to find the functions $A(f)$, $\lambda(f)$ and $\beta(f)$. These functions are described as:

$$A = 0.003845f^2 - 0.01889f + 0.03914. \tag{5.1}$$

$$\lambda = -0.201e^{-1.765f} + 0.4616. \tag{5.2}$$

$$\beta = -0.3758f + 5.248. \tag{5.3}$$

The sum of square errors of prediction (SSE) which reveal discrepancies between the data and the estimation models of $A(f)$, $\lambda(f)$, and $\beta(f)$ are $3.405 \times 10^{-7}$, $4.148 \times 10^{-5}$, and $1.421 \times 10^{-3}$, respectively. These are small values, indicating the sufficient fitness of the model to the data. Therefore, Eq. (3.15), Eq. (5.1) - Eq. (5.3) can be used

to estimate the thrust force created by the eel robot at any swimming frequency between 0.83 Hz and 1.67 Hz. For ease of calculation of the thrust force, function $\theta$ with variable $x$ was built. The values of angle $\theta$ at 21 points which were divided equally from x = 0 to x = $\lambda$ were calculated using Eq. (3.15). The curve fitting tool (Matlab R2018b), then, was utilized to find the function $\theta(x)$. Table 5.2 shows the equation of angle $\theta$ as a function of $x$ at four measured frequencies and the corresponding sum of square errors of prediction.

TABLE 5.2: The variation of $\theta$ depending on x at four testing frequencies

| f (Hz) | $\theta(x)$ | SSE |
|---|---|---|
| 0.83 | $0.925\sin(14.49x + 1.86) + 0.506\sin(20.36x + 5.13)$ | 0.013 |
| 1 | $0.907\sin(14.37x + 1.87) + 0.521\sin(19.74x + 5.12)$ | 0.010 |
| 1.25 | $0.91\sin(13.88x + 1.88) + 0.561\sin(18.26x + 5.09)$ | 0.034 |
| 1.67 | $1.027\sin(14.47x + 1.92) + 0.792\sin(17.33x + 5.12)$ | 0.015 |

Swimming postures shown in Fig. 5.7 are the representative bending shape of the robot. At low frequencies, due to the long opening time of the solenoid valves, the soft actuators receive a larger amount of pressured air. As a result, the robot body resulted in a large curvature and the curvature of the body decreased w.r.t the increase in frequency. As a matter of fact, a large curvature will create more lateral movement which impedes the forward movement of the robot. Fig. 5.8 shows calculations of propulsion created by the eel robot at 11 swimming frequencies. Since the drag coefficient $C_D$, which strongly depends on the geometrical characteristics of the eel body and swimming posture, may vary during the propulsion, it is difficult to specify a unique value for the eel robot. If the robot eel body is considered as a cylinder moving in a turbulent flow, $C_D$ will be equivalent to 0.3 [95]. Since the robot body performed anguilliform movement, drag reduction should be taken into account. In this case, drag reduction varied from 15 % to 70 %, compared to that expected of a rigid body [100]. Therefore, $C_D$ was chosen from 0.09 to 0.255. Fig. 5.8 indicates the area (with diagonal lines) limited by a minimum thrust force graph (green line, with $C_D$=0.09) and maximum thrust force graph (blue line, with

$C_D$=0.255). As two limitation graphs, the calculated propulsion increased gradually with an increase in frequency from 0.83 Hz to 1.5 Hz before rising slightly between 1.5 Hz and 1.67 Hz. The measured thrust force is expected to fall into this area, since the precise calculation of $C_D$ requires a much more experimental approach that is out of the scope of this thesis.

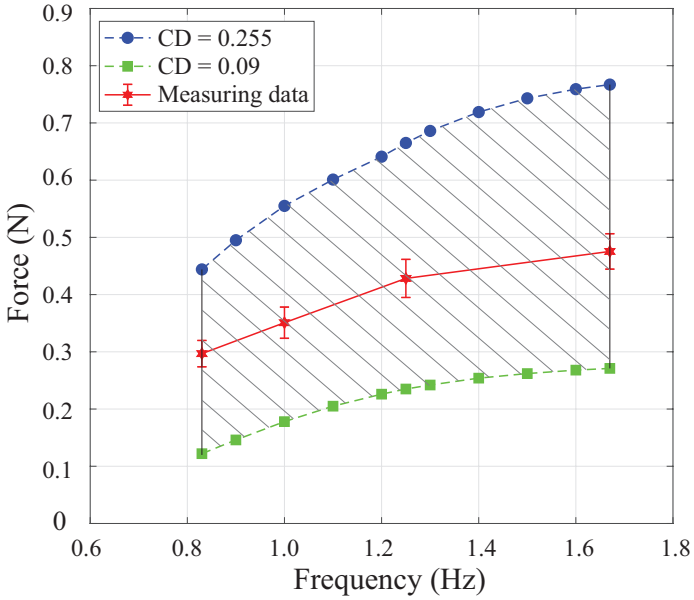


FIGURE 5.8: Comparison of calculated thrust force range and actual measured one at different frequencies. The calculated force range is limited by the upper border (in blue, with drag coefficient $C_D = 0.255$) and the lower border (in green, with $C_D = 0.09$). The actual measured thrust force value is within the calculated range, with approximated $C_D = 0.167$.

### 5.3.4 Thrust force measurement

Variation of propulsion depends on the movement of the robot body in sinusoidal waves according to Eq. (3.3). As mentioned above, propulsion reaches a maximum when the robot body assumes its maximum bending position. A range of generated forces at each swimming frequency was measured five times and the maximum value was extracted. Variation of propulsion by frequency is shown in Fig. 5.8. It is clear that generated thrust force increased with that of frequency and such variation is similar to calculated data at two limitation values of $C_D$. These measurement values were within the computed area as expected. Based on this measurement, we were able to estimate the drag coefficient $C_D$ at its maximum as approximately

0.167. It is considered that the drag coefficient of this soft eel robot takes into account the effect of the robot's surface (skin) morphology and the deformation of the robot body since such deformations directly affected the particular surface area.

A thrust force model presented in this thesis may be utilized for predicting variation in propulsion force w.r.t flapping frequency. Due to the strong dependence of the thrust force model on swimming parameters of a certain swimming system, it is necessary to conduct experiments with frequencies across the desired range of swimming frequencies, for determining a set of swimming parameters. Once constructed, the thrust force model, which is the function of frequencies, may be used to calculate generated propulsion of an anguilliform swimmer at any frequency. In this case, Eq. (3.15) can be used directly to calculate the thrust force at the maximum bending state of the robot. The thrust force calculation and experiment data indicated that an increase in swimming frequency (within the bandwidth of the actuator) results in a rise in propulsion. This model is also exploitable for the calculation of the robotic eel's thrust force when another condition varies, such as the chamber's input pressure or shifting phase. The drag coefficient $C_D$ also plays an important role in the estimation of the thrust force. Nonetheless, it requires a substantial experiment tool and approaches on fluid dynamics for estimation of a precise value of $C_D$, since it depends on many swimming factors of the robot and the surrounding water. Therefore, precise estimation of $C_D$ is out of the scope of this thesis.

## 5.4 Swimming velocity

Swimming speed is an important parameter that needed to be investigated during the evaluation of underwater robots' mobility. To measure the swimming velocity of the eel robot, it was set in a free condition (not attached to the supporting rod as in previous sections). Swimming speed was estimated based on consecutive images from the high speed camera. The velocity is calculated by total displacement divided by traveling time. To avoid the effect of bounce back wave, the robot was traveled along with the tank one time for each measurement. The next only be conducted after getting a stable water surface. Each measurement was repeated five times, then, took the average and standard deviation to minimize the inaccuracy due to

short distance of traveling (short length of the tank), other factors and estimate the convergence level of the measurement. Tail beat frequency, supplying air pressure, and shifting phase of control signal were among parameters to be varied to evaluate the influences of these conditions on the robot's movement ability.

### 5.4.1 Performing traditional mode

As aforementioned, operation parameters including air pressure, tail beat frequency, and control shifting phase strongly affect the swimming performance of the soft eel robot. Therefore, this section aims to evaluate swimming velocity depending on these parameters. To begin, the influence of air pressure that is attributed to tail beat amplitude formation is investigated. There are many combinations of supplying pressure at three segments. It might waste of time for doing all such testing to find out the potential range of pressure values. Thus, we depend on our previous results to reduce the number of experiments. The result from both simulation and experiment with a pair of the actuator indicated that the pair can perform high flapping amplitude at 60 kPa. Some raw experiments, which were conducted at around the value of supplying air pressure for two lower segments of the robot body, revealed that the combination of 50 kPa and 30 kPa at middle and tail segment, respectively, can generate large tail beat amplitude. For simplification, these values will be fixed for all next experiments. Hence, in order to evaluate the effect of air pressure on

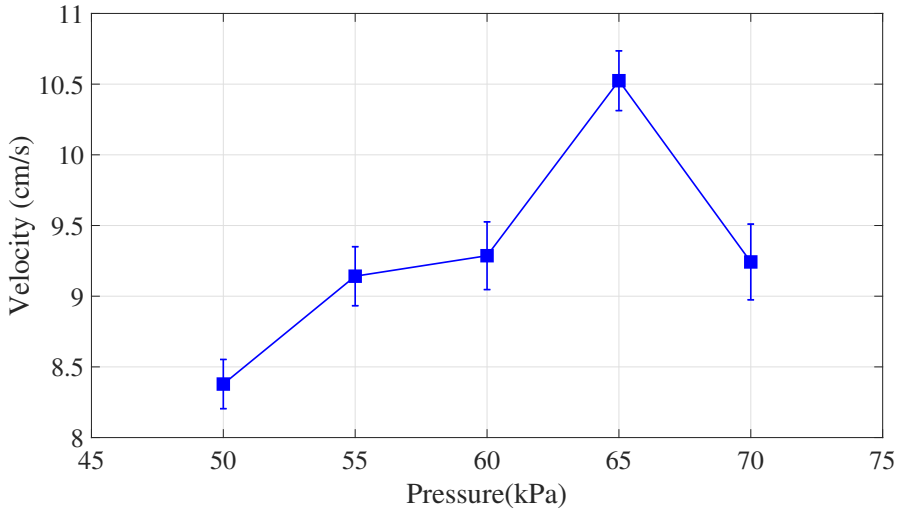


FIGURE 5.9: Pilot experimental results for evaluation of the eel robot's swimming velocity in variation of the first segment's input pressure.

swimming velocity, pressurized air at the first segment was varied, while the value of compressed air inside the others and shifting phase were kept unchanged. Tail beat frequency was set at 1.25 Hz and the control shifting phase was set at 40 %. Swimming velocities of the robot body at five pressure values (50 kPa, 55 kPa, 60 kPa, 65 kPa, and 70 kPa) of the first segment were measured and shown in Fig. 5.9. It reveals that when the air pressure increases from 50 kPa to 65 kPa, the velocity grows up from nearly 8.5 cm/s (0.16 BL/s) to 10.5 cm/s (0.198 BL/s). After that, the rise of air pressure results in the decrease of velocity (approximately 9.3 cm/s (0.175 BL/s) at 70 kPa). In this case, the variation of the first segment's pressure gradually affects the robot body's swimming velocity when the maximum difference of velocity is approximately 2 cm/s (around 20 % of the highest velocity). The velocity reaches a peak at 10.5 cm/s when the air pressure was at 65 kPa. As a result, air pressures of the first, second and third segment at 65 kPa, 50 kPa, and 30 kPa, respectively are chosen to be the best performing value set for the current eel robot's movement. The increase in air pressure to 70 kPa results in the rise of the first segment's bending, leading to the growth of a lateral movement of the eel robot's head segment which may result in the decrease in swimming velocity.

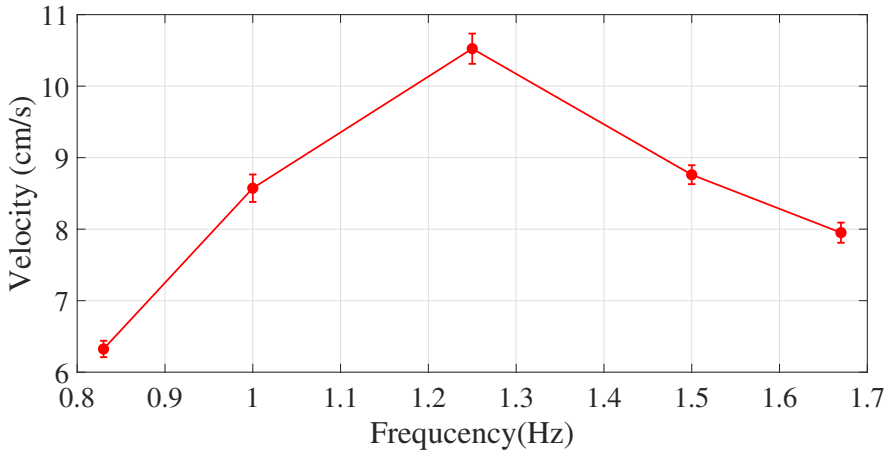


FIGURE 5.10: Pilot experimental results for evaluation of the eel robot's swimming velocity in variation of the tail beat amplitude.

To estimation the effect of tail beat frequency on the robot body's swimming performance, air pressure was set at 65 kPa, 50 kPa, and 30 kPa for the first, second, and third segment, respectively. Meanwhile, the tail beat frequency was varied, and the

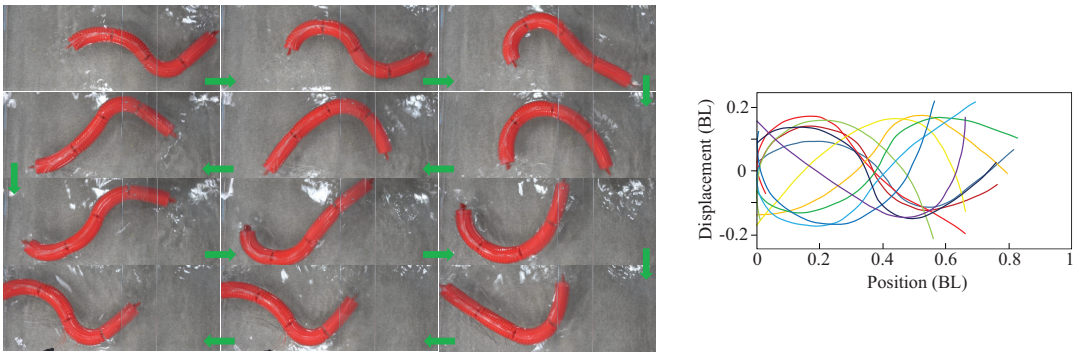


A - Eel soft body postures swimming (left) and midline kinematics (right) at 0.83 Hz

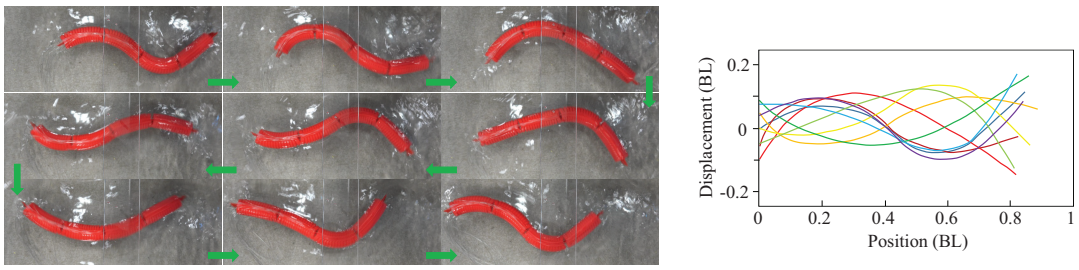


B - Eel soft body postures swimming (left) and midline kinematics (right) at 1.25 Hz

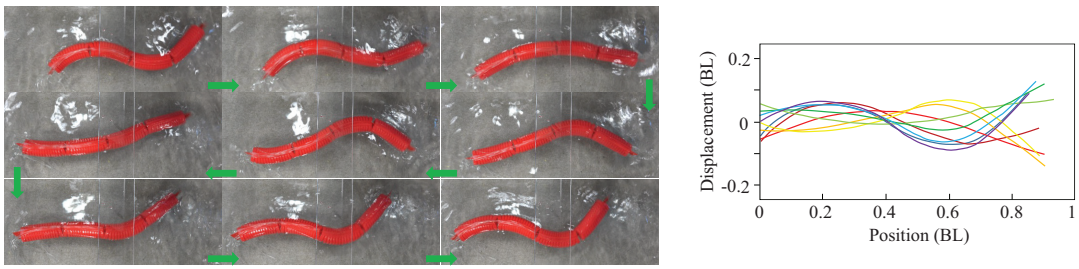


C - Eel soft body postures swimming (left) and midline kinematics (right) at 1.67 Hz

FIGURE 5.11: Robot eel body postures and its midline kinematics after 1 tail beat cycle at 3 different frequencies: the lowest frequency 0.83 Hz, the highest frequency: 1.67 Hz, and the frequency associated with the highest velocity of swimming 1.25 Hz. All are at shifting phase of 40 %. A related video of this experiment can be seen https://www.youtube.com/watch?v=C5XCXhUNN2s

shifting phase was still set at 40 %. Velocities were measured at five points including four frequencies (0.83 Hz, 1.0 Hz, 1.25 Hz, 1.67 Hz) for estimation of swimming parameters and thrust forces and 1.5 Hz witnessing the change of thrust force tendency from gradual increase to slight rise (see Fig. 5.8). Fig. 5.10 shows the variation of velocities depending on the robot's operation frequency. In the tested range, the velocity of the robot sharply increased corresponding to the increase in frequency to reach the maximum value of 10.5 cm/s (0.198 BL/s) at 1.25 Hz then gradually decreased at a higher frequency. The minimum velocity was 6.32 cm/s (0.119 BL/s) at 0.83 Hz.

The body postures of the robot eel when swimming at frequencies of 0.83 Hz, 1.25 Hz, and 1.67 Hz after one cycle are shown in Fig. 5.11. At the highest frequency,

although the robot eel body can create its greatest thrust force, the velocity of the body is rather low. The decrease of velocity at high frequency is caused by the low response (or bandwidth) of the soft actuator. This phenomenon prevents the body from adopting a maximum bending posture with sufficient amplitude, which impedes the eel robot's velocity through vortex formation relating to momentum flux. Larger tail beat amplitude creates larger momentum flux which is proportionate to a natural eel's velocity [22]. Meanwhile, at low frequencies, the robot eel body swimming with a large amplitude performs the large lateral movement. As a result, velocities associated with such frequencies are also low. This phenomenon was also reported on [82] in which eel robot velocity decreased from 5.45 cm/s to 4.08 cm/s when tail beat frequency decreased from 0.67 Hz to 0.5 Hz due to the increment of the head's beating amplitude. At frequencies ranging from 1 Hz to 1.5 Hz, the robot eel body shows quite good swimming efficiency, with velocities over 8.5 cm/s (0.16 BL/s).

The shifting phase $s$ of the control signal for three solenoid valves that deliver compressed air to three segments of the robot is one of the most important control parameters. The variation of the shifting phase influences the robot swimming's posture which directly affects the swimming speed. The Control signal's shifting phase was varied from 10 % to 100 % for investigating the effect of this parameter on the robot body movement ability. The other parameters were set as same as these create the highest velocity at two examinations above. Specifically, air pressures at the first, second, and third segments were set at 65 kPa, 50 kPa, and 30 kPa, respectively. Tail beat frequency was put at 1.25 Hz. Measurement data is shown in Fig. 5.12. The velocity starts to increase and reaches its peak when $s$ = 50 % at velocity of 10.5 cm/s (0.198 BL/s). Then, the velocity sharply decreases to zero at $s$ = 90 %. The decrease of the eel robot velocity can be explained based on the wave propagation phenomenon. At a high value of the shifting phase, when the head segment was bent to one side, the middle segment was bent to the opposite side almost simultaneously, and the tail segment was bent to the similar side of the head one. Such movements of three segments canceled out one to another, and the rise of the shifting phase led to the increase of the cancellation level. Therefore, three segments could not efficiently create wave propagation along the body. As a result, the eel

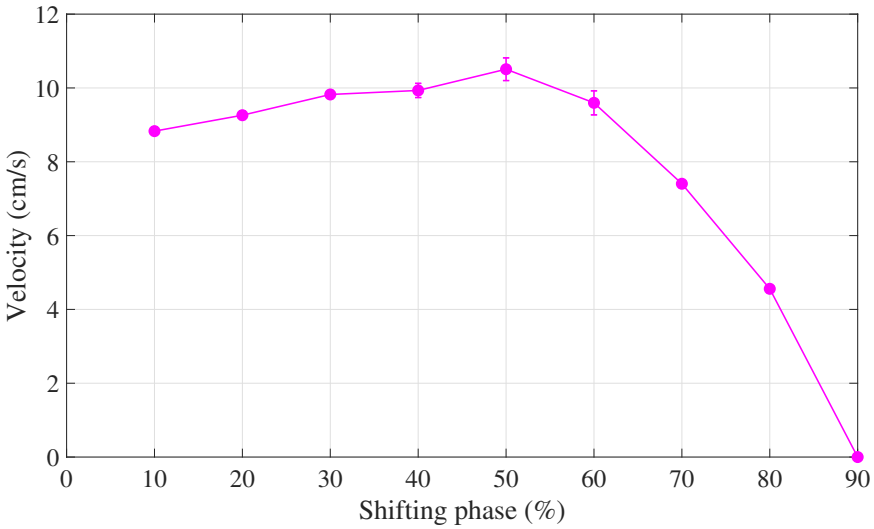


FIGURE 5.12: Experimental results for evaluation of the eel robot's swimming velocity in variation of the control shifting phase.

robot speed drops down sharply when the shifting phase increases. From the result shown in Fig. 5.12, it can be concluded that with the shifting phase from 30 % to 50 % the eel soft robot can generate smooth propagation waves from the anterior to the posterior robot body. The forward velocity at shifting phase of 0.3 $T$, 0.4 $T$, and 0.5 $T$ are 9.8 cm/s, 9.9 cm/s, and 10.5 cm/s respectively. Although the differences of the soft eel robot at three shifting phase values are very small, it can be said that at the highest velocity (corresponding to $s$ = 50 % ) the robot performed the smoothest propagation waves. It is difficult to determine time lag in the activation muscle of elongated body fish for straight swimming. Thus, the results of the robot investigation might be a foundation or reference for investigating the similar issue of original natural species. They are also worthy of the development of soft elongated body robots.

### 5.4.2 Performing C shape mode

This swimming mode was done by the combination of inverting air pipe connection at the middle segment that was detailed described in Section 5.2.2 and highest control shifting phase (100 %). Noting that the inverting air pipe connection at middle segment combining with shifting phase at around 40 % still create smooth propagation wave from head to tail. The images data shown in Fig. 5.7 and Fig. 5.11 prove this complaint. The C performing mode, interestingly, was discovered once the air

pipes system is reconnected. After some experiments with three to four $s$ values, we realized the connection problem due to the differences in swimming gaits. At $s$ = 30 % to 40 %, the robot seem to be performed propagation waves along its body. However, when the increased shifting phase the velocity went up instead of gone down as usual. Thus, we decided to carefully investigate this swimming mode. Operation parameters are set as same as those for the highest swimming velocity of traditional swimming strategy as described above, excluding the control shifting phase. The variation of swimming velocity versus shifting phase is shown in Fig. 5.13. The increase in shifting phase percentage results in the rise of swimming velocity significantly. The speed is at the lowest of just over 6.0 cm/s (0.113 BL/s) at 10 % of shifting phase $s$. It hits the peak at around 19.0 cm/s (0.36 BL/s) with the shifting phase of 100 %. At the maximum shifting phase, the first and third segments will be inflated at the same phase. This leads to the change in the swimming posture of the robotic eel. It did not perform a sinusoidal wave from the anterior to the posterior body (as seen in Fig. 5.11). Instead, a big curve in the body posture was formed then released, in order to generate forwarding movement (see Fig. 5.14), and the second segment obviously plays an important role in the robot's swimming. The importance of the second segment was proved by an experiment, in which the first and the third ones were actuated but the second one was inactive, and the robot could not move forward.

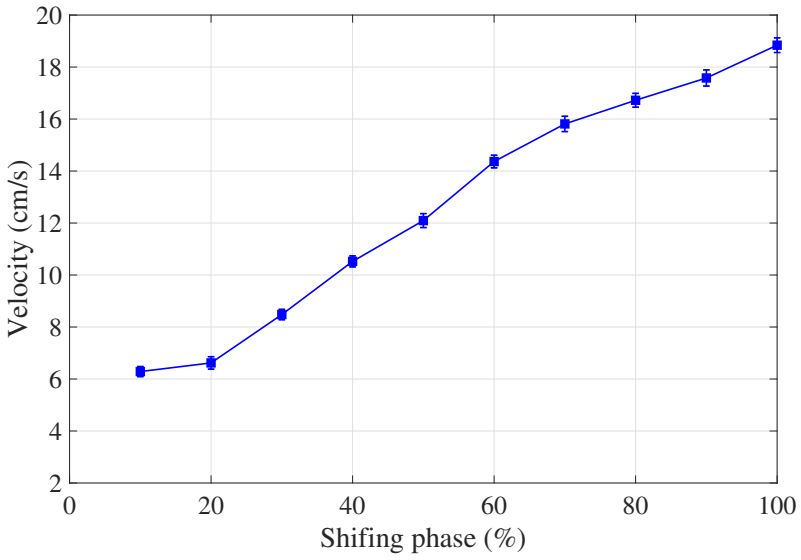


FIGURE 5.13: The variation of swimming velocity of the soft eel robot body as performing C mode.

In several frames of Fig. 5.14, for example 3 and 7, there seems to be a phase difference between the first and third segments, even though they were controlled properly with the same phase. This visually perceived difference may come from the inertia of the robotic system, and possible differences in the fabrication of related actuators. In fact, in such frames, the tail segment has reached its maximum displacement and is about to reverse the direction. In addition, due to the large time lag (100 % shifting phase), the movement of the tail segment also be strongly affected by water flow which is created by the first and second segments. As a result, the deformed shape of the third segment, in some moments, looked different from the first segment.

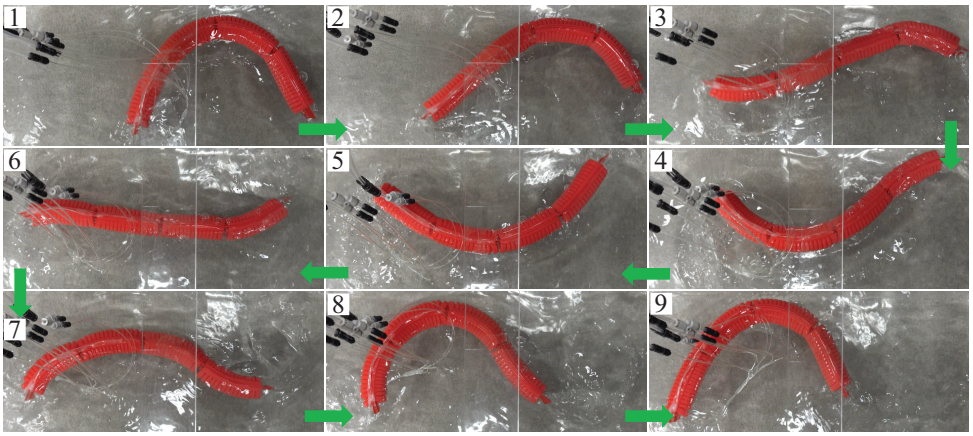


FIGURE 5.14: Eel robot body postures performing C mode after 1 tail beat cycle at 1.25 Hz with shifting phase of 100 %.

One concern with the case of swimming at shifting phase of 100 % is that there was a stronger interaction of the robot body with surrounding ambient water, which resulted in noise and bigger waves on the water surface compared to these generated by the robot performing anguilliform movement (as shown in Fig. 5.11). In fact, natural ones are not able to operate this swimming strategy (as the robot swims at 100 % shifting phase). This might relate to their muscle structures which only permit them to create continuously sine wave form. Meanwhile, the eel soft robot that is constructed from 4 independent muscle units is able to execute some certain type of movement depending on the combination of actuators' bending phase. As a result, for maximum swimming speed the eel robot may be controlled at shifting phase of 100 % with C mode's air pipe connection order; while for the accomplishment of natural eel-like undulatory movement with pleasant interaction with ambient fluid.

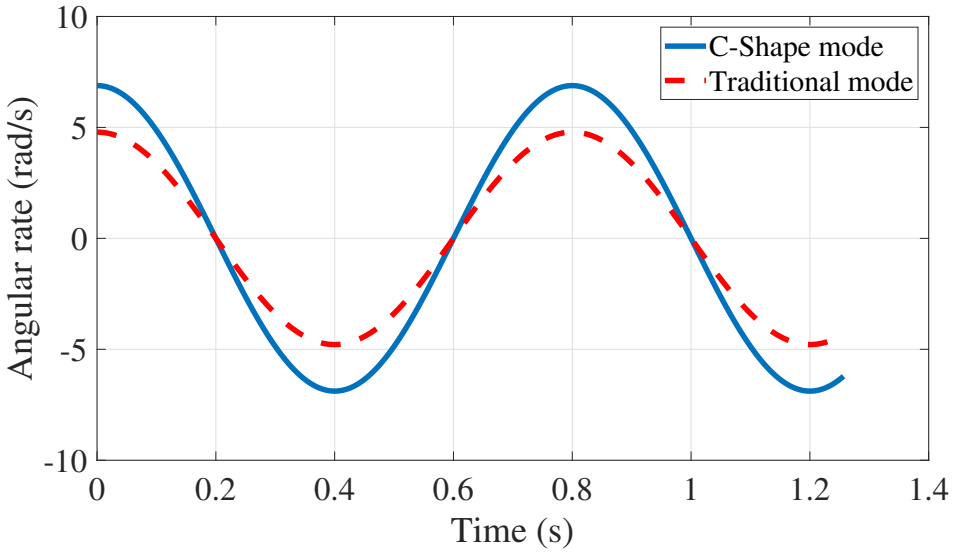


FIGURE 5.15: Head segment's angular velocity of traditional mode (tail beat frequency: 1.25 Hz, shifting phase: 50 %, working pressure at head - middle - tail segment: 65 kPa - 50 kPa - 30 kPa) and C-Shape mode (tail beat frequency: 1.25 Hz, shifting phase: 100 %, working pressure at head - middle - tail segment: 65 kPa - 50 kPa - 30 kPa).

According to Fig. 5.15, the robot's velocity can also be affected strongly by the angular velocity of the head segment. Compared to the traditional mode's angular velocity, the robot head segment's angular velocity when performing C-shape mode is over 30 % higher. As a result, about 85.7 % more velocity was achieved at similar working conditions (air pressure, tail beat frequency).

## 5.5 Cost of Transport

Energy consumption plays an important evaluation index in constructing robots because it would decide the selection of batteries and other driving parts, eventually resulting in the robot's shape and size. In this research, cost of transport (COT) that relates to the energy consumption of the robot was investigated. Additionally, cost of transport has been used to estimate the efficiency of the movement of animals and mobility robots [29], [101]. COT is defined as:

$$COT = \frac{Consumption\ \ Energy}{Mass \times g \times Distance}. \tag{5.4}$$

Cost of transport qualifies the amount of energy required to move a specific weight system to a specific distance. From Eq. (5.4), in the case of underwater robots, it is

clear that the lower COT value shows the higher swimming efficiency. For the soft eel robot body, consumption energy comes from two sources including electrical power and air pressure power. The former used to operate control system (control board, control circuit) can be calculated as $P_E = U.I.t$, where $U$, $I$, and $t$ stand for supplying voltage, current, and time respectively. Supplying voltage and current were measured by sensors integrated into power supply E3630A (Keysight, USA). Whereas the latter can be calculated as $P_A = p.Q.t$, where $p$, $Q$, and $t$ stand for supplying air pressure, flow rate, and time, respectively. Pressurized air was supplied from an air pressure compressor. The Air pressure and airflow rate used to operate the eel robot were measured by pressure sensor ISE20A-R-M (SMC, Japan) and flow rate sensor PFM710-01-A (SMC, Japan). Energy consumption for operating the eel robot is determined by the sum of electrical and air pressure energies.

TABLE 5.3: The variation of COT depending on swimming frequency ($s$: 40 %)

(The smallest value of COT is at 1.25 Hz)

| Frequency (Hz) | $P_E$ (J) | $P_A$ (J) | COT |
|---|---|---|---|
| 0.83 | 5.28 | 9.04 | 33.31 |
| 1.0 | 5.28 | 8.67 | 23.95 |
| 1.25 | 5.52 | 8.22 | 19.21 |
| 1.5 | 5.52 | 7.92 | 22.56 |
| 1.67 | 5.52 | 7.36 | 23.83 |

The air pressure power only is measured after pressurized air goes through throttle valves. This will avoid being taken into account energy loss from an air compressor. COT values corresponding to the variation of tail beat frequency and the first segment's air pressure were calculated. Table 5.3 shows the measured power consumption and calculated COT at five different frequencies. Cost of transport value decreases from 33.31 to 19.21 when tail beat frequency increases from 0.83 Hz to 1.25 Hz and then the value goes up corresponding to the rise of the tail beat frequency. The lowest value of COT is 19.21 at 1.25 Hz where the robot body swims with the highest velocity (see Fig. 5.16 (B)). This means that at this frequency the eel

soft robot body has higher swimming efficiency compared to the others.

TABLE 5.4: The variation of COT depending on first segment pressure ($f$: 1.25 Hz; $s$: 40 %)

(The smallest value of COT is at 65 kPa)

| Air pressure (kPa) | $P_E$ (J) | $P_A$ (J) | COT |
|---|---|---|---|
| 50 | 5.52 | 6.15 | 20.53 |
| 55 | 5.52 | 6.8 | 19.83 |
| 60 | 5.52 | 7.4 | 20.49 |
| 65 | 5.52 | 8.22 | 19.21 |
| 70 | 5.52 | 9.65 | 24.17 |

COT values of the robot body that swims at different pressure of the first segment were also calculated to estimate swimming efficiency. The robot body was operated at 1.25 Hz and the first segment's air pressure was varied from 50 kPa to 70 kPa with a step of 5 kPa. The results are shown in Table 5.4. The best value of COT, in this case, is 19.21 at 65 kPa. It can be seen that although total energy consumption when the robot body swims with the pressure of the first segment at 65 kPa is higher compared to those at 50 kPa, 55 kPa, and 60 kPa, the higher velocity that it created (see Fig. 5.16 (A)) results in the better COT. The variation of cost of transport as varying control shifting phase revealed the similar tendency with the two others since the best COT (18.84) drops to the highest velocity (10.5 cm/s (0.198 BL/s)).

To estimate the effect of control shifting phase on swimming efficiency of the robot body when the robot body performs C shape swimming mode, COT of swimming robot body at 10 different shifting phases (10 % to 100 % with step of 10 %) was calculated. Note that the robot, in this case, was controlled at 1.25 Hz and pressure of the first segment 65 kPa, which correspond to the best values in propagation waves mode. Fig. 5.17 shows the variation of COT depending on the control shifting phase. COT sharply declines from 32.18 to 14.07 when the shifting phase goes up from 10 % to 60 %. After that COT decreases gradually to the best value of 10.72 at 100 %. This variation of COT indicated that the robot body's swimming efficiency is greatly improved when the control shifting phase is raised from 10 % to 60 %, and gradually

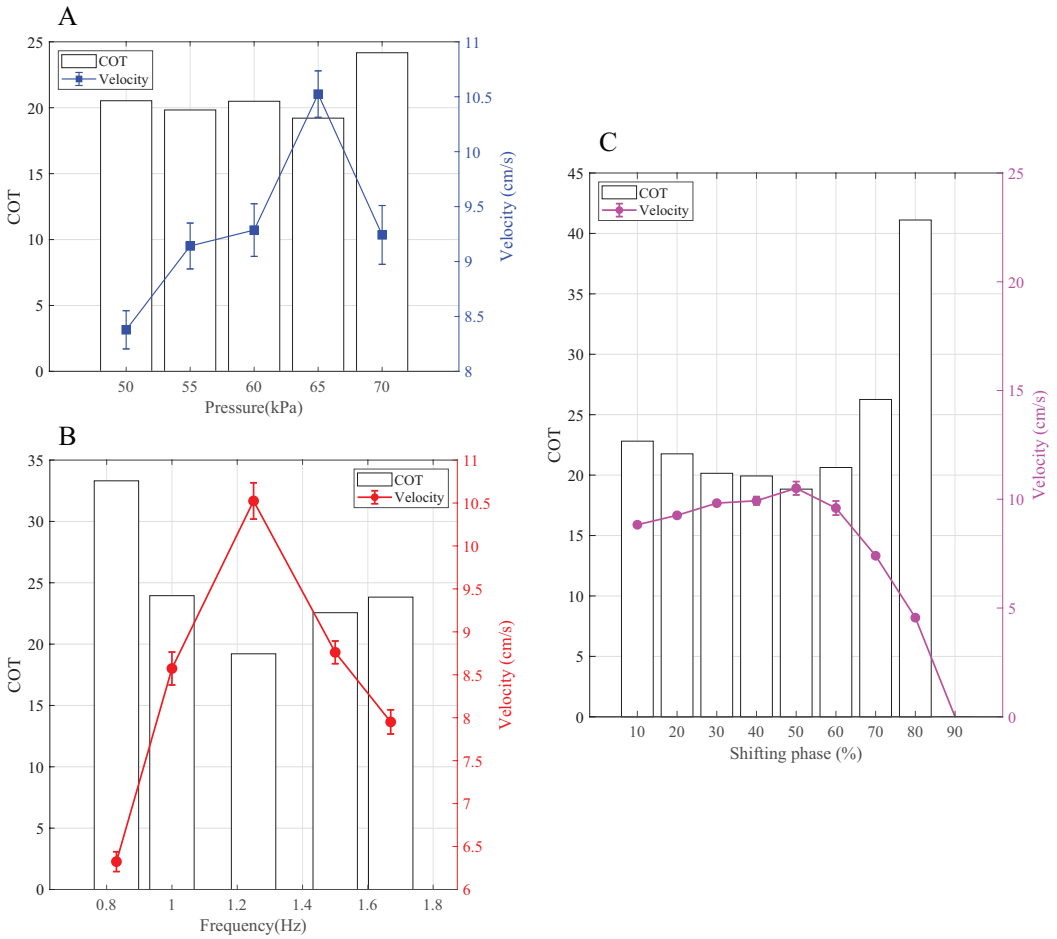


FIGURE 5.16: Pilot experimental results for comparison the eel robot's COT in various condition. (A) The influence of the first segment's input pressure on the eel robot's velocity. The maximum velocity is at 65 KPa, which corresponds to the lowest COT. (B) Eel robot's velocity measured at 5 swimming frequencies at shifting phase of 40 %. The maximum velocity is realized at 1.25 Hz, which corresponds to the lowest COT. (C) Effect of shifting phase of control signals on the velocity and COT value.

increases at the shifting phase from 60 % to 100 %. The data is meaningful for the development of the soft anguilliform swimmer. The novel swimming strategy is suitable for a task requiring fast movement.

## 5.6 Swimming efficiency discussion

The swimming efficiency of the soft eel robot is evaluated based on three factors including thrust force generation, swimming speed, and body posture. For wave generation swimming strategy, within the range of analyzed frequencies (bandwidth) from 0.83 Hz to 1.67 Hz, the thrust force performed a gradual increase. Meanwhile, swimming velocity sharply increased to a maximum at 10.5 cm/s (0.198 BL/s) with

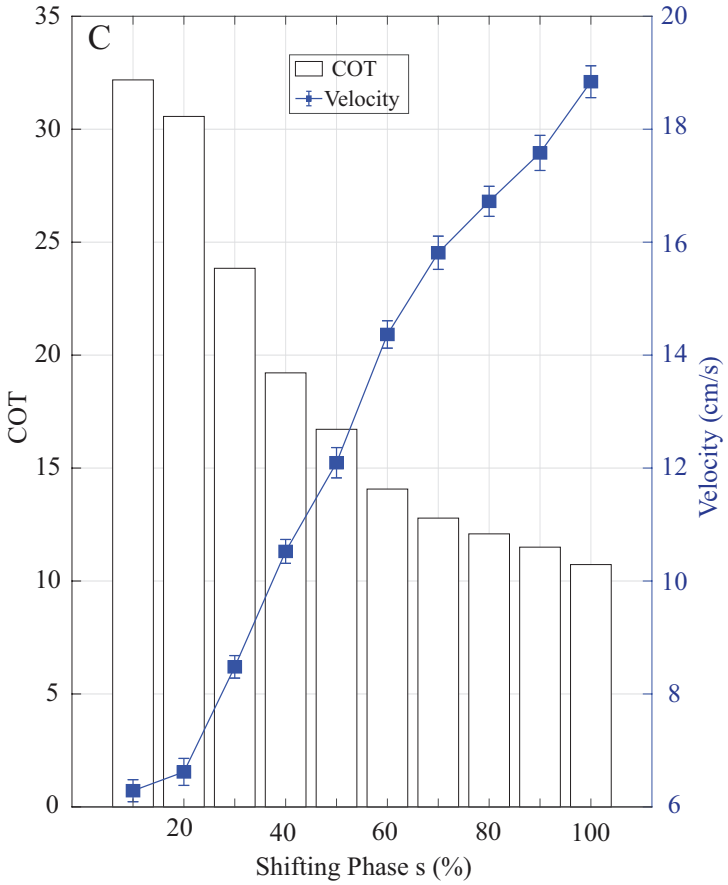


FIGURE 5.17: Effect of shifting phase of control signals on the velocity and COT value since the soft eel robot performing C mode. Interestingly, the velocity increases w.r.t. the rise of the shifting phase and the decrease of COT. Note that the robot in this case was controlled at 1.25 Hz and pressure at three segments from head to tail are 65 kPa, 50 kPa, and 30 kPa, respectively, which correspond to the best values in wave mode.

the best COT of 19.21 corresponding to a swimming frequency of 1.25 Hz (and shifting phase 50 %) and then gradually declined. From these data, we may conclude that swimming efficiency does not depend only on generated thrust force. This conclusion is supported by an analysis of body posture when swimming at different frequencies. The effect of body posture on swimming velocity and swimming efficiency was also further clarified with the experiment of changing the first segment's working air pressure. At the frequency of 1.25 Hz and control shifting phase of 40 % for C shape mode, or 50 % for wave generation mode, the combination of working air pressure at first, the second and third segment of 65 kPa, 50 kPa, and 30 kPa, respectively created the most swimming efficiency with high velocity and low COT. This forwarding speed is faster than that reported on previous research 0.19 cm/s

[50], and 5.45 cm/s [22], however, still lower than speed of natural eel (0.5-2.0 BL/s) [21]. This might come from the hydrodynamic shape of the robot, and the morphology of the robot skin that deserves insightful investigation in the future toward the creation of a high-efficiency robot that is close to a natural one.

**Chapter 5 conclusions**

Based on the experimental approach, the bandwidth of a pair of the soft actuator, which plays as a muscle unit of the soft eel robot, was determined. Air pipe connection method and control strategy was investigated for generating propagation waves from anterior to posterior robot body. A novel swimming strategy that can not be done by natural species and traditional rigid robots was also developed. Interestingly, the novel swimming mode performs swimming efficiency much better than that of the normal one. The experiment was employed to validate the established thrust model that was described in Chapter 3.

# Chapter 6

# Eel soft robot with partial passive body

It can be seen from both natural anguilliform swimmers [22] and traditional rigid anguilliform swimmer-like robots [102] that passive (disable or damage/un-controlled) tail prevented them from speedy movement. Meanwhile, research in [98] provided a piece of evidence about the ability to create propagation waves on a passive body part with suitable stiffness. Generally, an elongated soft eel robot, which is constructed by a series of soft actuators, might commit a failure in swimming forward since one or several actuators are not controlled (partially damaged). In these cases, the robot should be able to perceive the damage and switch to suitable swimming strategies. In this Chapter, we investigated the swimming efficiency of an eel-inspired robot with two levels of the passive tail (due to damage or un-controlled situation) with related control strategies. The main chapter's contents are as follows:

- Investigated swimming strategy of an eel soft robot to find out the suitable shifting phase of the control signal for smooth propagation of wave from anterior to posterior body part of the elongated body when some parts of the body are not in control.
- Evaluated swimming efficiency based on swimming ability and consumption energy of a tethered soft eel robot. Obtained results can be utilized for optimization of the eel robots' design, as well as applied to study movement behaviors of natural eels based on the robotic model.

## 6.1 Swimming efficiency of aquatic animal with partially damaged body

Natural creatures not only possess remarkable mechanisms for interacting and locomotion but also adaptability to a critical case when they break or lose control of their body part accidentally. Holtmaat *et al*. [103] indicated that the cortex and spine of a mouse can adjust to adapt with broken whiskers, which permits the mouse to use nearby whiskers to sense instead of the broken one. Meanwhile, Gemmell *et al*. [22] reported on the differences between negative pressure fields in water (which help create the moving force) that were produced by the normal lampreys and partly disable one (the spinal cord of the mid-body was cut). The disabled ones, after that, only can swim with half the body. The results indicated that the disabled ones could not perform swimming ability as well as the normal ones due to uncontrollable bending kinematics of the body (see Fig. 6.1 (A)). Contrary to these results, this research raised the hypothesis of what if an anguilliform robot swims with a passive body that can bend as close as to the normal/active one, which could not be observed in nature. In fact, the elongated body robot with a partially uncontrolled body might not be possible to test the above hypothesis, since such rigid robots using a series of motors that were discretely connected with heavy mass [4], [104], [105]. However, a soft robotic structure with light mass and a continuous body could be a suitable subject for the evaluation of such a hypothesis.

Some researchers investigated the role of a passive tail, or put a piece of the flexible plate at the end of the tail segment for enhancing the swimming efficiency of the robotic fishes. Zhong *et al*. [67] proposed a novel robot fish propelled by an active wire-driven mechanism with a soft passive tail to accomplish subcarangiform swimming. The fish robot could perform up to 3.5 Hz of the tail beat frequency with the maximum velocity of 2.15 BL/s at 3.0 Hz. Meanwhile, most of the research on fish-like robots used big and passive caudal fin as efficient propulsion supporting parts [29], [34]. Feilich *et al*. [104] investigated the effect of shape and stiffness of passive caudal fins on self-propulsion. The authors only used the simple model of the fish body (two-dimension raw foil caudal fin shape), however, the results can be used as a reference for taking advantage of a passive tail. Regarding the anguilliform

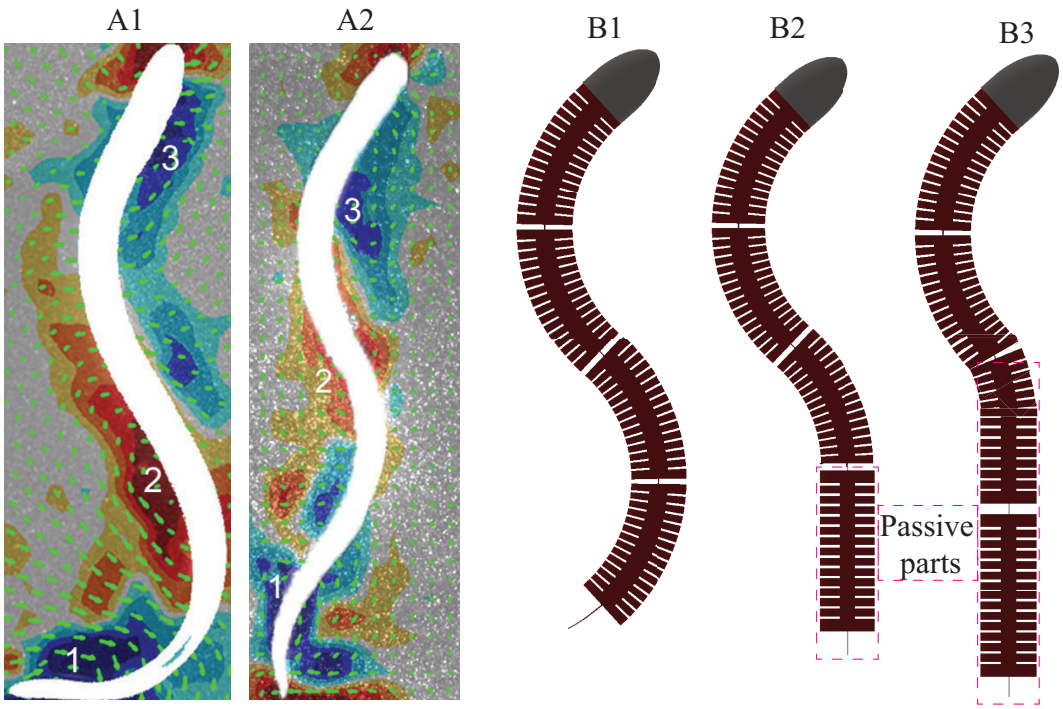


FIGURE 6.1: Natural anguilliform swimmer (A) [22] and the proposed design of anguilliform swimmer robot (B) with active and passive body. (A1) -A normal lamprey. (A2) - A lamprey with a passive half body. (B1) - Design of an eel robot. (B2) - Design of an eel robot with a passive one-fourth body (passive level 1). (B3) - Design of an eel robot with a passive half body (passive level 2).

movement, Leftwich *et al*. [106] addressed the wake structures of the lamprey robot with a passively flexible tail. The authors used three kinds of the passive tail with the same length of about 20 % of the total body length, and three different stiffness levels. The results indicated that the swimming speed of the robot with a passive tail was smaller than that of the original one (0.11 BL/s). Additionally, the robot speed decreased correspondingly to lowering the passive tail's stiffness.

## 6.2 Swimming efficiency of the eel soft robot with partially damaged body

The soft eel robot was set at two modes to investigate its swimming ability with a part of the passive body. Detail description of the two modes is shown in Fig. 6.2 and as follows:

1. Mode 1: The control of the tail segment was deactivated. In this mode, the robot operated with a passive tail (passive level 1).

2. Mode 2: The control of the middle and the tail segment was deactivated (passive level 2).

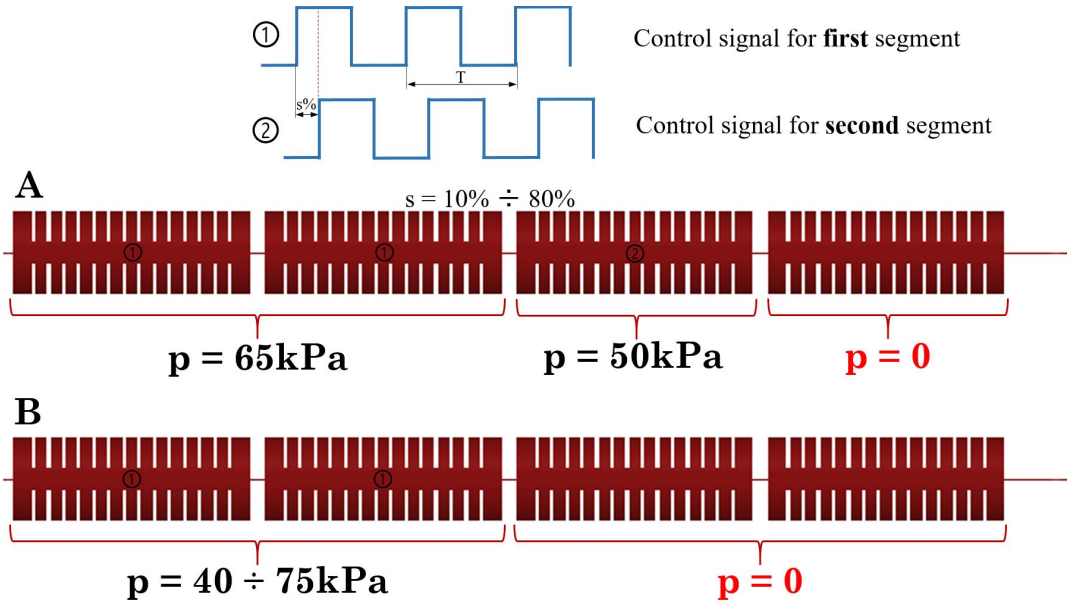


FIGURE 6.2: Two swimming mode with partial passive body. A - Tail segment is deactivated. B - Middle and tail segments are deactivated.

In order to measure the swimming velocity, the robot was placed in a water tank with dimensions of 450×450×900 mm in length, width, and depth, respectively. A high-speed camera (DSC-RX10M4, SONY, Japan) was set on top of the tank for recording the robot movement (see Fig. 5.6). To avoid the bounce back wave from the tank, the robot was controlled to travel along with the tank one time for each measurement trial. The next trial was only conducted after the water surface was stable. Each measurement was repeated five times (trials), then the average and the standard deviation of the speed were estimated. The robot swimming velocities were examined at the frequency range from 0.83 Hz to 1.67 Hz, which was suitable for the designed soft actuator.

### 6.2.1 Swimming efficiency of the soft eel robot performing Mode 1

The active head and middle segments were driven with nominal air pressure values as 65 kPa and 50 kPa, respectively, while the tail segment was deactivated (passively move). Fig. 6.3 shows the variation of robot velocity depending on the control signal's shifting phase s from 10 % to 80 % at four different frequencies. In the examined range, swimming velocity gradually increases corresponding to the rise of the

shifting phase and reaches the peak at range of s from 40 % to 50 % before sharply decreasing. In all four cases, the soft eel robot with a passive tail segment cannot swim forward at a shifting phase of more than 90 %. At 0.83 Hz, the robot speed reaches a peak of 10.5 cm/s (0.198 BL/s) at s = 50 %. The maximum swimming velocities of the eel soft robot with passive tail segment at 1.0 Hz, 1.25 Hz, 1.67 Hz were 14.3 cm/s (0.27 BL/s), 11.7 cm/s (0.22 BL/s), 14.1 cm/s (0.266 BL/s), respectively, at shifting phase of 40 %. The results indicated that the eel robot with a passive tail segment (Mode 1) performs the best locomotion efficiency at the shifting phase of 40 %, which differ from that of the robot driven by a fully active body as the highest velocity dropped to s = 50 %.

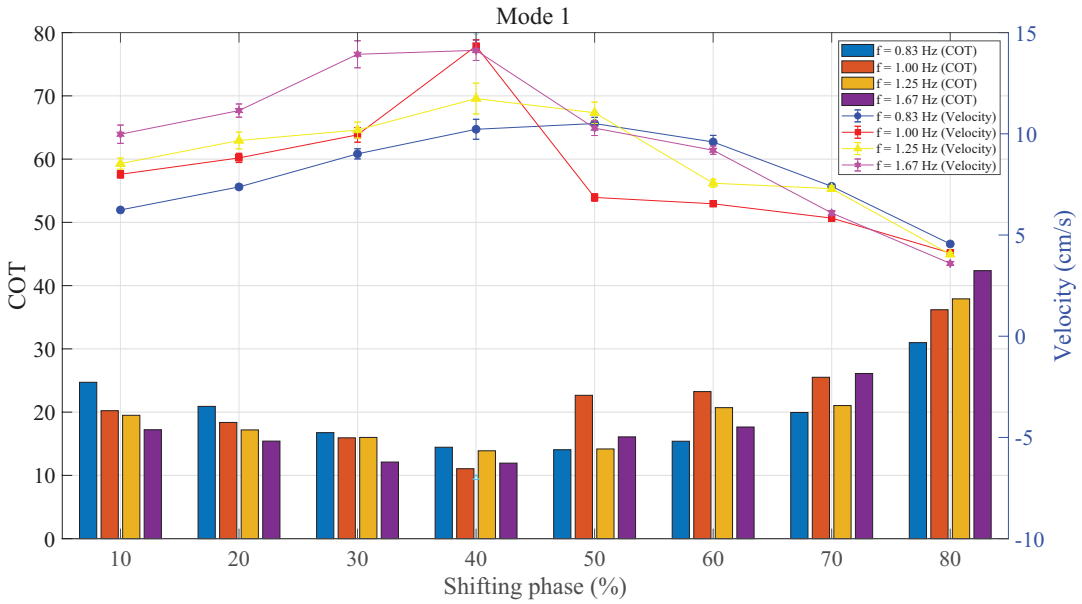


FIGURE 6.3: The variation of the eel robot's velocity and corresponding COT versus shifting phase of Mode 1 when the air pressure at the head, middle, and tail segments were at 65 kPa, 50 kPa, 30 kPa, respectively. The control signal frequency was set at 1.25 Hz.

Over the range of analyzed frequencies from 0.83 Hz to 1.67 Hz, the range of control signal's shifting phase from 10 % to 90 %, and the range of maximum air pressure at the robot's head segment, the variation of the robot's velocity showed the similar tendency. In passive Mode 1, the robot's velocities reach the peaks at the shifting phase around 40 %. Except at 0.83 Hz, the maximum velocity was recognized at the shifting phase $s$ = 50 %. However, the velocity at $s$ = 40 % is only slightly smaller by 2,7 % than that at $s$ = 50 %. There are a small difference of the robot speed at all cases in range of $s$ from 30 % to 50 % since the differences are 14 %, 13.23 %, and 27.2 %

for 0.83 Hz, 1.25 Hz, and 1.67 Hz, respectively. At 1.0 Hz, there was a sudden change in swimming speed tendency, in which the velocity gradually rises from $s$ = 10 % to 30 % before increasing to the peak at $s$ = 40 %, and decreasing to the point at 50 %. Additionally, when the robot swims without any passive/disabled body part, the highest velocities also drop to the range of shifting phase from 30 % to 50 % (see Fig. 5.12). With these velocity variations, it can be concluded that the control's signal shifting phase from 30 % to 50 % is the best range for the movement of the elongated body soft robots that employ a series of pneumatic/hydraulic soft actuator for construction of their body. This relates to wave propagation efficiency. Therefore, to mimic the eel movement, the key point is to create smooth propagation waves from head to tail of the robot by researching the suitable control signal's shifting phase $s$. The changing tendency of acquired data here differs from those in C shape mode, where the swimming speed increased when the shifting phase expanded. The differences come from the variations of swimming postures caused by the pipe order connections (see Chapter 5 for a detailed explanation of the phenomenon).

### 6.2.2 Swimming efficiency of the soft eel robot performing Mode 2

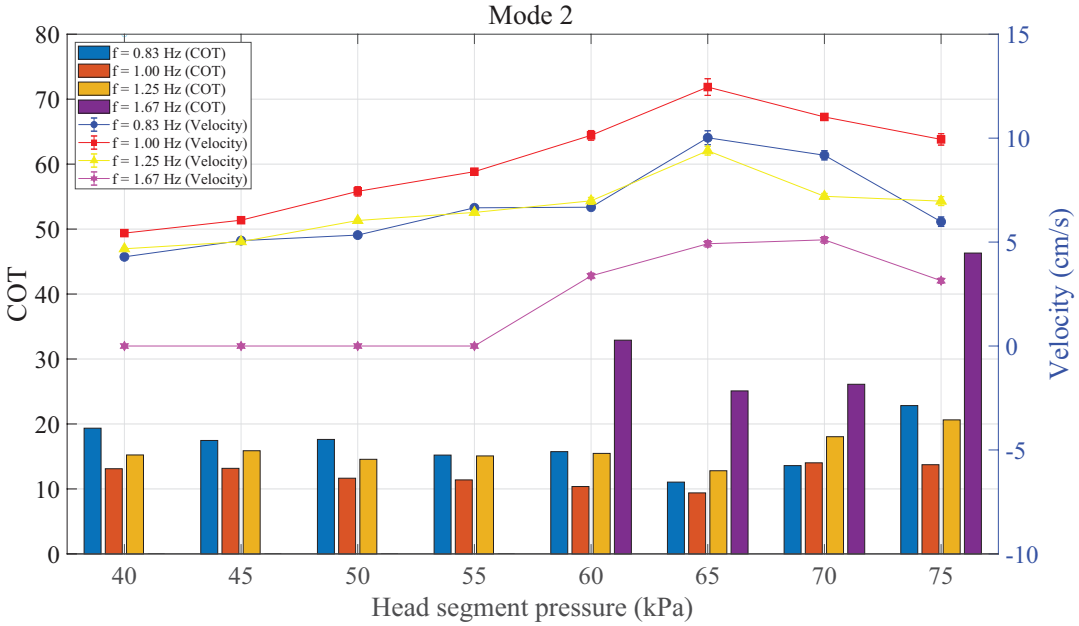


FIGURE 6.4: The variation of swimming velocity (line graphs) and corresponding COT (bar graphs) of the eel robot with passive body level 2 versus maximum pressure value at the head segment at four different frequencies.

In this passive mode, the eel robot body was only driven at the head segment, where the maximum pressure was varied from 40 kPa to 75 kPa with a step of 5 kPa. Fig. 6.4 shows the variation of the robot swimming speed depending on the head segment's pressurization at four different frequencies. In general, the robot velocity rises significantly before reaching the peak at 65 kPa, then decreases. At 1.67 Hz, the maximum velocity is just over 5 cm/s at 70 kPa. Meanwhile, the velocity at 65 kPa, which is slightly smaller than that at 70 kPa, is just under 5 cm/s. The highest velocity is 12.5 cm/s (0.236 BL/s) at operating frequency of 1.0 Hz. The highest speed at 0.83 Hz and 1.25 Hz are 10 cm/s and 9.4 cm/s, respectively. These values are still smaller than the robot velocity at 1.0 Hz with the maximum head segment pressure of 70 kPa that is the second-fastest speed at this working frequency regime (just over 11 cm/s).

### 6.2.3 Elaboration and discussion on active and passive Modes

In this Chapter, the eel body robot was set to swim at two levels of the passive body as aforementioned at Mode 1 and Mode 2. Different from natural eel, which could not perform proper movement when the lower part of its body was deactivated, the robotic eel was proven experimentally to be able to swim even with uncontrolled parts. The success in swimming with a partially disabled body suggests that robotic eel may need fewer degrees of freedom in terms of controlling, thus reducing the necessary resource used in fully-activated mode. This is considered crucial in the design of underwater soft robots, especially when the robot is designed untethered, where passive body parts do not require actuation or consume energy. Additionally, the eel soft robot that swims efficiently with a passive tail will provide evidence for the advantages of the locomotion of bioinspired robots that are not only able to mimic the movement of the natural one, but also perform special locomotion strategies in an effective way that cannot be done by animals. Fig. 6.3 shows the variation of swimming velocity of the soft eel robot when swimming with a passive tail segment, and the robot performs equally compared to a fully activated case. The mostly unchanged performance of the eel robot with a passive tail proves that the robot can create smooth propagation waves along its body based on the morphology of the passive tail segment, which is suitable for receiving and propagating

sinusoidal waves from the head and middle segments. This conclusion can also be supported by the midline kinematics of the robot, extracted by the high speed cameras, as shown in Fig. 6.5 (A) and (B). The displacement amplitude of the tails is almost similar among swimming modes.

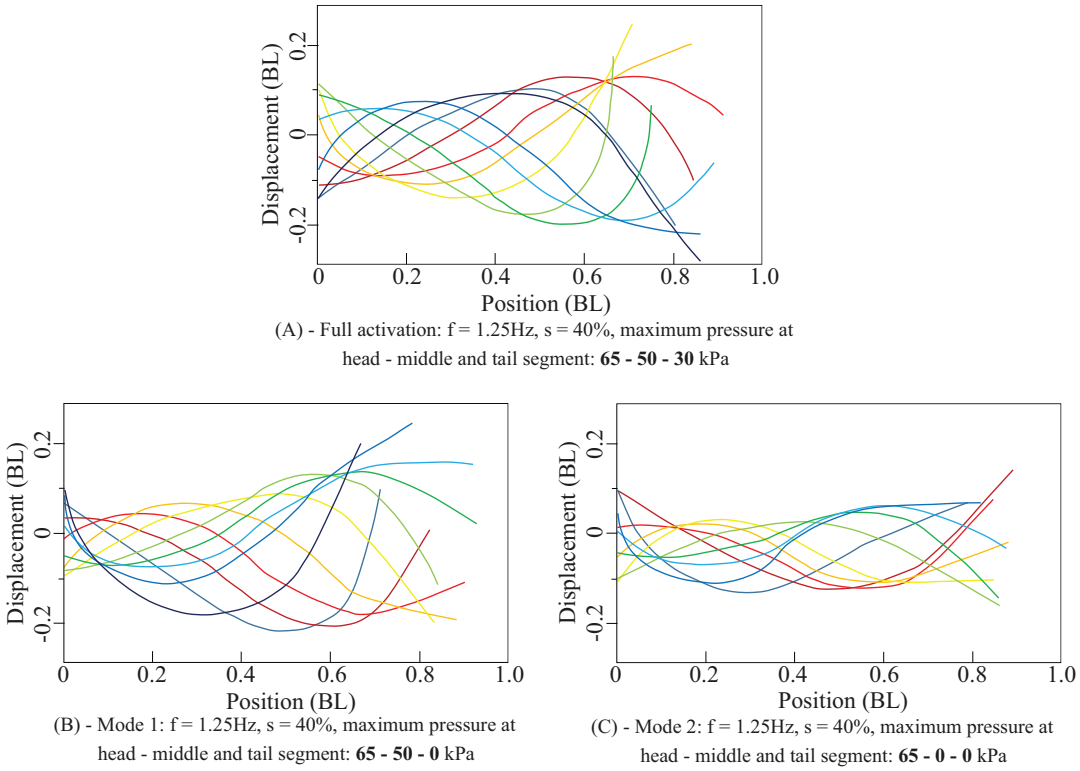


(A) - Full activation: f = 1.25Hz, s = 40%, maximum pressure at head - middle and tail segment: **65 - 50 - 30** kPa

(B) - Mode 1: f = 1.25Hz, s = 40%, maximum pressure at head - middle and tail segment: **65 - 50 - 0** kPa

(C) - Mode 2: f = 1.25Hz, s = 40%, maximum pressure at head - middle and tail segment: **65 - 0 - 0** kPa

FIGURE 6.5: Robot's midline kinematics of the soft eel robot body swimming at different modes. (A) - Swimming at full activation mode. (B) - Swimming at passive level 1 - Mode 1. (C) - Swimming at passive level 2 - Mode 2).

In passive level 2, with an uncontrolled middle and tail segment, the robot did not show efficient swimming performance as the two other modes. At 1.25 Hz, the robot could only swim at 9.39 cm/s which is slower than that of Mode 1 and 2 (9.93 cm/s and 11.74 cm/s, respectively). The body midline's kinematics in Fig. 6.5 (C) also supports this claim, since the displacement amplitude of the tail segment in Mode 3 is much smaller compared to the two others. The low tail beat displacement might come from the inertia of the long passive part of the body at a high frequency (in comparison with frequency bandwidth from 0.83 Hz to 1.67 Hz). However, there is a remarkable point at 1.0 Hz (see Fig. 6.4), at which the robot reaches the forwarding speed of 12.46 cm/s (0.235 BL/s). This working mode is valuable for designing an untethered design of this robot since it consumes the least energy compared to the others.

The main purpose of evaluating the soft robotic eel with damaged (or uncontrolled) body parts is to examine the swimming efficiency relating to energy used. Even though the robot design allows to control segments independently, the robot can still perform swimming when part of the body is deactivated and utilized as a passive tail. This implies that the passive part is helpful for saving energy, especially when the robot becomes untethered. The energy consumption levels at each swimming mode are shown in Table 6.1. It can be seen that the total energy consumption goes down corresponding to the increase of the passive level, in terms of both electrical energy and air pressure (mechanical) energy. The robot speed at passive modes is also higher than that at active mode. The reason is partly due to the stiffness of the robot body, which is considered mitigating wave propagation from head to tail. When performing active mode, pressurized air is distributed to the whole robot body, thus increasing stiffness and preventing wave propagation. At Mode 1 (one-fourth passive body), the robot velocity is higher than at Mode 2 (one-half passive body). This phenomenon is caused by a higher energy expenditure for wave generation.

TABLE 6.1: Comparison of the highest velocity and COT at different Modes

| Working mode (*level*-$f$-$s$ or $p$)* | $P_E$ (J) | $P_A$ (J) | Average velocity (cm/s) | COT |
|---|---|---|---|---|
| 0 - 1.25 - 50 (s) | 5.52 | 7.94 | 10.5 | 18.84 |
| 1 - 0.83 - 50 (s) | 3.96 | 6.09 | 10.51 | 14.06 |
| 1 - 1.00 - 40 (s) | 4.18 | 6.6 | 14.34 | 11.06 |
| 1 - 1.25 - 40 (s) | 4.18 | 6.91 | 11.74 | 13.88 |
| 1 - 1.67 - 40 (s) | 4.18 | 7.29 | 14.12 | 11.94 |
| 2 - 0.83 - 65 (p) | 2.64 | 4.88 | 10.02 | 11.05 |
| 2 - 1.00 - 65 (p) | 2.64 | 5.32 | 12.46 | 9.39 |
| 2 - 1.25 - 65 (p) | 2.64 | 5.54 | 9.39 | 12.8 |
| 2 - 1.67 - 65 (p) | 2.64 | 5.75 | 4.92 | 25.09 |

* *level* 0: Full activation mode, 1: Mode 1, 2: Mode 2, $f$: tail beat frequency, $s$: shifting phase, $p$: head segment pressure

The efficiency of swimming also can be estimated by examining the robot velocity and its corresponding COT. Fig. 6.3 and 6.4 present the correlation between the robot's forwarding velocity and its COT. Because of the small differences in energy consumption among operating modes, the rise of the robot velocity mostly results in the decrease of COT (i.e., higher efficiency). Generally, when the robot performs at the highest velocity, it also implies its high efficiency in energy consumption and swimming. The robot has the best COT of 9.39 in Mode 2 at a frequency of 1.0 Hz and the maximum pressure of 65 kPa of the head segment, at which the speed is performed at 0.12 BL. On the other hand, the highest velocity is 14.34 cm/s (0.27 BL/s) in Mode 2 at a frequency of 1.0 Hz, and control shifting phase of 40 %, however, the COT in this mode is 11.06 larger 15.1 % than the case with the best COT. The analysis of the best COT and the highest velocity of the robot in various operating modes can be applied for designing a similar robot for long-term and long-haul operation tasks.

**Chapter 6 conclusions**

We introduced the soft eel robot's swimming strategy with two (uncontrolled) passive body levels including a one-fourth passive body (Mode 1) and a half passive body (Mode 2). The experiment data indicated that the robot performed the good swimming efficiency at both passive swimming modes, even at a quarter passive body, the robot revealed the swimming ability better than of the robot with fully-controlled mode. Such design enlarges the working ability of the robot at high frequency given the wider bandwidth of the soft actuator or performs backward swimming when the robot works at very narrow area. Moreover, research on the soft eel robot swimming with a partly passive (uncontrolled) body also brings valuable data for the development of the robot swimming strategy for different kinds of tasks.

# Chapter 7

# Undulatory movement for self-propelled colonoscopy

Applications of soft robots are of great interest in endoscopic surgery due to their inherent gentle interactions with the human body. Based on the success of creating propagation waves along the elongated robot body for locomotion, we come up with the idea of scaling the aquatic soft eel robot for colonoscopy purposes. This Chapter will address the following issues:

- Proposed the preliminary design of a soft robot using a series of soft actuators which can be fabricated by molding technique resulting in the miniaturized size of the robot that is suitable for colonoscopy task.
- Investigated on control strategy, in which pulse control signals with suitable shifting phase are found out, to provide undulatory movement (creating smooth propagation waves along the robot body) with high locomotion velocity.

## 7.1 Potential application of soft robot in colonoscopy

Surgery robots including minimally invasive surgery (MIS), endoscopy, laparoscopy, bronchoscopy, and colonoscopy robots play an important role in the medical process due to their small size so that they can provide access to all target anatomy. In recent decades, colonoscopy robots have been rapidly developed on both quantity and quality [107]. Despite the developments, minimally invasive surgery robots still face many challenges such as difficulty to use, patient's discomfort [108], [109], or pain due to the stiffness of instruments [110], or time-consuming medical process [111].

This requires further investigation on the mechanism, working principles, materials to invent new endoscope robots for ease of using, reducing medical time processing, and creating gentle interaction with the human body. Soft robots, which are constructed from soft and deformable materials with multiple degrees of freedom (DOF) and gentle contact with the surroundings, are believed to have great potential for MIS robots applications.

### 7.1.1 Soft surgery robots

Preliminary ideas of soft surgery robots were based on the continuum principle, from which the robots' structure does not contain any rigid link but an infinitive number of dofs with continuous bendability. Cianchetti *et al*. [112] proposed soft and stiffness-controllable medical devices inspired by the octopus. With a stiffness platform and surgical manipulator at end of the device, the proposed device was expected to perform precise intervention for better target reaching. The soft surgery robots that employed this working principle have to engage with a solid base or support structure to manipulate surgery tasks [113], [114]. This does not allow the robots to perform surgery tasks in narrow and long spaces such as the colon. Another approach was to use the magnetism principle to construct and control soft continuum robots for surgery purposes. Kim *et al*. [115] used ferromagnetic composite ink to form ferromagnetic soft continuum robots with omnidirectional steering abilities under outside magnetic actuation. With promising preliminary results, the working principle is expected for potential medical applications. Based on a similar principle, Dario deployed Endoo Project, in which the idea of a magnetic-driven soft-tethered endoluminal robot was investigated to develop an active colonoscopic platform for the navigation of colonoscopy robot with magnetic head [116].

### 7.1.2 Self-propelled soft colonoscopy robots

Performing endoscopy is a technical procedure and it is considered difficult even for experienced doctors. To tackle this issue, researchers put effort to develop self-propelled colonoscopy robots. Suzumori *et al*. [117] proposed two mechanisms called "thin tube wave generation" and "round bubbler" applying for colonoscopes.

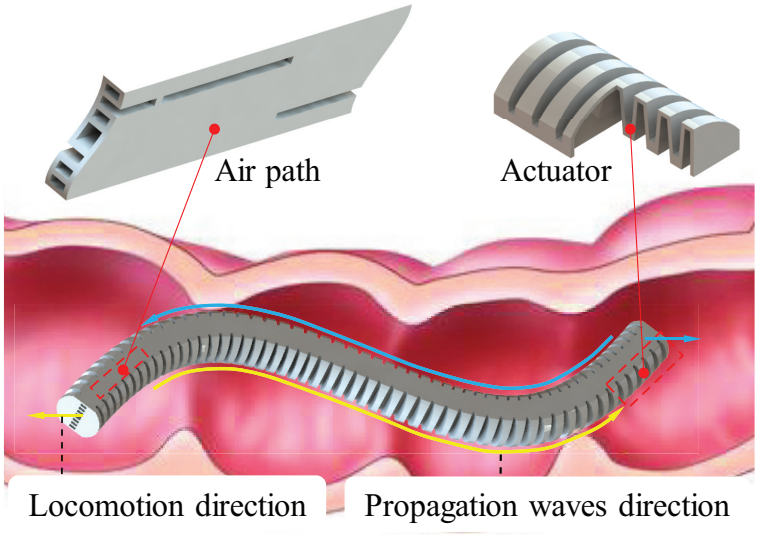


FIGURE 7.1: self-propelled colonoscopy robot constructed from series of soft actuators using undulatory movement to travel in colon in both forward and backward directions.

The colonoscopy robot covered with a thin tube wave generator reached a speed of 40 mm/s, meanwhile, that equipped with a round bubbler has a velocity of 1.3 mm/s. These are promising results for the future development of soft self-propelled colonoscopy robots. Nonetheless, it has been required to make an investigation on the efficient locomotion of these types of robots in large diameter environments like the colon when the robot only moved efficiently in small tubes. Other researches were mainly inspired by inchworm, earthworm, or snake. Bernth *et al*. [118] introduced an untethered robot constructed by three separate segments that were covered by elastic mesh and driven by tendons actuated by an on-board motor. The robot is able to move forward and backward and reaches the highest velocity in a simulated colon environment at 1.21 mm/s. Meanwhile, Manfredi *et al*. [119] reported a soft pneumatic inchworm double-balloon mini-robot for colonoscopy constructed by three dofs soft pneumatic actuator with two balloons at both ends. The robot was able to move in different sizes of a tube from 36 to 72 mm in diameter. The self-propelled velocity of the robot can reach 2.8 mm/s in the colon's simulated geometry environment.

It can be seen that there have been many pieces of researches on self-propelled soft colonoscopy robots as aforementioned. However, all of them performed at low velocities resulting in taking a long time to finish medical procedures. Hence, in this

Chapter, we propose a self-propelled soft colonoscopy robot with the target of high-speed locomotion in a simulated colon geometry environment (phantom model). The robot employs a series of soft actuators (see Fig. 7.1 and a pulse control signal with a suitable shifting phase to create propagation waves to move forward or backward.

## 7.2 Soft conoloscopy robot design, fabrication, and control

### 7.2.1 Development of a physical model of the robot

Soft elongated body robots have been investigated on both terrestrial and aquatic movement [120], [121], in which the soft robots employed a series of pneumatic actuators and pulse signals with suitable shifting phase to create propagation waves from head to tail to move forward. In these researches, two opposite actuators are activated by two pressurized air sources that are supplied in opposite phases, while adjacent actuators are activated by these in the shifting phase. This robot structure and operating principle seem to be suitable for aquatic soft robots [121] but terrestrial soft robots without any supporting mechanism such as wheels. We also conducted experiments with a mini scale of the soft eel robot (similar structure and working principle). Two types of body robots including three and four pairs of soft actuators were fabricated. The highest velocity was at approximately 3.7 mm/s that was very low and was not suitable to develop a colonoscopy robot. Thus, in order to overcome the drawback for soft elongated body terrestrial robot, Qi *et al*. [122] introduced a novel pneumatic soft snake robot for working in a constrained environment. The robot whole design is suitable for 3D printing technique leading to large size (approximately 520 mm in length) and high energy consumption for operation. The design and fabrication technique, therefore, is not suitable for miniature colonoscopy robots. Based on that proposed working principle, we come up with the idea of a new design of a self-propelled colonoscopy soft robot using a series of soft actuators that are designed to get a suitable structure for fabrication by molding technique.

The robot is constructed from two main parts including air path and actuators

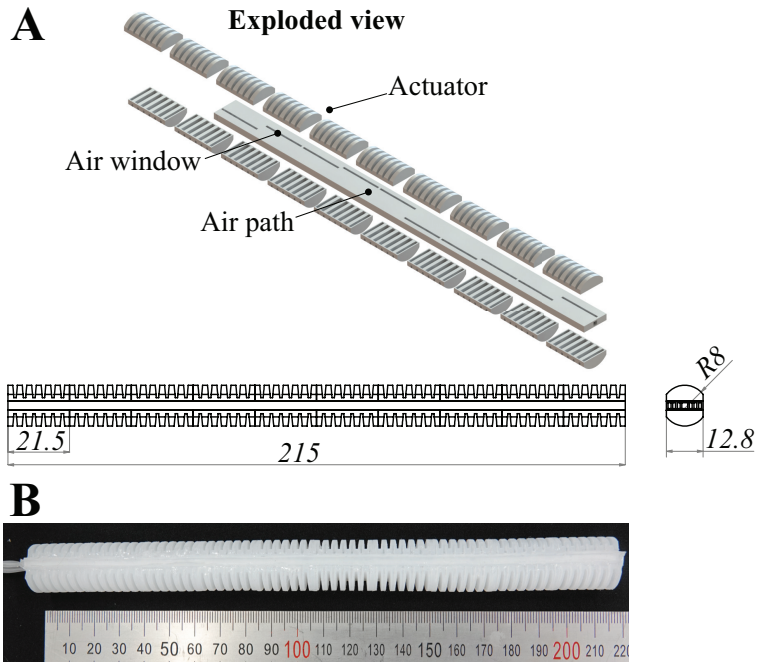


FIGURE 7.2: Soft colonoscopy robot. A - Design of the soft self-propelled colonoscopy robot using series of soft actuator to creating undulatory movement. B - Fabricated robot

as shown in Fig. 7.2. The air path includes four air channels for air supply to create undulatory movement. In the air path, air windows are arranged to distribute pressurized air from air channels to corresponding actuators. Pressurized air is distributed in order that the robot is able to generate sinusoidal wave-like locomotion, in which there are transient zones between crest and trough for creating smooth serpentine waves. Toward this end, four actuators are grouped into one segment and air windows are arranged so that one segment can perform four modes including crest, trough, transient from crest to trough, and transient from trough to crest (see Section Control strategy for wave propagation for more detail). In this research, only one type of actuator was used combined with the distribution of air windows on the air path for creating the four states of a segment, meanwhile, in [121], four types of actuators were introduced.

### 7.2.2 Fabrication

After finishing the robot design, molds for fabricating the robot parts (air path and actuator) were designed and fabricated. Fig. 7.3 shows the design and fabrication process of the robot parts. Based on the design of the robot (as shown in Fig. 7.2),

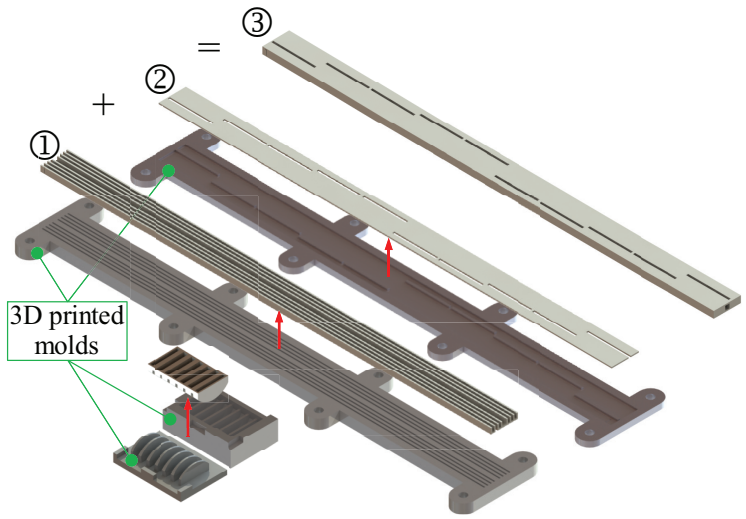


FIGURE 7.3: Design of the robot parts' molds and basic fabrication process of the robot parts.

molds for the robot's parts including actuator molds and air path molds were designed by SolidWorks (Dassault Systemes). The molds, then, were fabricated by a 3D printing technique, in which actuator mold was made by Acrylonitrile butadiene styrene (ABS) using Zortrax M200 printer, and air path molds were made by Polylactic acid (PLA) using Prusa i3 MK3. Silicone rubber Dragon skin 30 (Smooth-On, Inc., USA) was chosen for fabricating the robot. After being fabricated, the separate parts of the robot were glued together by Dragon skin 30 when it is still in liquid state.

### 7.2.3 Control strategy for wave propagation

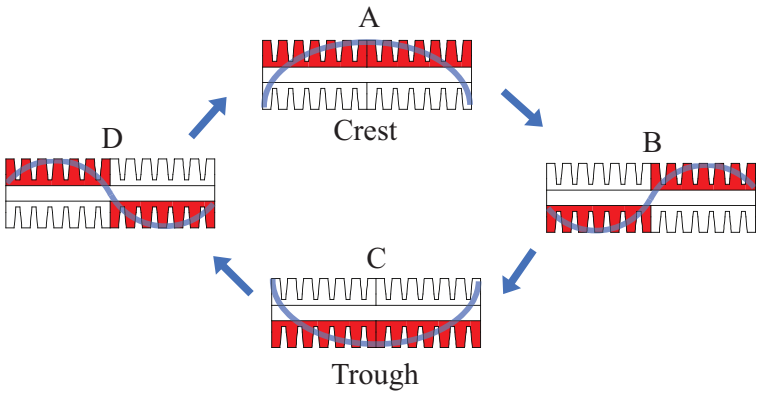


FIGURE 7.4: Deformation modes of one segment, where the actuators colored in red are filled with air, and blue curves indicates the shapes of the segment.

To create smooth propagation waves along the robot body, besides shaping crest and trough, each body segment called actuation unit should be able to perform transient shape. Therefore, four actuators were grouped into one actuation unit, from which four bending modes can be carried out as shown in Fig. 7.4. Four modes were named $A$, $B$, $C$, and $D$, where $A$ stands for crest mode, $C$ stands for trough mode, $B$ is transient mode from crest to trough, and $D$ is transient mode from trough to crest. Pressurized air is supplied so that the actuation unit change status between four modes periodically (for more detail on working principle see [122]). By periodically supplying air to four air channels, the five segments deform orderly resulting in propagation waves from end to end of the robot body, which allows the robot to move forward or backward depending on propagation direction (see Fig. 7.1).

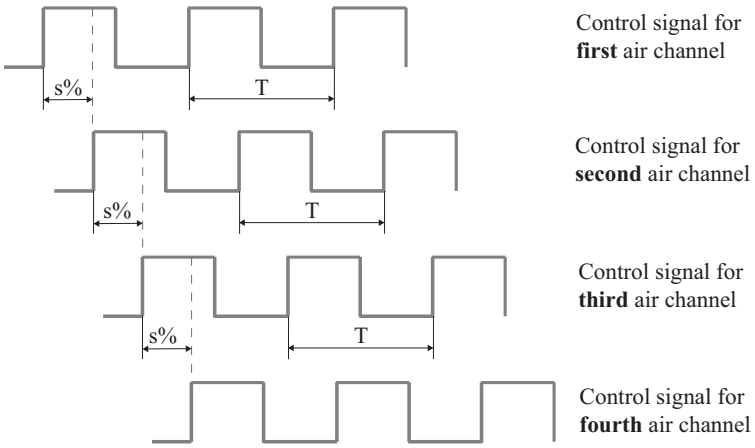


FIGURE 7.5: Diagram of control signals for four segments of the colonoscopy robot, where $T$ is cycle time, and $s$ is shifting percentage ($s$=100% corresponds to half of the cycle $T$).

In order to achieve such undulatory locomotion, the control signals for four solenoid valves that dispense pressurized air to the four air channels are planned as shown in Fig. 7.5. By adding a shifting phase between each control signal, actuation units are active sequentially leading to sinusoidal waves along the robot body. The shifting between control signals of the air paths' distribution is $s$ percent of the cycle time $T$. By changing the length of the shifting phase, the period of each mode is manipulable, thus, the travel velocity is alternated. The effect of shifting phase and frequency (one over cycle time) on the performance of locomotion will be investigated.

Regarding the robot activation, each air channel is connected to a solenoid valve

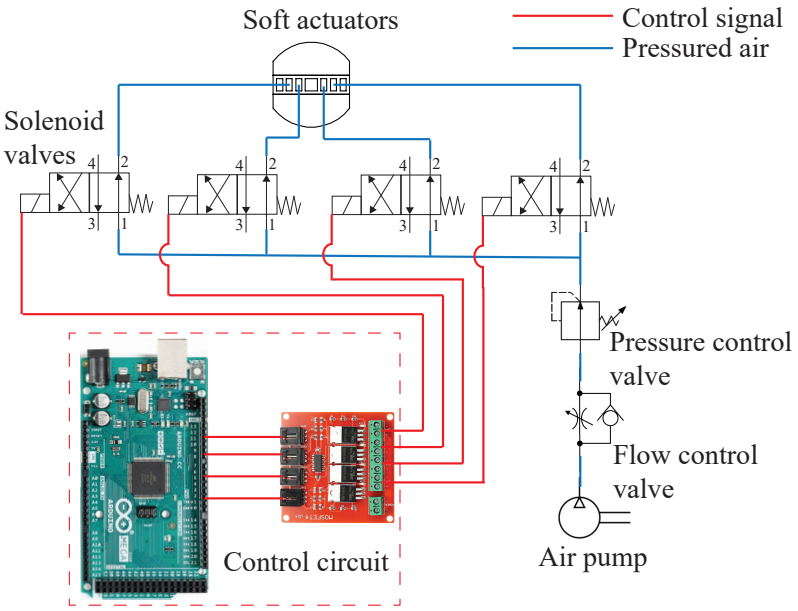


FIGURE 7.6: Diagram of control system. Arduino and Mosfet were used to control the on/off status of four solenoid valves that contribute pressurized air to four air channel. Mechanical flow control and pressure control valves were used to adjust total air pressure working on the robot.

(VQD 1121-5L; SMC, Japan), which is 4/2 way and has four ports named 1 to 4. Port 1 is the inlet port, port 2 is the outlet port, port 3 is the exhaust port, and port 4 is unused. The opening of the solenoid valves is regulated through a four-channel switch (MOSFET 4, UO 4) by a control program written on an Arduino (Arduino, Mega 2560). Arduino control code is similar to that shown in Appendix A (for the soft eel robot) by adding a task for solenoid valve number 4. To provide pressurized air for the system, the four solenoid valves are linked to a compressor (JUN-AIR). Before going through four solenoid valves, a pair of the throttle valve and pressure regulator valve are used to adjust the flow rate and pressure of the air input into each of the air paths. The control system is illustrated in Fig. 7.6.

## 7.3 Experiment and validation

The colonoscopy robot was placed inside an acrylic tube having a length of 500 mm and an inside diameter of 45 mm. To record the sequential images of the robot's self-propelled, a DSC-RX10M4 camera (Sony, Japan), which was situated 500 mm above the tube was used. To evaluate the locomotion ability of the robot, its tail beat

frequencies were varied between 2.0 Hz and 4.0 Hz with the step of 0.5 Hz, while the shifting phase was set to be between 30 % and 55 % of cycle time. The system operated at 60 kPa, 70 kPa, 80 kPa, and 90 kPa of air pressure. The robot will be moved along an acrylic tube and the frame data of locomotion in a marked section of 100 mm were extracted using Matlab R2020b (MathWorks). The best-resulted parameters were then used for the experimenting of the robot inside a rubber colon-rectum tube for the same 100 mm distance. The colon model was situated on a clear glass surface, and an LED photography light (Neewer, China) was placed 120 mm above the examined section, while the position of the camera was 400 mm under the glass surface. Since the rubber wall was hardly transparent, objects inside the colon model could not be observed, thus the light was used to produce detectable shadows of the moving robot (see Fig. 7.9 (A)).

### 7.3.1 Locomotion in acrylic tube

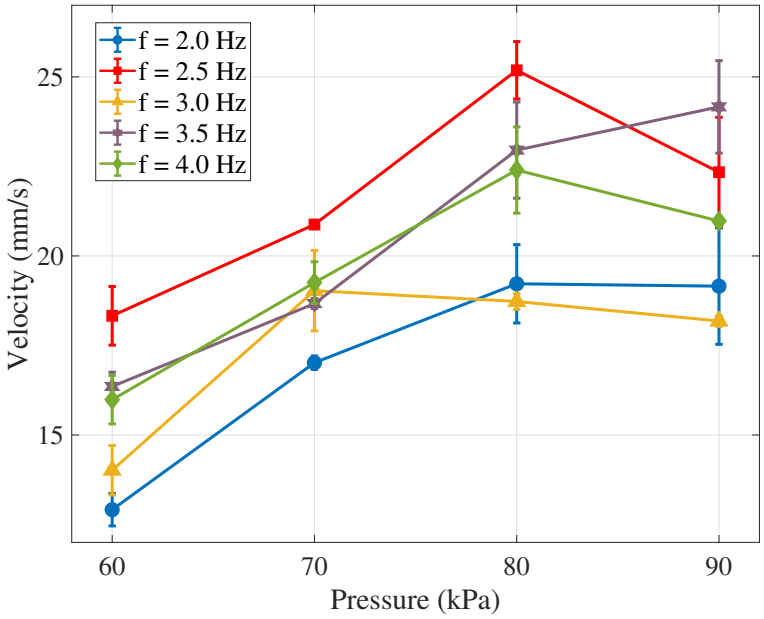


FIGURE 7.7: The variation of straight locomotion velocity in plastic tube of colonoscopy robot versus pressure at five different frequencies.

Firstly, the best pair of values for frequency and pressure were identified by measuring the velocity of straight locomotion in an acrylic tube with a diameter of 45 mm that roughly equal to the average diameter of the human colon. Each test

run was repeated three times (trials) for each set of the above parameters. Regarding the shifting phase for the first experiment, according to our previous research on anguilliform swimming performance, the most cost-effective shifting phase mainly dropped into 50 %, therefore, this value was fixed at 50 %. Fig. 7.7 shows the variation of velocity corresponding to the applied pressure, which ranges from 60 kPa to 90 kPa, at five frequencies. The reason for choosing the pressure range is locomotion efficiency and the limitation of endurance of the robot. Specifically, at below 60 kPa, the robot cannot perform efficient serpentine waves along its body, meanwhile, over 90 kPa might break the robot at the actuators' position. The results reveal that both tail beat frequency and working pressure affect the robot locomotion's ability. The velocity reached a peak of 25.18 mm/s when the robot operated at 80 kPa of pressure, and 2.5 Hz of frequency. The reason for the decrease of locomotion velocity at higher frequency could be that the contact period was not enough to generate sufficient friction for advancing. On the other hand, a pressure value greater than 80 kPa would result in large deformation of the robot, which limited the maneuverability in confined space.

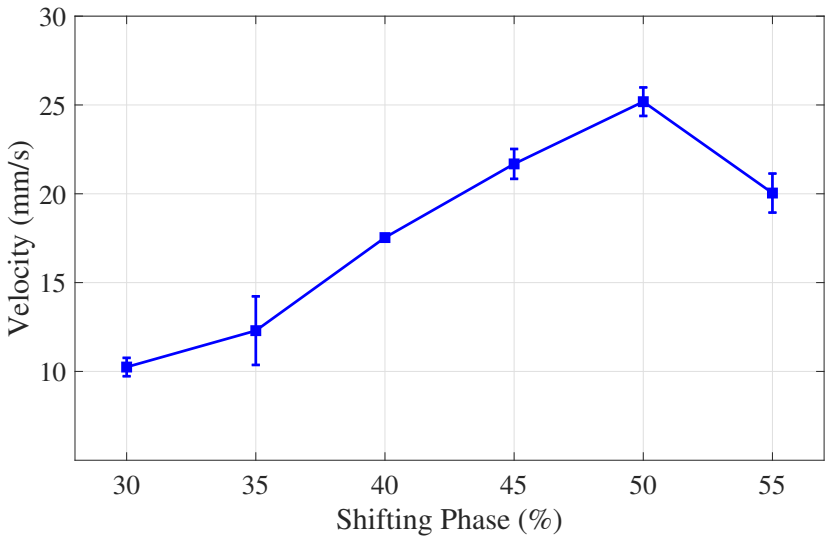


FIGURE 7.8: The effect of control shifting phase on movement velocity of the robot on acrylic tube.

In the next phase, because of the differences of design principle and working environment between the elongated robot body as mentioned in previous Chapters - an aquatic robot and the robot in this research - a terrestrial robot, effect of control shifting phase at the best locomotion velocity was re-investigated. The pressure and

frequency were set at 80 kPa and 2.5 Hz, respectively, meanwhile the control shifting phase was varied from 30 % to 55 % with the step of 5 %. The result is shown in Fig. 7.8. The velocity gradually increases corresponding to the stepping up of the control shifting phase and reaches a peak at $s$ = 50 % before gradually decreasing. This result is similar to researches on the elongated body soft aquatic robots.

### 7.3.2 Locomotion in colon model

Experiment on straight locomotion of the robot was conducted in a colon model to preliminary evaluation working ability of the colonoscopy robot. The robot was moved in a dry and straight colon model as shown in Fig. 7.9 (A) at working parameters of $f$ = 2.5 Hz, $s$ = 50 %, and air pressure was varied from 70 kPa to 90 kPa. The data of the highest and lowest robot velocity at 2.5 Hz and 2.0 Hz, respectively, when working at the acrylic tube were extracted to compare with the locomotion ability of the robot at the colon model as shown in Fig. 7.9 (B). It can be seen that the robot velocities at the colon model are smaller than those at acrylic tube and working pressure still strongly affects the robot locomotion ability. Differing from the trending of velocity data when the robot moved in the acrylic tube, the robot velocity, in this case, goes up corresponding to the increase of working pressure when the speed reaches the peak of 19.26 mm/s at 90 kPa.

The experimental results have proven the ability of the proposed colonoscopy robot in locomotion inside cylinder-shaped objects. The variation of the robot velocity in Fig. 7.7 indicated that working pressure strongly affects the robot locomotion capability. The variation closely relates to locomotion gait, in which higher pressure creates bigger lateral displacement resulting in higher thrust force generation that is created by reaction force between the robot body and the surrounding (acrylic tube inside wall). Effect of locomotion gait on elongated body soft robot also analyzed in the Chapter 5. The velocities, however, decrease regardless of the increase of working pressure. The phenomenon can be explained due to the increase of both contact area and action force between the robot body (at serpentine locomotion) and the tube wall leading to the going up of friction force that impedes the robot movement. Fig. 7.10, which shows the variation of the robot body deformation when moving in the rigid tube, provides the evidence for our claims. The red arrows indicate the large

deformation of the robot body at high working pressure due to the constrain of the working environment.

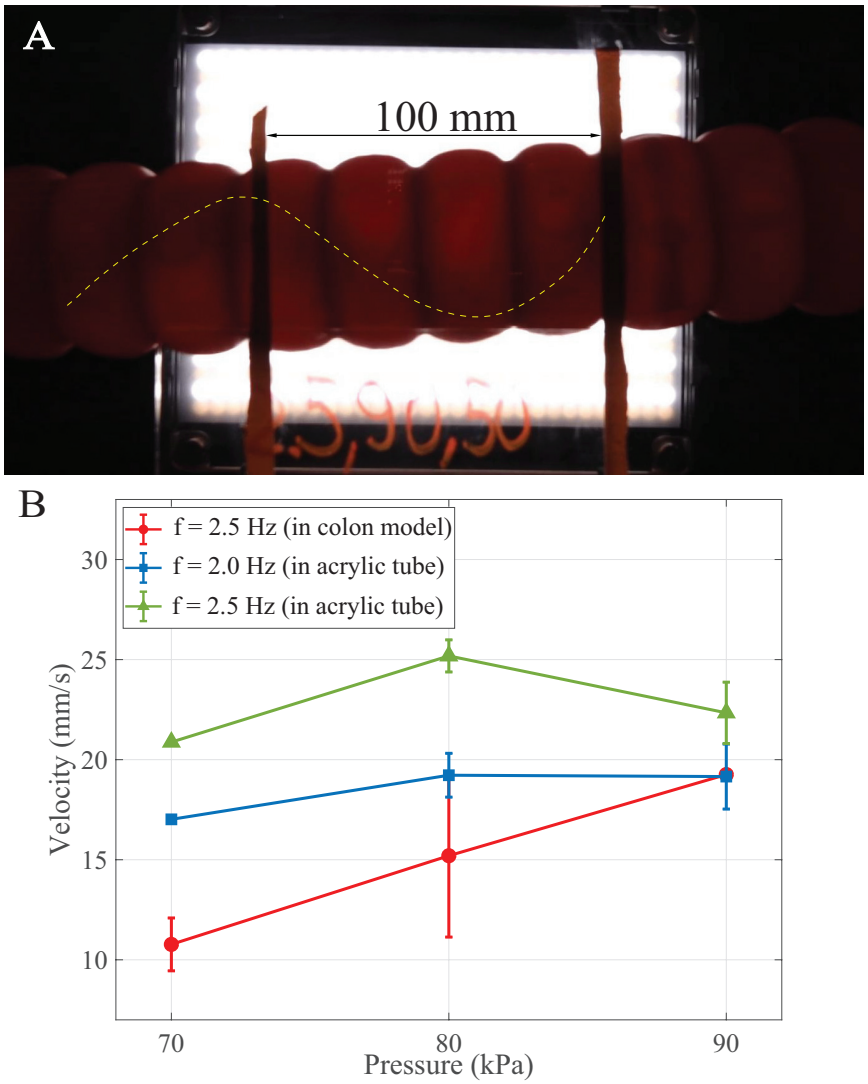


FIGURE 7.9: A - The soft colonoscopy robot moves in the colon model. B - The variation of the robot velocity moving in the colon model at 2.5 Hz depends on working air pressure in comparison with that working in the acrylic tube at 2.0 Hz and 2.5 Hz (two robot's speed boundaries).

Another parameter strongly affecting the robot velocity is the control shifting phase $s$. Data in Fig. 7.8 shows the best value of $s$ for the soft colonoscopy robot is at 50 %. The control shifting phase determines the propagation ability of waves along the robot body. The actuation unit on the robot body was activated sequentially from end to end to form such propagation waves. The sequence degree depends on the value of $s$, and at $s$ = 50 %, the smoothest propagation waves are generated. In other words, with this design principle at this value of $s$, four consecutive actuation units will be in states of A, B, C, then D cyclically. This result is quite similar to that of

elongated body soft aquatic robots as shown in Chapter 5.

Meanwhile, there are dissimilarities in the performance of the robot in the two working environments. Particularly, at 90 kPa, there was an improvement in the speed of the robot inside the colon model, compared to the compromise of increasing pressure on the velocity seen in the acrylic tube setting. It can be seen that greater tail beat amplitude would be more tolerable in the stretchable rubber colon, while a hard glass surface would result in more resistance as the deformation increased. Therefore, the dissimilarities could be explained due to the deformation of the colon wall. The deformation leads to less constrain of serpentine wave locomotion of the robot at 90 kPa compared to that working in the rigid tube. In other words, the robot moving in a deformation environment, in this case, suffer less friction at the two side surfaces. If suffering less friction, why does the robot move slower (19.26 mm/s compared to 22.34 mm/s)? This also comes from the deformation of the working environment that partly absorbs active forces of the robot body for locomotion resulting in lower thrust generated compared to that in the rigid environment. The increase of robot velocity corresponding to the stepping up of the working pressure might also come from more energetic movement when supplying more pressurized air helped the robot overcome ridges on the inside of the colon model.

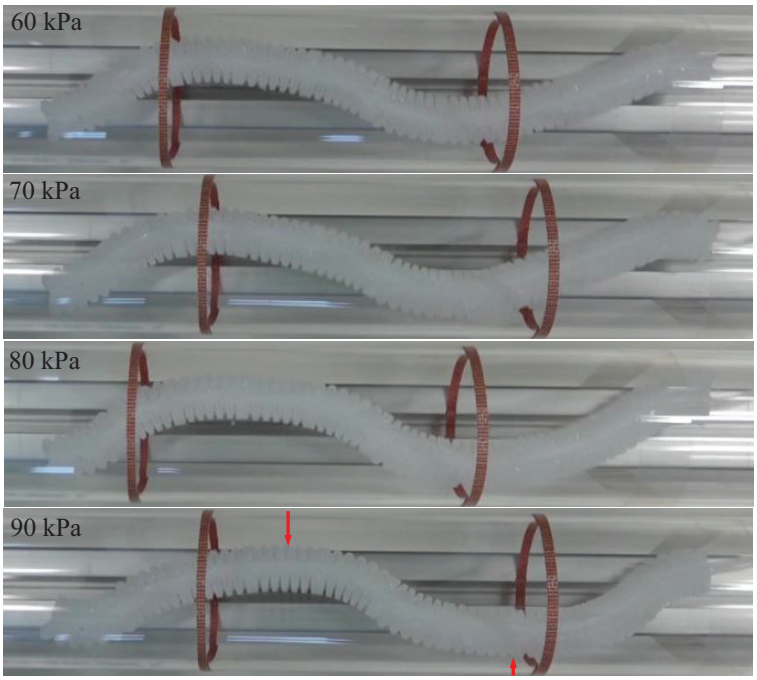


FIGURE 7.10: The variation of the robot body deformation when working in the acrylic tube at $f$ = 2.5 Hz, $s$ = 50 %, and air pressure is varied from 60 kPa to 90 kPa.

**Chapter 7 conclusions**

In this Chapter, the novel self-propelled soft robot for colonoscopy was developed. The robot used a series of soft actuators, which are fabricated by molding technique, and pulse control signal with shifting phase to generate undulatory movement. The robot can move with the highest velocity of 25.18 mm/s (with working parameters: $f$ = 2.5 Hz, $s$ = 50 %, $p$ = 80 kPa, moving in acrylic tube with diameter of 45 mm) that much higher than the previous self-propelled soft colonoscopy robot (2.8 mm/s) moving in large tube diameter. In the colon model, the robot velocity reaches the peak at 19.26 mm/s. This result reveals the potential application of the proposed robot for tasks related to medical treatments of the human colon.

Nonetheless, there are some important aspects that have not been investigated yet. Firstly, the interactive force between the robot body and colon wall should be studied because it determines the patients' comfort that is the most important characteristic of a colonoscopy robot along with velocity (procedure time). Therefore, the balance between the robot velocity and its active force on the colon wall is very important. Secondly, the structure of the human colon contains a vertical segment. The colonoscopy robot is called self-propelled when it is able to move over this segment without outside pushes. Thus, a mechanism or a new locomotion strategy must be invented for vertical movement. Finally, basic accessories including a camera and a turning segment at the robot head for colonoscopy procedure have to be equipped. The structure and attaching method of these accessories should have no/little effect on the robot locomotion ability. Three aforementioned issues will be addressed in our next research to invent the complete novel self-propelled soft colonoscopy robot.

# Chapter 8

# Conclusions and visions

## 8.1 Summary

Up to now, more and more efforts have been put into creating a new robot generation that can interact gently and safely with the surrounding environments. Animals have evolved their body structures and a remarkable diversity of mechanisms to interact with their surrounding environment and other creatures. Accordingly, replicating natural creatures' movements and behaviors in robotics systems, which utilize soft and deformable materials for their body constructions, can achieve animal-like capabilities for our use in both practical purposes such as transportation, medical devices, and scientific investigation on natural life and behaviors. These reasons motivated us to create soft bio-inspired robots. Toward contributing to the biomimetic soft robot community, the elongated body soft robots that can perform anguilliform/wave-like locomotion were investigated for all design, modeling, control, and locomotion strategy, and application aspects.

### 8.1.1 Design and fabrication

Regarding the design of the soft eel robot, we presented a pneumatic semi-cylindrical soft actuator with a segmented and chambered structure accompanied by narrow air connecting channel which allows the soft actuator to bend easily as actuated. A simulation method was employed to determine the suitable structure. A pair of the semi-cylindrical soft actuators form the circular cross-section mimicked from the eel body. Each pair of the pneumatic soft actuator plays a role of a muscle unit that can perform a flapping movement. A series of soft actuators were used to form a soft

eel robot body. With the modulation design, in which each pair of soft actuators was a cell, the soft body can be constructed from any number of the cell. Nonetheless, in this thesis, toward replication anguilliform swimming performance, four pairs of soft actuators that were divided into three segments were used. The fabrication process of the soft actuator (by molding technique) and of the soft eel robot was also detailed described.

For a miniature scale of the elongated body soft robot, different air contribution method for smoother wave propagation that can perform better terrestrial locomotion efficiency was employed. A totally soft robot body design was introduced. The small robot is divided into two-part including a soft actuator and a soft air path, which can easily fabricate by a molding technique. The fabrication process for the colonoscopy robot was introduced. The modular design also permits the robot length as much as possible. The special point of the design is that it only requires four air channels to actuate an infinitive number of soft actuators.

### 8.1.2 Control and locomotion strategy

The bandwidth (tail beat working frequency range) of the soft eel robot was determined by an experiment in a similar working condition of the robot. Due to the modular design, the determination process is only performed on a pair of soft actuators. For wave generation along the robot body, pulse control signals with shifting phase, which allow the soft actuator to be actuated orderly, was introduced. Research results indicated that tail beat frequency, supplying pressurized air, and control shifting phase strongly affect the swimming efficiency of the soft eel robot body. The control shifting phase puts the biggest influence on the robot's swimming efficiency, in which the value from 30 % to 50 % is the best range for creating smooth propagation waves along the robot body. We introduced a simple control system that used only one pressurized air source (one air pump), solenoid valves are driven by pulse signal controls with equal shifting phases were used to contribute air to corresponding segments.

Three swimming strategies were innovated. The first one is propagation wave mode that the robot body creates sinusoidal waves from head to tail or vice versa. The second one is the C shape mode, in which the robot body from a C curve is then

released to interact with surrounding water for locomotion. To perform this mode, the air pipe connection at the second segment is inverted and the control shifting phase is set at 100 %. The last one is the passive mode that the lower part(s) of the robot body is deactivated simulating the broken state of these parts. Two passive levels include deactivating one-fourth of the robot body (tail segment) - passive level 1 and deactivating half the robot body (tail and middle segments) - passive level 2 were introduced. Interestingly, the swimming velocity at C shape mode and passive mode level 1 is bigger than that of traditional mode. Additionally, the two novel modes can not be done by natural species and traditional rigid elongated body robots. They might be very useful for the development of a soft robot for fast-moving tasks (C shape mode), long journey tasks due to low power consumption (passive mode), and also enlarge the working condition of the soft eel robot since the lower body parts are damaged.

Regarding the miniature one, although there is a little different structure (difference in air contribution to actuators), the control strategy is similar. Four air channels were driven by four pulse signal controls were used to actuate 20 actuators affixing symmetric from both sides of the air path. The best locomotion performance drop to the control shifting phase of 50 %. Air pressure and flapping frequency also strongly affect the straight velocity of the colonoscopy robot. Due to the construction, the mini soft eel robot can only perform wave-like locomotion mode.

### 8.1.3 Modeling

The hydrodynamic model that considers the effect of whole-body movement of the eel-like body's locomotion was constructed. The model was built based on the continuum approach, in which the reactive force at any point (an element reactive force) along the mid-line, and the angle ($\theta_i$) between its vector and swimming direction are determined. The total reactive force, thus, can be calculated by integrating the horizontal component of the element reactive force along a wavelength $\lambda$ forming by the eel body as performing anguilliform locomotion. The model was then utilized to predict the propulsion of the eel robot at different working regimes. Also, the model brings in an approach for estimating the drag force coefficient of anguilliform movements, even when it is difficult to set up an experiment and conduct measurement

due to the complex motion of the object.

### 8.1.4 Application areas

Regarding the soft robotic eel, we demonstrated the ability of the anguilliform performance of the soft robot body with four pairs of actuators. Thanks to the soft body, the robot is able to create gentle contact with surrounding environments. Thus it has potential applications for monitoring aquatic ecosystems. Additionally, the thin long body is also the advantage of the eel-like robot. The robot can entrance to and work in a narrow space. The capability is suitable for inspection and search tasks in narrow and/or collapsed structures.

The mini scale of the soft eel robot is aimed to apply for the colonoscopy process. Experimental results indicated that the robot can generate smooth propagation waves along the body for terrestrial locomotion in constrained environments. Based on this structure, the robot can move forward and backward by inverting propagation waves directions. Additionally, the robot's body is totally soft and deformable. These characteristics are very suitable for a self-propelled colonoscopy robot. Such working principles and structure are also for inspection robots in tube environments.

## 8.2 Summary of Contributions

The major contributions of the research presented in this thesis are as follows:

- A soft eel robot design using a series of soft actuators that have semi-cylindrical, chambered, and segmented structure. The design permits the soft eel robot can self-balance when actuated.
- Processes for fabrication of the soft actuator and whole robot body.
- Methodology and process for determining bandwidth of a pair of the soft actuator.
- Control strategy for anguilliform swimming performance, in which pulse signals with shifting phase are used to operate solenoid valves that contribute pressurized air from one source to the soft actuators.

- Hydrodynamic model and its establishment process for prediction thrust generation of an anguilliform swimmer with an anchor at a very first point of the anterior part.
- Novel swimming strategies (C shape mode, passive mode) that can perform better swimming efficiency than the traditional one.
- A total soft body robot design scaled in mini size for self-propelled colonoscopy robot.
- Fabrication process using molding technique that suitable for the small size of the robot.
- Control strategy for wave-like locomotion of the self-propelled colonoscopy robot.

## 8.3 Limitations

A simulation approach was employed for choosing a suitable soft actuator. The bandwidth of a pair of soft actuators was determined by experiment. Nonetheless, the effect of air supplying pipe was not taken into account. In some extra experiments that were not included in this thesis, we found that the air pipe diameter partly affected the working capability of the soft actuator, thus, the soft eel robot. Regarding actuation sources, this thesis only investigated pneumatic sources that are suitable for an aquatic soft robot working at the water surface or locations having a small distance from the water surface. To dive and work at deeper locations, hydraulic actuation must be added. The actuator structure is totally appropriate for hydraulic actuation. Nonetheless, solenoid valves need to be changed for water working conditions. The segmented structure of the soft actuator allows the large bending angle in the actuation of low pressure resulting in low consumption energy. Although there was no experimental evidence (measuring data), such a structure certainly has a bad influence on the hydrodynamics of the robot's swimming performance. To solve this phenomenon, it requires to come up with the idea of covering the soft actuator surface. The cover layer can create a continuous and smooth surface and it must not affect the bending capability at low pressure of the soft actuator.

The soft eel robot was operated at low-level control. There are two important factors, which require for applying high-level control (velocity and position control through input parameters such as air pressure, tail beat frequency), including an analytical model that describes the effect of input control parameters on the robot velocity, and suitable sensor integrated to the robot body must be investigated. As reviewed in Chapter 1, the analytical model for soft robots that are constructed from non-linear materials is being a big challenge up to now. Additionally, having to include hydrodynamic phenomena in the model increases the difficulty of this work. Thus, in our opinion, it requires to take a period to address completely these issues, which, then, should be validated on an untethered soft eel robot.

Three separated swimming strategies were innovated and studied. The investigation included examination, analysis, and choosing input parameters for the best performance of each mode. However, there was a lack of deep explanation of how each mode work. For wave propagation mode, it can easily understand by using explanations from previous researches on original natural species (eel, lamprey, *etc*.). For two novel modes that cannot be done by natural creatures or rigid elongated body robots, they require more experimental analysis for deep understanding. For example, the following information must be collected for logical explanations: How does the vortex ring form when the soft elongated body performs such movements? How is the pressure of the surrounding water distributed? These require building a complex dedicated system (as described in [21], [23]) combined with using PIV (Particle Image Velocimetry) technique or collaborating with an aquatic biological laboratory.

## 8.4 Visions

All the above issues are big from both academia and technique and also have potential applications. Therefore, we have a plan to develop the undulatory movement of a soft elongated body robot. Regarding the underwater soft robot, an untethered soft eel robot has been investigated. All control parts (a miniature pump, control circuit, solenoid valves, batteries, sensors) are integrated. At first, the control strategy

for turning performance also has been explored combining with a camera and remote control, the developing robot can perform inspection tasks at the nearby water surface. To develop high-level control, an analytical model that describes the relationship between the robot velocity, the robot swimming posture, and input control parameters including tail beat frequency, air pressure supplying to each segment, and the robot body geometrical parameters must be established. The model has to take into account the effect of hydrodynamic behavior on the robot movement as similar as the thrust force model. The non-linear behavior of soft and deformable materials forming the robot body is also included in the model. The characteristic might examine by experiment combined with Matlab fitting tool as we proposed in this thesis. Novel swimming strategies will be applied in the untethered robot for different kinds of tasks or enlarging the working conditions of the robot (*e.g*. when one actuator at tail segment is damaged). An autonomous robot with an adaptive control algorithm currently is set as the final target. More detail for the phase "adaptive control", the robot is able to switch swimming mode automatically adapt with working conditions (long journey tasks, fast swimming, *etc*.). One of the most important capabilities is that it can "sense" the damage position and deactivate corresponding actuators to switch to passive swimming modes. This will become one of the most advantages of the autonomous soft eel robot as it still work efficiently despite a damaged body.

Hydrodynamic behavior that will be used to explain the swimming performance of the different swimming strategies is very worth deeply investigating. Besides the development of a complex dedicated system as aforementioned, one approach comes from the combination between FEM model and simple experiment validations. The latter approach seems to be suitable for our existing equipment. Some potential FEM candidates that can be employed for this research direction deployment can be mentioned as Abaqus, OpenFOAM, SOFA.

self-propelled soft colonoscopy robots are also a potential direction and are developing. In this thesis, we proposed and developed wave-like locomotion small-scale robots with a total soft body as the first step in exploring research. To complete the colonoscopy robot, some other works must be done. Firstly, a steering part has to

introduce for turning when working in complex structures as colon and for inspecting desired positions. Secondly, due to the complex colon structure, the locomotion strategy for vertical colon parts must be investigated. This strategy might be combined with a novel added structure and control method. Finally, a camera ought to be integrated into the robot. The final target at this phase is a complete self-propelled colonoscopy robot that can work safely and reliably in a colon environment. The soft property will create gentle contact with the colon resulting in decreasing pain and uncomfortable feeling in the endoscope process, meanwhile, the self-propelled capability will reduce the dependence on doctor skills and also reduce the processing time.

Recognizing that the soft proposed elongated body robots performing wave-like movement have potential applications. We intend to continuously enlarge the application of such a working principle. The first research direction is haptic devices that are able to create continuous touching on human skin to mimic stroke activities. Such movement cannot be done by any devices before. This idea was filed for a patent with application number 2021-168206.

# Appendix A

# Achievements

**Journal**

**Dinh Quang Nguyen** and Van Anh Ho, "Anguilliform Swimming Performance of an Eel-Inspired Soft Robot", Soft Robotics, https://doi.org/10.1089/soro.2020.0093, (**Q1, IF 8.071, No. 2 in Robotics**).

**Conference proceedings**

1. **Dinh Quang Nguyen** and Van Anh Ho, "Kinematic Evaluation of a Series of Soft Actuators in Designing an Eel-inspired Robot", 2020 IEEE/SICE International Symposium on System Integration (SII), pp. 1288-1293, Honolulu, Hawaii, USA, January 12-15, 2020.

2. **Dinh Quang Nguyen**, and Van Anh Ho, "Evaluation on Swimming Efficiency of an Eel-inspired Soft Robot with Partially Damaged Body", 2021 IEEE 4th International Conference on Soft Robotics (RoboSoft), pp. 289-294, Yale University, USA, April 12-16 2021.

3. **Dinh Quang Nguyen** and Van Anh Ho, "Experimental Investigation of Locomotive Efficiency of a Soft Robotic Eel with a Largely Passive Body", Robotics for Sustainable Future. CLAWAR 2021. Lecture Notes in Networks and Systems, vol 324. Springer, Cham. $https://doi.org/10.1007/978-3-030-86294-710$

4. **Dinh Quang Nguyen**, Giuseppe Loianno, Van Anh Ho, "Towards design of a deformable propeller for drone safety", 2020 IEEE International Conference on Soft Robotics (RoboSoft), pp. 464-469, Yale University, USA, April 2020.

5. Nhan Huu Nguyen, Trung Dung Ngo, **Dinh Quang Nguyen** and Van Anh Ho,

"Contact Distance Estimation by a Soft Active Whisker Sensor Based on Morphological Computation," 2020 8th IEEE RAS/EMBS International Conference for Biomedical Robotics and Biomechatronics (BioRob), pp. 322-327, NewYork, USA, 29 Nov.-1 Dec. 2020.

**Patents**

1. Van Anh Ho and **Dinh Quang Nguyen**, Deformable propeller, Application number: 2019-198143 (filed on 2019/10/31).

2. Van Anh Ho, **Dinh Quang Nguyen**, Quan Khanh Luu, Nhat Dinh Minh Le, Drone and drone control device, Application number: 2021-147818 (filed on 2021/9/10).

3. Van Anh Ho, **Dinh Quang Nguyen**, Tuan Tai Nguyen, Tactile presentation device and tactile presentation method, Application number: 2021-168206 (filed on 2021/10/13).

## Appendix B

# Program for multitasks

```
#include <Arduino_FreeRTOS.h>

void HeadValve( void *pvParameters);
void MiddleValve( void *pvParameters);
void TailValve( void *pvParameters);
void Analog( void *pvParameters);

  float t=800;
  float s=0.4*t;
void setup() {

  // put your setup code here, to run once:
  Serial.begin(9600);
  while (!Serial);

  xTaskCreate(
    HeadValve
    , (const portCHAR *)"valve 1"
    , 128
    , NULL
    , 1 // priority,with 3 being the highest, and 0 being the lowest
    , NULL );
```

```
  xTaskCreate(
    MiddleValve
    , (const portCHAR *)"valve 2"
    , 128
    , NULL
    , 1 // priority,with 3 being the highest, and 0 being the lowest
    , NULL );

  xTaskCreate(
    TailValve
    , (const portCHAR *)"valve 3"
    , 128
    , NULL
    , 1 // priority,with 3 being the highest, and 0 being the lowest
    , NULL );
}

void loop() {

}
void HeadValve(void *pvParameters)
{
  (void) pvParameters;
  pinMode(2, OUTPUT);

  for (;;)
  {

    digitalWrite(2, HIGH);
    vTaskDelay(t / portTICK_PERIOD_MS);
    digitalWrite(2, LOW);
```

```
    vTaskDelay(t / portTICK_PERIOD_MS);
  }
}
void MiddleValve(void *pvParameters)
{
  (void) pvParameters;
  pinMode(3, OUTPUT);
vTaskDelay(s / portTICK_PERIOD_MS);
  for (;;)
  {

    digitalWrite(3, HIGH);
    vTaskDelay(t / portTICK_PERIOD_MS);
    digitalWrite(3, LOW);
    vTaskDelay(t / portTICK_PERIOD_MS);
  }
}
void TailValve(void *pvParameters)
{
  (void) pvParameters;
  pinMode(4, OUTPUT);
vTaskDelay(2*s / portTICK_PERIOD_MS);
  for (;;)
  {

    digitalWrite(4, HIGH);
    vTaskDelay(t / portTICK_PERIOD_MS);
    digitalWrite(4, LOW);
    vTaskDelay(t / portTICK_PERIOD_MS);
  }
}
```

## Appendix C

# MATLAB code for collecting thrust force data

```
clear all;
clc;
if ~isempty(instrfind)
     fclose(instrfind);
     delete(instrfind);
end
C = [0.0051599 -0.0070484 -0.336193 -6.621657 0.632099 6.509378;
      0.388494 8.08554 -0.219520 -3.77063 -0.4122007 -3.80373;
      7.500814 0.0550485 7.60797 -0.166813 7.383399 -0.220088;
      2.130068/1000 49.363983/1000 41.38694/1000 -23.76404/1000

      -43.8207702/1000 -22.018714/1000;
      -48.3382644/1000 -0.28956/1000 26.52380/1000 39.978233/1000

      20.597137/1000 -40.53733/1000;
      1.446445/1000 30.286844/1000 1.7388979/1000 29.9991512/1000

      3.0322103/1000 28.57239/1000];
%
u = daq.createSession('ni');
u.Rate=5000;
```

```
u.addAnalogInputChannel('Dev1',0:7,'Voltage');
offset=inputSingleScan(u)';
Y = [0 0 0 0 0 0];
Ys = [0 0 0 0 0 0];
%#########################################################

position = 0;
Y_calib=[0];
posX=[0];
posY=[0];
forceATI = [0 0 0 0 0 0];
straingauge=[0];

tic
for j=1:1000

    data=inputSingleScan(u)'-offset;
    force_cal = C*data(1:6);
    force_cal = force_cal';
    forceATI = [forceATI;force_cal];
    straingauge=[straingauge;data(8)];
end
toc

figure
plot(forceATI,'LineWidth',2)
grid on
xlswrite('Eel thrust force.xls',forceATI, 1)
```

## Appendix D

# MATLAB code for extracting images

```
a=VideoReader('videoname.mp4');
for img = 1:a.NumberOfFrames;
    filename=strcat('frame',num2str(img),'.jpg');
    b = read(a, img)
    imwrite(b,filename);
end
```

# Bibliography

[1] Malcolm Gordon, Reinhard Blickhan, John Dabiri, et al. *Animal Locomotion: Physical Principles and Adaptations*. May 2017, pp. 1–268. ISBN: 9781315265155. DOI: 10.1201/b22011.

[2] Brian Dean and Bharat Bhushan. "Shark-skin surfaces for fluid-drag reduction in turbulent flow: a review". In: *Philosophical Transactions of the Royal Society A: Mathematical, Physical and Engineering Sciences* 368.1929 (2010), pp. 4775–4806. DOI: 10.1098/rsta.2010.0201. eprint: https://royalsocietypublishing.org/doi/pdf/10.1098/rsta.2010.0201. URL: https://royalsocietypublishing.org/doi/abs/10.1098/rsta.2010.0201.

[3] Hoang Vu Phan and Hoon Cheol Park. "Insect-inspired, tailless, hover-capable flapping-wing robots: Recent progress, challenges, and future directions". In: *Progress in Aerospace Sciences* 111 (2019), p. 100573. ISSN: 0376-0421. DOI: https://doi.org/10.1016/j.paerosci.2019.100573. URL: https://www.sciencedirect.com/science/article/pii/S0376042119300545.

[4] Alessandro Crespi, Konstantinos Karakasiliotis, André Guignard, et al. "Salamandra Robotica II: An Amphibious Robot to Study Salamander-Like Swimming and Walking Gaits". In: *IEEE Transactions on Robotics* 29.2 (2013), pp. 308–320. DOI: 10.1109/TRO.2012.2234311.

[5] *TRENDING SCIENCE: How are elephant trunks inspiring tomorrow's robots?* URL: https://cordis.europa.eu/article/id/430627-trending-science-how-are-elephant-trunks-inspiring-tomorrow-s-robots.

[6] Sangbae Kim, Cecilia Laschi, and Barry Trimmer. "Soft robotics: a bioinspired evolution in robotics". In: *Trends in Biotechnology* 31.5 (2013), pp. 287–294. ISSN: 0167-7799. DOI: https://doi.org/10.1016/j.tibtech.2013.

03.002. URL: https://www.sciencedirect.com/science/article/pii/S0167779913000632.

[7] Siegfried Bauer, Simona Bauer-Gogonea, Ingrid Graz, et al. "25th Anniversary Article: A Soft Future: From Robots and Sensor Skin to Energy Harvesters". In: *Advanced materials (Deerfield Beach, Fla.)* 26 (Jan. 2014). DOI: 10.1002/adma.201303349.

[8] C. J. PENNYCUICK. "Predicting Wingbeat Frequency and Wavelength of Birds". In: *Journal of Experimental Biology* 150.1 (May 1990), pp. 171–185. ISSN: 0022-0949. DOI: 10.1242/jeb.150.1.171. eprint: https://journals.biologists.com/jeb/article-pdf/150/1/171/1228331/171.pdf. URL: https://doi.org/10.1242/jeb.150.1.171.

[9] Dinh Quang Nguyen, Giuseppe Loianno, and Van Anh Ho. "Towards Design of a Deformable Propeller for Drone Safety". In: *2020 3rd IEEE International Conference on Soft Robotics (RoboSoft)*. 2020, pp. 464–469. DOI: 10.1109/RoboSoft48309.2020.9115983.

[10] R.M.N. Alexander. *Principles of Animal Locomotion*. Jan. 2013, pp. 1–371. ISBN: 9781400849512. DOI: 10.1515/9781400849512.

[11] Priyaranjan Biswal and Prases K. Mohanty. "Development of quadruped walking robots: A review". In: *Ain Shams Engineering Journal* 12.2 (2021), pp. 2017–2031. ISSN: 2090-4479. DOI: https://doi.org/10.1016/j.asej.2020.11.005. URL: https://www.sciencedirect.com/science/article/pii/S2090447920302501.

[12] Alessandro Crespi, Konstantinos Karakasiliotis, André Guignard, et al. "Salamandra Robotica II: An Amphibious Robot to Study Salamander-Like Swimming and Walking Gaits". In: *IEEE Transactions on Robotics* 29.2 (2013), pp. 308–320. DOI: 10.1109/TRO.2012.2234311.

[13] Raymond H. Plaut. "Mathematical model of inchworm locomotion". In: *International Journal of Non-Linear Mechanics* 76 (2015), pp. 56–63. ISSN: 0020-7462. DOI: https://doi.org/10.1016/j.ijnonlinmec.2015.05.007. URL: https://www.sciencedirect.com/science/article/pii/S0020746215001080.

[14] Chi Zhang, Wei Zou, Liping Ma, et al. "Biologically inspired jumping robots: A comprehensive review". In: *Robotics and Autonomous Systems* 124 (2020), p. 103362. ISSN: 0921-8890. DOI: https://doi.org/10.1016/j.robot.2019.103362. URL: https://www.sciencedirect.com/science/article/pii/S0921889019301861.

[15] Yumo Wang, Shunxiang Pang, Hu Jin, et al. "Development of a biomimetic scallop robot capable of jet propulsion". In: *Bioinspiration & Biomimetics* 15.3 (Mar. 2020), p. 036008. DOI: 10.1088/1748-3190/ab75f6. URL: https://doi.org/10.1088/1748-3190/ab75f6.

[16] Mather J. A. "How do octopuses use their arms?" In: *Journal of comparative psychology* 112.3 (Sept. 1998), pp. 306–316. DOI: https://doi.org/10.1037/0735-7036.112.3.306.

[17] Mahdi Tabatabaei Malazi, Ali Olcay, Mehmet Gökçen, et al. "Drag force and jet propulsion investigation of a swimming squid". In: *EPJ Web of Conferences* 92 (May 2015), p. 02092. DOI: 10.1051/epjconf/20159202092.

[18] M. EDWIN DEMONT and JOHN M. GOSLINE. "Mechanics of Jet Propulsion in the Hydromedusan Jellyfish, Polyorchis Penicillatus: II. Energetics of the Jet Cycle". In: *Journal of Experimental Biology* 134.1 (Jan. 1988), pp. 333–345. ISSN: 0022-0949. DOI: 10.1242/jeb.134.1.333. eprint: https://journals.biologists.com/jeb/article-pdf/134/1/333/1227003/333.pdf. URL: https://doi.org/10.1242/jeb.134.1.333.

[19] M. Sfakiotakis, D.M. Lane, and J.B.C. Davies. "Review of fish swimming modes for aquatic locomotion". In: *IEEE Journal of Oceanic Engineering* 24.2 (1999), pp. 237–252. DOI: 10.1109/48.757275.

[20] Daiki Satoi, Mikihiro Hagiwara, Akira Uemoto, et al. "Unified Motion Planner for Fishes with Various Swimming Styles". In: *ACM Trans. Graph.* 35.4 (July 2016). ISSN: 0730-0301. DOI: 10.1145/2897824.2925977. URL: https://doi.org/10.1145/2897824.2925977.

[21] Eric D. Tytell. "The hydrodynamics of eel swimming II. Effect of swimming speed". In: *Journal of Experimental Biology* 207 (2004), pp. 3265–3279.

[22] Brad J. Gemmell, Stephanie M. Fogerson, John H. Costello, et al. "How the bending kinematics of swimming lampreys build negative pressure fields for suction thrust". In: *Journal of Experimental Biology* 219.24 (Dec. 2016), pp. 3884–3895. ISSN: 0022-0949. DOI: 10.1242/jeb.144642. eprint: https://journals.biologists.com/jeb/article-pdf/219/24/3884/1893682/jeb144642.pdf. URL: https://doi.org/10.1242/jeb.144642.

[23] Eric Tytell and George Lauder. "The hydrodynamics of eel swimming. I. Wake structure". In: *The Journal of experimental biology* 207 (June 2004), pp. 1825–41. DOI: 10.1242/jeb.00968.

[24] Nils B. Tack, Kevin T. Du Clos, and Brad J. Gemmell. "Anguilliform Locomotion across a Natural Range of Swimming Speeds". In: *Fluids* 6.3 (2021). ISSN: 2311-5521. DOI: 10.3390/fluids6030127. URL: https://www.mdpi.com/2311-5521/6/3/127.

[25] Fumiya Iida and Auke Jan Ijspeert. "Biologically Inspired Robotics". In: *Springer Handbook of Robotics*. Ed. by Bruno Siciliano and Oussama Khatib. Cham: Springer International Publishing, 2016, pp. 2015–2034. ISBN: 978-3-319-32552-1. DOI: 10.1007/978-3-319-32552-1_75. URL: https://doi.org/10.1007/978-3-319-32552-1_75.

[26] Sangok Seok, Albert Wang, Meng Yee Chuah, et al. "Design principles for highly efficient quadrupeds and implementation on the MIT Cheetah robot". In: *2013 IEEE International Conference on Robotics and Automation*. 2013, pp. 3307–3312. DOI: 10.1109/ICRA.2013.6631038.

[27] Chi Zhang, Wei Zou, Liping Ma, et al. "Biologically inspired jumping robots: A comprehensive review". In: *Robotics and Autonomous Systems* 124 (2020), p. 103362. ISSN: 0921-8890. DOI: https://doi.org/10.1016/j.robot.2019.103362. URL: https://www.sciencedirect.com/science/article/pii/S0921889019301861.

[28] Lee-Hee Drory and David Zarrouk. "Locomotion Dynamics of a Miniature Wave-Like Robot, Modeling and Experiments". In: *2019 International Conference on Robotics and Automation (ICRA)*. 2019, pp. 8422–8428. DOI: 10.1109/ICRA.2019.8794015.

[29] Jizhong Zhu, Carl H. White, Dylan K. Wainwright, et al. "Tuna robotics: A high-frequency experimental platform exploring the performance space of swimming fishes". In: *Science Robotics* 4 (2019).

[30] Gursel Alici. "Softer is Harder: What Differentiates Soft Robotics from Hard Robotics?" In: *MRS Advances* 3 (2018), pp. 1557–1568.

[31] Bobak Mosadegh, Panagiotis Polygerinos, Christoph Keplinger, et al. "Pneumatic Networks for Soft Robotics that Actuate Rapidly". In: *Advanced Functional Materials* 24.15 (2014), pp. 2163–2170. DOI: https://doi.org/10.1002/adfm.201303288. eprint: https://onlinelibrary.wiley.com/doi/pdf/10.1002/adfm.201303288. URL: https://onlinelibrary.wiley.com/doi/abs/10.1002/adfm.201303288.

[32] Ardian Jusufi, Daniel M. Vogt, Robert J. Wood, et al. "Undulatory Swimming Performance and Body Stiffness Modulation in a Soft Robotic Fish-Inspired Physical Model". In: *Soft Robotics* 4.3 (2017). PMID: 29182079, pp. 202–210. DOI: 10.1089/soro.2016.0053. eprint: https://doi.org/10.1089/soro.2016.0053. URL: https://doi.org/10.1089/soro.2016.0053.

[33] Jiaqi Liu, Saverio Iacoponi, Cecilia Laschi, et al. "Underwater Mobile Manipulation: A Soft Arm on a Benthic Legged Robot". In: *IEEE Robotics Automation Magazine* 27.4 (2020), pp. 12–26. DOI: 10.1109/MRA.2020.3024001.

[34] Andrew D. Marchese, Cagdas D. Onal, and Daniela Rus. "Autonomous Soft Robotic Fish Capable of Escape Maneuvers Using Fluidic Elastomer Actuators". In: *Soft Robotics* 1.1 (2014). PMID: 27625912, pp. 75–87. DOI: 10.1089/soro.2013.0009. eprint: https://doi.org/10.1089/soro.2013.0009. URL: https://doi.org/10.1089/soro.2013.0009.

[35] Seppe Terryn, Joost Brancart, Dirk Lefeber, et al. "Self-healing soft pneumatic robots". In: *Science Robotics* 2.9 (2017), eaan4268. DOI: 10.1126/scirobotics.aan4268. eprint: https://www.science.org/doi/pdf/10.1126/scirobotics.aan4268. URL: https://www.science.org/doi/abs/10.1126/scirobotics.aan4268.

[36] Robert Shepherd, Filip Ilievski, Wonjae Choi, et al. "Multigait Soft Robot". In: *Proceedings of the National Academy of Sciences of the United States of America* 108 (Nov. 2011), pp. 20400–3. DOI: 10.1073/pnas.1116564108.

[37] Pham H. Nguyen, Imran I. B. Mohd, Katherine Duford, et al. "Design, Fabrication, and Characterization of a Helical Twisting, Contracting, and Bending Fabric Soft Continuum Actuator". In: *2021 IEEE 4th International Conference on Soft Robotics (RoboSoft)*. 2021, pp. 567–570. DOI: 10.1109/RoboSoft51838.2021.9479350.

[38] Jan Fras and Kaspar Althoefer. "Soft Fiber-Reinforced Pneumatic Actuator Design and Fabrication: Towards Robust, Soft Robotic Systems". In: *Towards Autonomous Robotic Systems*. Ed. by Kaspar Althoefer, Jelizaveta Konstantinova, and Ketao Zhang. Cham: Springer International Publishing, 2019, pp. 103–114. ISBN: 978-3-030-23807-0.

[39] Rongzhen Xie, Manjia Su, Yihong Zhang, et al. "3D-PSA: A 3D Pneumatic Soft Actuator with Extending and Omnidirectional Bending Motion". In: *2018 IEEE International Conference on Robotics and Biomimetics (ROBIO)*. 2018, pp. 618–623. DOI: 10.1109/ROBIO.2018.8665051.

[40] Roman Balak and Yi Chen Mazumdar. "Multi-Modal Pneumatic Actuator for Twisting, Extension, and Bending". In: *2020 IEEE/RSJ International Conference on Intelligent Robots and Systems (IROS)*. 2020, pp. 8673–8679. DOI: 10.1109/IROS45743.2020.9341555.

[41] Wen Zhou and Yiqing Li. "Modeling and Analysis of Soft Pneumatic Actuator with Symmetrical Chambers Used for Bionic Robotic Fish". In: *Soft Robotics* 7.2 (2020). PMID: 32255420, pp. 168–178. DOI: 10.1089/soro.2018.0087. eprint: https://doi.org/10.1089/soro.2018.0087. URL: https://doi.org/10.1089/soro.2018.0087.

[42] Robert K Katzschmann, Austin de Maille, David L Dorhout, et al. "Cyclic hydraulic actuation for soft robotic devices". In: *2016 IEEE/RSJ International Conference on Intelligent Robots and Systems (IROS)*. 2016, pp. 3048–3055. DOI: 10.1109/IROS.2016.7759472.

[43] Dylan Drotman, Saurabh Jadhav, David Sharp, et al. "Electronics-free pneumatic circuits for controlling soft-legged robots". In: *Science Robotics* 6 (Feb. 2021), eaay2627. DOI: 10.1126/scirobotics.aay2627.

[44] K. Suzumori, T. Hama, and T. Kanda. "New pneumatic rubber actuators to assist colonoscope insertion". In: *Proceedings 2006 IEEE International Conference on Robotics and Automation, 2006. ICRA 2006.* 2006, pp. 1824–1829. DOI: 10.1109/ROBOT.2006.1641971.

[45] Sangok Seok, Cagdas D. Onal, Robert Wood, et al. "Peristaltic locomotion with antagonistic actuators in soft robotics". In: *2010 IEEE International Conference on Robotics and Automation*. 2010, pp. 1228–1233. DOI: 10.1109/ROBOT.2010.5509542.

[46] Cecilia Laschi, Matteo Cianchetti, Barbara Mazzolai, et al. "Soft Robot Arm Inspired by the Octopus". In: *Advanced Robotics* 26.7 (2012), pp. 709–727. DOI: 10.1163/156855312X626343. eprint: https://doi.org/10.1163/156855312X626343. URL: https://doi.org/10.1163/156855312X626343.

[47] Je-Sung Koh and Kyu-Jin Cho. "Omega-Shaped Inchworm-Inspired Crawling Robot With Large-Index-and-Pitch (LIP) SMA Spring Actuators". In: *IEEE/ASME Transactions on Mechatronics* 18.2 (2013), pp. 419–429. DOI: 10.1109/TMECH.2012.2211033.

[48] YuFeng Chen, Siyi Xu, Zhijian Ren, et al. "Collision Resilient Insect-Scale Soft-Actuated Aerial Robots With High Agility". In: *IEEE Transactions on Robotics* (2021), pp. 1–13. DOI: 10.1109/TRO.2021.3053647.

[49] Yufeng Chen, Hongqiang Wang, E. Farrell Helbling, et al. "A biologically inspired, flapping-wing, hybrid aerial-aquatic microrobot". In: *Science Robotics* 2.11 (2017), eaao5619. DOI: 10.1126/scirobotics.aao5619. eprint: https://www.science.org/doi/pdf/10.1126/scirobotics.aao5619. URL: https://www.science.org/doi/abs/10.1126/scirobotics.aao5619.

[50] Caleb Christianson, Nathaniel N. Goldberg, Dimitri D. Deheyn, et al. "Translucent soft robots driven by frameless fluid electrode dielectric elastomer actuators". In: *Science Robotics* 3.17 (2018), eaat1893. DOI: 10.1126/scirobotics.aat1893. eprint: https://www.science.org/doi/pdf/10.1126/scirobotics.

aat1893. URL: https://www.science.org/doi/abs/10.1126/scirobotics.aat1893.

[51] Tao Ren, Yingtian Li, Menghong Xu, et al. "A Novel Tendon-Driven Soft Actuator with Self-Pumping Property". In: *Soft Robotics* 7.2 (2020). PMID: 31584322, pp. 130–139. DOI: 10.1089/soro.2019.0008. eprint: https://doi.org/10.1089/soro.2019.0008. URL: https://doi.org/10.1089/soro.2019.0008.

[52] M Calisti, M Giorelli, G Levy, et al. "An octopus-bioinspired solution to movement and manipulation for soft robots". In: *Bioinspiration & Biomimetics* 6.3 (June 2011), p. 036002. DOI: 10.1088/1748-3182/6/3/036002. URL: https://doi.org/10.1088/1748-3182/6/3/036002.

[53] Dorin-Sabin Copaci, Dolores Blanco, Alejandro Martin-Clemente, et al. "Flexible shape memory alloy actuators for soft robotics: Modelling and control". In: *International Journal of Advanced Robotic Systems* 17.1 (2020), p. 1729881419886747. DOI: 10.1177/1729881419886747. eprint: https://doi.org/10.1177/1729881419886747. URL: https://doi.org/10.1177/1729881419886747.

[54] Pablo Valdivia y Alvarado and Kamal Youcef-Toumi. "Soft-Body Robot Fish". In: *Robot Fish: Bio-inspired Fishlike Underwater Robots*. Ed. by Ruxu Du, Zheng Li, Kamal Youcef-Toumi, et al. Berlin, Heidelberg: Springer Berlin Heidelberg, 2015, pp. 161–191. ISBN: 978-3-662-46870-8. DOI: 10.1007/978-3-662-46870-8_6. URL: https://doi.org/10.1007/978-3-662-46870-8_6.

[55] Lora Kolodny Brian Heater. *How marine biology inspired Soft Robotics' industrial grippers*. URL: https://techcrunch.com/2017/04/01/soft-robotics-grippers/.

[56] Adam Conner-Simons. *Soft robotic fish swims alongside real ones in coral reefs*. URL: https://news.mit.edu/2018/soft-robotic-fish-swims-alongside-real-ones-coral-reefs-0321.

[57] Zhongkui Wang and Shinichi Hirai. "Soft Gripper Dynamics Using a Line-Segment Model With an Optimization-Based Parameter Identification Method". In: *IEEE Robotics and Automation Letters* 2.2 (2017), pp. 624–631. DOI: 10.1109/LRA.2017.2650149.

[58] Longchuan Li, Shugen Ma, Isao Tokuda, et al. "Generation of Efficient Rectilinear Gait Based on Dynamic Morphological Computation and Its Theoretical Analysis". In: *IEEE Robotics and Automation Letters* 6.2 (2021), pp. 841–848. DOI: 10.1109/LRA.2021.3052421.

[59] III Robert J. Webster and Bryan A. Jones. "Design and Kinematic Modeling of Constant Curvature Continuum Robots: A Review". In: *The International Journal of Robotics Research* 29.13 (2010), pp. 1661–1683. DOI: 10.1177/0278364910368147. eprint: https://doi.org/10.1177/0278364910368147. URL: https://doi.org/10.1177/0278364910368147.

[60] Robert K. Katzschmann, Cosimo Della Santina, Yasunori Toshimitsu, et al. "Dynamic Motion Control of Multi-Segment Soft Robots Using Piecewise Constant Curvature Matched with an Augmented Rigid Body Model". In: *2019 2nd IEEE International Conference on Soft Robotics (RoboSoft)*. 2019, pp. 454–461. DOI: 10.1109/ROBOSOFT.2019.8722799.

[61] Federico Renda, Frédéric Boyer, Jorge Dias, et al. "Discrete Cosserat Approach for Multisection Soft Manipulator Dynamics". In: *IEEE Transactions on Robotics* 34.6 (2018), pp. 1518–1533. DOI: 10.1109/TRO.2018.2868815.

[62] Frédéric Boyer, Vincent Lebastard, Fabien Candelier, et al. "Dynamics of continuum and soft robots: a strain parametrization based approach". In: *IEEE Transactions on Robotics* (Nov. 2020). DOI: 10.1109/TRO.2020.3036618. URL: https://hal.archives-ouvertes.fr/hal-02318617.

[63] Taogang Hou, Xingbang Yang, Haohong Su, et al. "Design and Experiments of a Squid-Like Aquatic-Aerial Vehicle with Soft Morphing Fins and Arms". In: *2019 International Conference on Robotics and Automation (ICRA)*. 2019, pp. 4681–4687. DOI: 10.1109/ICRA.2019.8793702.

[64] Jennifer Frame, Nick Lopez, Oscar Curet, et al. "Thrust force characterization of free-swimming soft robotic jellyfish". In: *Bioinspiration & Biomimetics* 13.6 (Sept. 2018), p. 064001. DOI: 10.1088/1748-3190/aadcb3. URL: https://doi.org/10.1088/1748-3190/aadcb3.

[65] Ziyu Ren, Wenqi Hu, Xiaoguang Dong, et al. "Multi-functional soft-bodied jellyfish-like swimming". In: *Nature Communications* 10 (July 2019). DOI: 10.1038/s41467-019-10549-7.

[66] Caleb Christianson, Christopher Bayag, Guorui Li, et al. "Jellyfish-Inspired Soft Robot Driven by Fluid Electrode Dielectric Organic Robotic Actuators". In: *Frontiers in Robotics and AI* 6 (2019), p. 126. ISSN: 2296-9144. DOI: 10.3389/frobt.2019.00126. URL: https://www.frontiersin.org/article/10.3389/frobt.2019.00126.

[67] Yong Zhong, Zheng Li, and Ruxu Du. "A Novel Robot Fish With Wire-Driven Active Body and Compliant Tail". In: *IEEE/ASME Transactions on Mechatronics* 22.4 (2017), pp. 1633–1643. DOI: 10.1109/TMECH.2017.2712820.

[68] Bingxing Chen and Hongzhou Jiang. "Swimming Performance of a Tensegrity Robotic Fish". In: *Soft Robotics* 6 (Aug. 2019). DOI: 10.1089/soro.2018.0079.

[69] Sander C. van den Berg. "Design of a high speed soft robotic fish". In: 2019.

[70] Zheng Li and Ruxu Du. "Wire-Driven Robot Fish". In: *Robot Fish: Bio-inspired Fishlike Underwater Robots*. Ed. by Ruxu Du, Zheng Li, Kamal Youcef-Toumi, et al. Berlin, Heidelberg: Springer Berlin Heidelberg, 2015, pp. 51–92. ISBN: 978-3-662-46870-8. DOI: 10.1007/978-3-662-46870-8_3. URL: https://doi.org/10.1007/978-3-662-46870-8_3.

[71] Robert K. Katzschmann, Joseph DelPreto, Robert MacCurdy, et al. "Exploration of underwater life with an acoustically controlled soft robotic fish". In: *Science Robotics* 3.16 (2018), eaar3449. DOI: 10.1126/scirobotics.aar3449. eprint: https://www.science.org/doi/pdf/10.1126/scirobotics.aar3449. URL: https://www.science.org/doi/abs/10.1126/scirobotics.aar3449.

[72] Robert K Katzschmann, Austin de Maille, David L Dorhout, et al. "Cyclic hydraulic actuation for soft robotic devices". In: *2016 IEEE/RSJ International Conference on Intelligent Robots and Systems (IROS)*. 2016, pp. 3048–3055. DOI: 10.1109/IROS.2016.7759472.

[73] Robert Katzschmann, Andrew Marchese, and Daniela Rus. "Hydraulic Autonomous Soft Robotic Fish for 3D Swimming". In: vol. 109. June 2014, pp. 405–420. DOI: 10.1007/978-3-319-23778-7_27.

[74] Yu-Hsiang Lin, Robert Siddall, Fabian Schwab, et al. "Modeling and Control of a Soft Robotic Fish with Integrated Soft Sensing". In: *Advanced Intelligent Systems* n/a.n/a (), p. 2000244. DOI: https://doi.org/10.1002/aisy.202000244. eprint: https://onlinelibrary.wiley.com/doi/pdf/10.1002/aisy.202000244. URL: https://onlinelibrary.wiley.com/doi/abs/10.1002/aisy.202000244.

[75] Jun Shintake, Vito Cacucciolo, Herbert Shea, et al. "Soft Biomimetic Fish Robot Made of Dielectric Elastomer Actuators". In: *Soft Robotics* 5.4 (2018). PMID: 29957131, pp. 466–474. DOI: 10.1089/soro.2017.0062. eprint: https://doi.org/10.1089/soro.2017.0062. URL: https://doi.org/10.1089/soro.2017.0062.

[76] Zhenlong Wang, Guanrong Hang, Jian Li, et al. "A micro-robot fish with embedded SMA wire actuated flexible biomimetic fin". In: *Sensors and Actuators A: Physical* 144.2 (2008), pp. 354–360. ISSN: 0924-4247. DOI: https://doi.org/10.1016/j.sna.2008.02.013. URL: https://www.sciencedirect.com/science/article/pii/S0924424708001283.

[77] M. Muralidharan and I.A. Palani. "Development of Subcarangiform Bionic Robotic Fish Propelled by Shape Memory Alloy Actuators". In: *Defence Science Journal* 71.1 (Feb. 2021), pp. 94–101. DOI: 10.14429/dsj.71.15777. URL: https://publications.drdo.gov.in/ojs/index.php/dsj/article/view/15777.

[78] William Vorus and Brandon Taravella. "Anguilliform fish propulsion of highest hydrodynamic efficiency". In: *Journal of Marine Science and Application* 10 (June 2011), pp. 163–174. DOI: 10.1007/s11804-011-1056-3.

[79] K. H. Low, Jie Yang, Anjan P. Pattathil, et al. "Initial Prototype Design and Investigation of an Undulating Body by SMA". In: *2006 IEEE International Conference on Automation Science and Engineering*. 2006, pp. 472–477. DOI: 10.1109/COASE.2006.326927.

[80] A. Westphal, Nikolai Rulkov, Joseph Ayers, et al. "Controlling a lamprey-based robot with an electronic nervous system". In: *Smart Structures and Systems* 8 (July 2011). DOI: 10.12989/sss.2011.8.1.039.

[81] Anthony Westphal. "Controlling a lamprey-based robot with an electronic nervous system". PhD dissertation. Boston, Massachusetts : Northeastern University, 2012.

[82] Hui Feng, Yi Sun, Peter A. Todd, et al. "Body Wave Generation for Anguilliform Locomotion Using a Fiber-Reinforced Soft Fluidic Elastomer Actuator Array Toward the Development of the Eel-Inspired Underwater Soft Robot". In: *Soft Robotics* 7.2 (2020). PMID: 31851869, pp. 233–250. DOI: 10.1089/soro.2019.0054. eprint: https://doi.org/10.1089/soro.2019.0054. URL: https://doi.org/10.1089/soro.2019.0054.

[83] Michael James Lighthill. "Large-amplitude elongated-body theory of fish locomotion". In: *Proceedings of the Royal Society of London. Series B. Biological Sciences* 179.1055 (1971), pp. 125–138. DOI: 10.1098/rspb.1971.0085. eprint: https://royalsocietypublishing.org/doi/pdf/10.1098/rspb.1971.0085. URL: https://royalsocietypublishing.org/doi/abs/10.1098/rspb.1971.0085.

[84] Liang Li, Anquan Liu, Wei Wang, et al. "Bottom-level motion control for robotic fish to swim in groups: modeling and experiments". In: *Bioinspiration & Biomimetics* 14.4 (May 2019), p. 046001. DOI: 10.1088/1748-3190/ab1052. URL: https://doi.org/10.1088/1748-3190/ab1052.

[85] Li Wen, Tianmiao Wang, Guanhao Wu, et al. "Novel Method for the Modeling and Control Investigation of Efficient Swimming for Robotic Fish". In: *IEEE Transactions on Industrial Electronics* 59.8 (2012), pp. 3176–3188. DOI: 10.1109/TIE.2011.2151812.

[86] Angus Webb, Christopher Phillips, Dominic Hudson, et al. "Can Lighthill's Elongated Body Theory Predict Hydrodynamic Forces in Underwater Undulatory Swimming?" In: *Procedia Engineering* 34 (Dec. 2012), pp. 724–729. DOI: 10.1016/j.proeng.2012.04.123.

[87] Pichet Suebsaiprom and Chun-Liang Lin. "Maneuverability modeling and trajectory tracking for fish robot". In: *Control Engineering Practice* 45 (Dec. 2015), pp. 22–36. DOI: 10.1016/j.conengprac.2015.08.010.

[88] Deniz Korkmaz, Ümit Budak, Cafer Bal, et al. "Modeling and implementation of a biomimetic robotic fish". In: June 2012, pp. 1187–1192. ISBN: 978-1-4673-1299-8. DOI: 10.1109/SPEEDAM.2012.6264510.

[89] Stefan Kern and Petros Koumoutsakos. "Simulations of optimized anguilliform swimming". In: *Journal of Experimental Biology* 209.24 (Dec. 2006), pp. 4841–4857. ISSN: 0022-0949. DOI: 10.1242/jeb.02526. eprint: https://journals.biologists.com/jeb/article-pdf/209/24/4841/1258105/4841.pdf. URL: https://doi.org/10.1242/jeb.02526.

[90] Hui Feng, Zhaomeng Wang, Peter Todd, et al. "Simulations of self-propelled anguilliform swimming using the immersed boundary method in OpenFOAM". In: *Engineering Applications of Computational Fluid Mechanics* 13 (Jan. 2019), pp. 438–452. DOI: 10.1080/19942060.2019.1609582.

[91] Palmani Duraisamy, Rakesh Sidharthan, and Manigandan Santhanakrishnan. "Design, Modeling, and Control of Biomimetic Fish Robot: A Review". In: *Journal of Bionic Engineering* 16 (Nov. 2019), pp. 967–993. DOI: 10.1007/s42235-019-0111-7.

[92] Sadatoshi Taneda and Yoshimasa Tomonari. "An Experiment on the Flow around a Waving Plate". In: *Journal of the Physical Society of Japan* 36.6 (1974), pp. 1683–1689. DOI: 10.1143/JPSJ.36.1683. eprint: https://doi.org/10.1143/JPSJ.36.1683. URL: https://doi.org/10.1143/JPSJ.36.1683.

[93] John J. Magnuson. "4 - Locomotion by Scombrid Fishes: Hydromechanics, Morphology, and Behavior". In: *Fish Physiology* 7 (1978), pp. 239–313.

[94] Webb PW. "Form and function in fish swimming". In: *Scientific America* 251.1 (1984), pp. 72–83.

[95] Cimbala JM Cengel JA. *Fluid mechanics: Fundamentals and Application*. 3rd ed. McGraw-Hill, 2 Penn Plaza, New York, NY 10121 USA, 2013.

[96] Miguel Piñeirua, Ramiro Godoy-Diana, and Benjamin Thiria. "Resistive thrust production can be as crucial as added mass mechanisms for inertial undulatory swimmers". In: *Physical Review E* 92 (July 2015). DOI: 10.1103/PhysRevE.92.021001.

[97] Cagdas D. Onal and Daniela Rus. "A modular approach to soft robots". In: *2012 4th IEEE RAS EMBS International Conference on Biomedical Robotics and Biomechatronics (BioRob)*. 2012, pp. 1038–1045. DOI: 10.1109/BioRob.2012.6290290.

[98] Sophie Ramananarivo, Ramiro Godoy-Diana, and Benjamin Thiria. "Passive elastic mechanism to mimic fish-muscle action in anguilliform swimming". In: *Journal of The Royal Society Interface* 10.88 (2013), p. 20130667. DOI: 10.1098/rsif.2013.0667. eprint: https://royalsocietypublishing.org/doi/pdf/10.1098/rsif.2013.0667. URL: https://royalsocietypublishing.org/doi/abs/10.1098/rsif.2013.0667.

[99] Smits AJ Quinn DB Lauder GV. "Maximizing the efficiency of a flexible propulsor using experimental optimization". In: *Journal of Fluid Mechanics* 767 (2015), pp. 430–448.

[100] D. S. BARRETT, M. S. TRIANTAFYLLOU, D. K. P. YUE, et al. "Drag reduction in fish-like locomotion". In: *Journal of Fluid Mechanics* 392 (1999), pp. 183–212. DOI: 10.1017/S0022112099005455.

[101] Lauder GV Di Santo V Kenaley CP. In: *Proceedings of the National Academy of Sciences of the United States of America*. National Academy of Sciences. Chicago, USA, Dec. 2017, pp. 13048–13053.

[102] Megan C. Leftwich, Eric D. Tytell, Avis H. Cohen, et al. "Wake structures behind a swimming robotic lamprey with a passively flexible tail". In: *Journal of Experimental Biology* 215.3 (Feb. 2012), pp. 416–425. ISSN: 0022-0949. DOI: 10.1242/jeb.061440. eprint: https://journals.biologists.com/jeb/article-pdf/215/3/416/1283393/416.pdf. URL: https://doi.org/10.1242/jeb.061440.

[103] Anthony Holtmaat and Karel Svoboda. "Experience-dependent structural synaptic plasticity in the mammalian brain". In: *Nature reviews. Neuroscience* 10 (Oct. 2009), pp. 647–58. DOI: 10.1038/nrn2699.

[104] Pål Liljebäck, Øyvind Stavdahl, Kristin Y. Pettersen, et al. "Mamba - A waterproof snake robot with tactile sensing". In: *2014 IEEE/RSJ International Conference on Intelligent Robots and Systems*. 2014, pp. 294–301. DOI: 10.1109/IROS.2014.6942575.

[105] Shumei Yu, Shugen Ma, Bin Li, et al. "An amphibious snake-like robot: Design and motion experiments on ground and in water". In: *2009 International Conference on Information and Automation*. 2009, pp. 500–505. DOI: 10.1109/ICINFA.2009.5204975.

[106] Kara Feilich and George Lauder. "Passive mechanical models of fish caudal fins: Effects of shape and stiffness on self-propulsion". In: *Bioinspiration biomimetics* 10 (June 2015), p. 036002. DOI: 10.1088/1748-3190/10/3/036002.

[107] Gastone Ciuti, Karolina Skonieczna-Żydecka, Wojciech Marlicz, et al. "Frontiers of Robotic Colonoscopy: A Comprehensive Review of Robotic Colonoscopes and Technologies". In: *Journal of Clinical Medicine* 9.6 (2020). ISSN: 2077-0383. DOI: 10.3390/jcm9061648. URL: https://www.mdpi.com/2077-0383/9/6/1648.

[108] Patrick L. Anderson, Ray A. Lathrop, and Robert J. Webster III. "Robot-like dexterity without computers and motors: a review of hand-held laparoscopic instruments with wrist-like tip articulation". In: *Expert Review of Medical Devices* 13.7 (2016). PMID: 26808896, pp. 661–672. DOI: 10.1586/17434440.2016.1146585. eprint: https://doi.org/10.1586/17434440.2016.1146585. URL: https://doi.org/10.1586/17434440.2016.1146585.

[109] Valentina Vitiello, Su-Lin Lee, Thomas Cundy, et al. "Emerging Robotic Platforms for Minimally Invasive Surgery". In: *IEEE reviews in biomedical engineering* 6 (Dec. 2012). DOI: 10.1109/RBME.2012.2236311.

[110] Ario Loeve, Paul Breedveld, and Jenny Dankelman. "Scopes Too Flexible...and Too Stiff". In: *IEEE Pulse* 1.3 (2010), pp. 26–41. DOI: 10.1109/MPUL.2010.939176.

[111] Axel Eickhoff, Jacques Dam, Ralf Jakobs, et al. "Computer-Assisted Colonoscopy (The NeoGuide Endoscopy System): Results of the First Human Clinical Trial ("PACE Study")". In: *The American journal of gastroenterology* 102 (Mar. 2007), pp. 261–6. DOI: 10.1111/j.1572-0241.2006.01002.x.

[112] Matteo Cianchetti, Tommaso Ranzani, Giada Gerboni, et al. "Soft Robotics Technologies to Address Shortcomings in Today's Minimally Invasive Surgery: The STIFF-FLOP Approach". In: *Soft Robotics* 1.2 (2014), pp. 122–131. DOI: 10.1089/soro.2014.0001. eprint: https://doi.org/10.1089/soro.2014.0001. URL: https://doi.org/10.1089/soro.2014.0001.

[113] Hesheng Wang, Runxi Zhang, Weidong Chen, et al. "A cable-driven soft robot surgical system for cardiothoracic endoscopic surgery: preclinical tests in animals". In: 31.8 (Nov. 2016), pp. 3152–3158. DOI: 10.1007/s00464-016-5340-9. URL: https://doi.org/10.10072Fs00464-016-5340-9.

[114] Kit-Hang Lee, Denny K.C. Fu, Martin C.W. Leong, et al. "Nonparametric Online Learning Control for Soft Continuum Robot: An Enabling Technique for Effective Endoscopic Navigation". In: *Soft Robotics* 4.4 (2017). PMID: 29251567, pp. 324–337. DOI: 10.1089/soro.2016.0065. eprint: https://doi.org/10.1089/soro.2016.0065. URL: https://doi.org/10.1089/soro.2016.0065.

[115] Yoonho Kim, German A. Parada, Shengduo Liu, et al. "Ferromagnetic soft continuum robots". In: *Science Robotics* 4.33 (2019), eaax7329. DOI: 10.1126/scirobotics.aax7329. eprint: https://www.science.org/doi/pdf/10.1126/scirobotics.aax7329. URL: https://www.science.org/doi/abs/10.1126/scirobotics.aax7329.

[116] *Endoo EU Project*. URL: https://www.endoo-project.eu/.

[117] K. Suzumori, T. Hama, and T. Kanda. "New pneumatic rubber actuators to assist colonoscope insertion". In: *Proceedings 2006 IEEE International Conference on Robotics and Automation, 2006. ICRA 2006.* 2006, pp. 1824–1829. DOI: 10.1109/ROBOT.2006.1641971.

[118] Julius E. Bernth, Alberto Arezzo, and Hongbin Liu. "A Novel Robotic Meshworm With Segment-Bending Anchoring for Colonoscopy". In: *IEEE Robotics*

*and Automation Letters* 2.3 (2017), pp. 1718–1724. DOI: 10.1109/LRA.2017.2678540.

[119] Luigi Manfredi, Elisabetta Capoccia, Gastone Ciuti, et al. "A Soft Pneumatic Inchworm Double balloon (SPID) for colonoscopy". In: *Scientific Reports* 9 (July 2019), p. 11109. DOI: 10.1038/s41598-019-47320-3.

[120] C.D. Onal and Daniela Rus. "Autonomous undulatory serpentine locomotion". In: *Bioinspiration biomimetics* 8 (Mar. 2013), p. 026003. DOI: 10.1088/1748-3182/8/2/026003.

[121] Dinh Quang Nguyen and Van Anh Ho. "Anguilliform Swimming Performance of an Eel-Inspired Soft Robot". In: *Soft Robotics* 0.0 (0). PMID: 34134542, null. DOI: 10.1089/soro.2020.0093. eprint: https://doi.org/10.1089/soro.2020.0093. URL: https://doi.org/10.1089/soro.2020.0093.

[122] Xinda Qi, Hongyang Shi, Thassyo Pinto, et al. "A Novel Pneumatic Soft Snake Robot Using Traveling-Wave Locomotion in Constrained Environments". In: *IEEE Robotics and Automation Letters* 5.2 (2020), pp. 1610–1617. DOI: 10.1109/LRA.2020.2969923.